

WCIO 2014

NEW YORK CITY



CONFERENCE PROGRAM

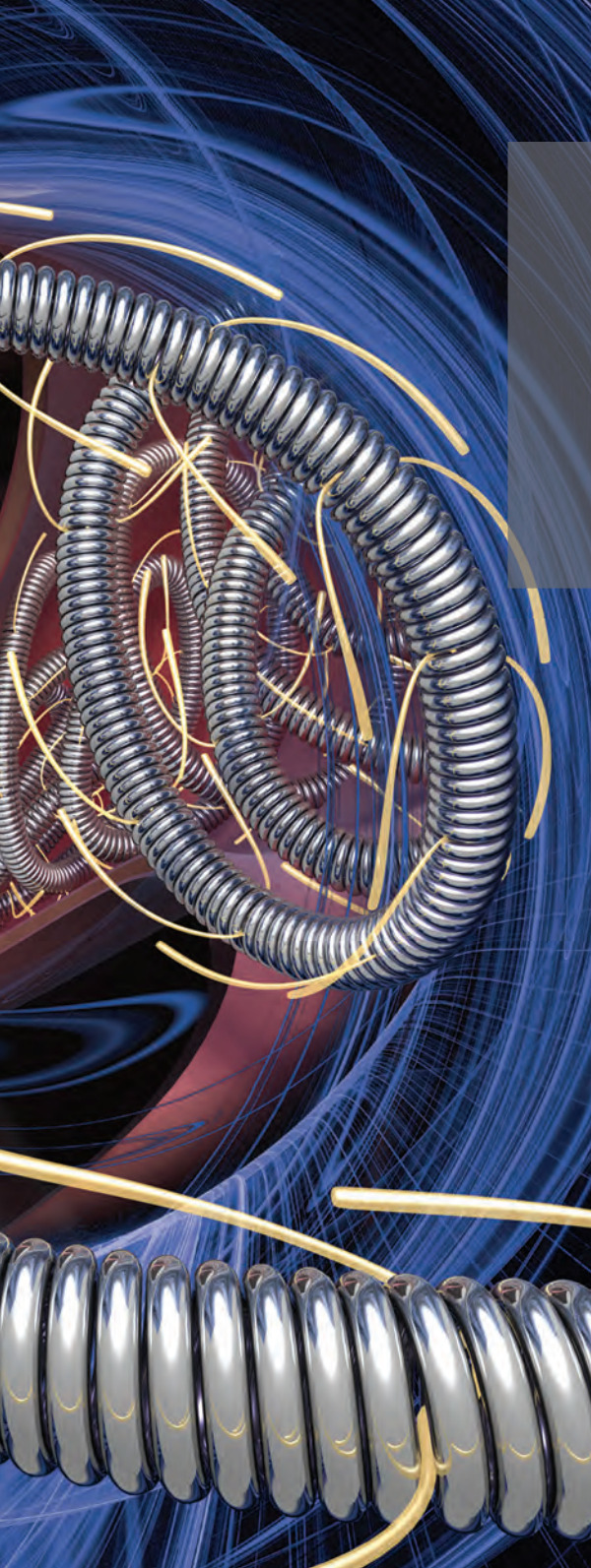
11-14 MAY 2014 / NEW YORK HILTON MIDTOWN / NEW YORK CITY

WWW.WCIOEVENTS.ORG

Brought to you by

WCIO

Advancing Interventional Oncology



More Ease. More Precision. More Control.

The Concerto™ detachable coil system is designed to deliver *more* at every stage of peripheral vasculature coil embolization.

EASIER DELIVERY

Inherently soft fibered coils travel smoothly through the microcatheter—enabling navigation of torturous anatomy and access to distal locations for targeted focal embolization.¹

PRECISE DEPLOYMENT

Superb distal performance provides easier loop formation for accurate coil deployment and secure positioning.

CONTROLLED DETACHMENT

Unique articulation zone enables instant detachment.

[VASCULAR THERAPIES]

Arterial | Venous | Neurovascular



COVIDIEN

1. Gandras E, Greben C, Putterman D, et al. Visceral arterial embolization. *Endovascular Today*. 2008;6:66-74.

Indications, contraindications, warnings, and instructions for use can be found on the product labeling supplied with each device. CAUTION: Federal (USA) law restricts this device to sale by or on the order of a physician.

COVIDIEN, COVIDIEN with logo, and Covidien logo are US and internationally registered trademarks of Covidien AG. Other brands are trademarks of a Covidien company. ©2014 Covidien. MK1063022014A

Visit Covidien
at WCIO Booth 104

SCHEDULE-AT-A-GLANCE

Time	IO Primer for Early Career – East Ballroom	Advanced IO Techniques and Applications – West Ballroom	
Sunday, 11 May			
8:50-9:00	Welcome		
9:00-10:30	IO Fundamentals – Part 1	Imaging, Therapy Planning, and Guidance	
10:30-11:00	Break & Exhibits		
11:00-12:30	IO Fundamentals - Part 2	Update on New Therapeutic Modalities	
12:30-13:10	Lunch Symposium: NeuWave Medical, Inc., <i>Growing Your Practice with Microwave Ablation</i>		
13:10 – 13:50	Lunch Symposium: Siemens Medical Solutions, <i>Syngo Dyna CT – Staying a Step Ahead in Solid Tumor Treatment</i>		
13:50-14:15	Break & Exhibits		
14:15-15:30	IO Practice Development – Part 1	Case-Based Review of Advanced IO Techniques – Part 1	
15:30-16:00	Break & Exhibits		
16:00-18:00	IO Practice Development – Part 2	Case-Based Review of Advanced IO Techniques – Part 2	
18:00-19:15	Symposium: Covidien, <i>Evolution of Embolization: The Columbia Experience with Fully Retrievable Coil Technology</i>		
18:00-19:30	Fellows' Program		
Time	General Sessions – East Ballroom	Abstracts and Allied Health Program – West Ballroom	Workshops
Monday, 12 May			
8:00-9:30		Scientific Abstracts: HCC	Workshop: Tumor Embolization (Bland, cTACE, DEB TACE) – East Ballroom
9:30-10:00	Break & Exhibits		
10:00-11:30	Plenary Session – Primary Liver Cancer*	Allied Health Program	
11:30 -12:30	Plenary Session – HCC Tumor Board		
12:30-13:45	Lunch Symposium: <i>Global Evolution of Techniques and Guidelines for the HCC Treatment**</i>		
13:50-14:15	Break & Exhibits		
14:15-15:00	Plenary Session – MSK, Pain Palliations		
15:00 – 15:30	MSK Tumor Board		
15:30-16:00	Break & Exhibits		
16:00-17:30		Scientific Abstracts: Palliative Care and Radioembolization	Hands-on Workshop: Bone, Spine, Soft Tissue and Palliative Care Therapies – Trianon
17:30-18:30	Poster Viewing – Americas Hall 1		
18:00-19:00	Reception in Exhibit Hall		
Tuesday, 13 May			
8:00-9:30		Scientific Abstracts: Pre-Clinical Research: Ablation and TACE	Workshop: Ablation, Kidney/Lung – East Ballroom
9:30-10:00	Break & Exhibits		
10:00-11:00	Plenary Session - Molecular Oncology	Allied Health Program	
10:00-11:00	Fellows' Program Exhibitor Time		
11:00-12:00	Plenary Session - Renal		Hands-on Workshop: Guidance, Targeting, Monitoring and Assessment – Trianon
12:00-12:30	Renal Tumor Board		
12:30-13:10	Lunch Symposium: GE Healthcare, <i>3D Applications in the Angio Suite: Gadgets or Must-Have? A Case Review</i>		
13:10 – 13:50	Lunch Symposium: Covidien, <i>Closing the Gap on Predictable Outcomes</i>		
13:50-14:15	Break & Exhibits		
14:15-15:55	Plenary Session - Lung		Workshop: Liver Ablation – West Ballroom
15:15-15:55	Lung Tumor Board		
16:00-16:30	Break & Exhibits		
16:30-18:00	Case of the Week: Live! – Americas Hall 1	Scientific Abstracts: Image Guidance and Follow-Up	Hands-on Workshop: RFA, MW, and Cryoablation – Trianon
18:00-19:30	Corporate Advisory Council Reception (Invitation only) – 44th Floor Executive Lounge		
Wednesday, 14 May			
8:00-9:30		Scientific Abstracts: Ablation	Workshop: Y90 Radioembolization – East Ballroom
9:30-10:00	Break & Exhibits		
10:00-11:30	Plenary Session - Liver Mets (mCRC, NET)*		
11:30-12:30	Liver Mets Tumor Board		

* SA-CME Credit

**Supported by an educational grant from BTG and Guerbet

CONTENTS

- 3 Message from the Chairs
- 5 WCIO Board of Directors
- 5 General Information
- 6 CME Information
- 7 Faculty
- 8 Acknowledgements
- 9 Industry Symposia Information
- 10 Program
- 15 Allied Health Program
- 16 Exhibit Hall Map
- 17 Exhibitors
- 19 Abstracts



MESSAGE FROM THE PROGRAM COMMITTEE

Dear Colleagues,

Welcome to New York City for WCIO 2014. WCIO 2014 is the leading interventional oncology (IO) conference, bringing together medical experts from around the world for a multidisciplinary approach to IO. WCIO 2014 is a unique conference developed by an international team of experts from multiple specialties, to further the goal of cross-disciplinary collaboration and education.

During the next several days, we will come together to hear state-of-the-art lectures on innovative IO topics, participate in tumor boards highlighting real-world techniques, acquire cutting-edge best practices, and learn bench-to-bedside program content.

Session topics will span private practice, hospital, and institutional settings. Medical students, residents and fellows, advanced practice providers, IO experts, and less experienced operators alike are participating in this truly dynamic learning and networking experience. We look forward to engaging with you to discuss available and emerging therapies in the field.

Additionally, WCIO features the most comprehensive early career program available for fellows and those looking to advance within the multidisciplinary field of interventional oncology or establish their own private practice.

This is your opportunity to explore best practices as well as new discoveries, and you will be sure to bring back insights and strategies for the fight against cancer in your own practice, hospital, or institution.

WCIO is a global community whose mission is to establish, nurture, and support interventional oncology (IO) as the 4th pillar of cancer therapy alongside medical, surgical, and radiation oncology worldwide. Please visit www.io-central.org to join our interventional oncology community if you have not already done so. We look forward to meeting with you this week in New York and are excited you've joined us for this one-of-a-kind event.

Welcome to New York City! We're happy you're here.

WCIO Program Committee:

William S. Rilling, MD

Program Chair
Medical College of Wisconsin
Milwaukee, Wisconsin, USA

Riccardo A. Lencioni, MD

Past Chair
Pisa University School of Medicine
Pisa, Italy

Thierry De Baere, MD

Science and Technology Chair
Institut Gustave Roussy
Villejuif, France

Hyun S. "Kevin" Kim, MD, FSIR

Workshop Chair
University of Pittsburgh School of Medicine
Pittsburgh, Pennsylvania, USA

Matthew R. Callstrom, MD, PhD

Program Committee Member
Mayo Clinic
Rochester, Minnesota, USA

Jeffrey F. Geshwind, MD

Program Committee Member
Johns Hopkins School of Medicine
Baltimore, Maryland, USA

Constantinos T. Sofocleous, MD, PhD

Program Committee Member
Memorial Sloan-Kettering Cancer Center
New York, New York, USA

3

WCIO would like to thank all those who participated in the abstract reviewing process. Without your diligent work, WCIO 2014 would not be possible.

Matthew Callstrom, MD, PhD

Jeffrey Geschwind, MD

David Madoff, MD

Stephen Solomon, MD

Thierry de Baere, MD

S. Nahum Goldberg, MD

William Rilling, MD

Michael Soulen, MD

Afshin Gangi, MD

Hyun S. "Kevin" Kim, MD

Riad Salem, MD, MBA

Debra Gervais, MD

Riccardo Lencioni, MD

Constantinos Sofocleous, MD, PhD



New Design. Same Great Content.

IO Central - Connecting the Interventional Oncology Community

We are bringing you the same great content you've come to expect from WCIO with a fresh, organized new look. Visit www.IO-Central.org and access unique features designed to bring together physicians, researchers, industry, and members of the IO community at large for online dialogue and learning.

- Discussion Forum
- IO News Feeds
- Industry Directory
- IO Event Calendar
- IO Video Library
- IO Insights Monthly Newsletter
- Case of the Week Education Series

Engage 24/7, 365 days a year with a network of world class leaders in IO. Joining IO Central is 100 percent free of cost!

www.IO-Central.org



GENERAL INFORMATION

Board of Directors

Riccardo A. Lencioni, MD **Chair**

Pisa University School of Medicine
Pisa, Italy

Jeffrey F. Geschwind, MD **Vice Chair**

Johns Hopkins University School of
Medicine
Baltimore, Maryland, USA

Michael C. Soulen, MD **Past Chair**

University of Pennsylvania
Philadelphia, Pennsylvania, USA

Thierry De Baere, MD

Institut Gustave Roussy
Villejuif, France

Afshin Gangi, MD, PhD

University Hospital of Strasbourg
Strasbourg, Bas-Rhin, France

David Lu, MD

University of California, Los Angeles
Los Angeles, California, USA

Riad Salem, MD, MBA

Northwestern University
Chicago, Illinois, USA

Luigi Solbiati, MD

General Hospital of Busto Arsizio
Busto Arsizio, Italy

Stephen Solomon, MD

Memorial Sloan-Kettering Cancer Center
New York, New York, USA



New York Hilton Midtown

1335 Avenue of the Americas
New York, NY 10019

Registration

Ballroom Promenade

Sunday, 11 May	8:00 – 19:00
Monday, 12 May	7:30 – 18:00
Tuesday, 13 May	7:30 – 17:00
Wednesday, 14 May	7:30 – 12:00

Exhibit Hall

Ballroom Foyer and Promenade

Sunday, 11 May	10:30 – 11:00	12:30 – 14:15	15:30 – 16:00
Monday, 12 May	8:00 – 10:00	12:30 – 14:15	15:30 – 19:00
Tuesday, 13 May	8:00 – 10:00	12:30 – 14:15	16:00 – 16:30
Wednesday, 14 May	8:00 – 10:00		

Speaker Ready Room

Midtown Suite

Sunday, 11 May	6:30 – 18:00
Monday, 12 May	6:30 – 18:00
Tuesday, 13 May	6:30 – 18:00
Wednesday, 14 May	6:30 – 12:00

Posters

Americas Hall 1

Sunday, 11 May	12:30 – 16:00
Monday, 12 May	8:00 – 19:00
Tuesday, 13 May	8:00 – 14:30

WCIO 2014 On Demand – Share Sessions with Your Colleagues

WCIO 2014 On Demand provides you web access to WCIO 2014 sessions* including speaker slides, videos, and pointer movements so you can follow along with the recorded presentations from the convenience of your home or office. Your purchase includes the conference session library and sessions for online download. On Demand is available for purchase at the registration desk for \$100.

**Abstract sessions are not included.*

Participate Like Never Before!

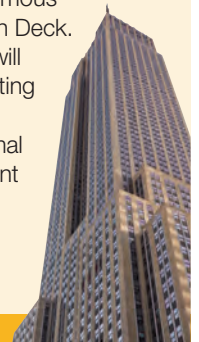
New for 2014! Be sure to take part in the audience response systems that will be used in selected sessions. Keypads are available at the Registration desk. Participate in audience polling, type questions directly to the moderators, earn SA-CME credit, and complete session evaluations all from one device.

WCIO Social Event – Experience NYC as a VIP

Saturday, 10 May 2014
5:30 pm – 9:00 pm

Kick off WCIO 2014 when you join fellow attendees for a relaxing evening at New York City's favorite attraction – **The Empire State Building**. An exclusive WCIO usher will be guiding the group with front-of-the-line access to the world famous 86th Floor Observation Deck. Afterward, our group will participate in Beer Tasting 101 at the Heartland Brewery with an informal presentation on different types of beer.

Bring your spouse, friend, or colleague!



CONTINUING MEDICAL EDUCATION (CME) INFORMATION

Accreditation Statement



This activity has been planned and implemented in accordance with the Essentials and Standards of the Accreditation Council for Continuing Medical Education (ACCME) through joint

sponsorship of the Society of Interventional Radiology (SIR) and WCIO. SIR is accredited by the ACCME to provide continuing medical education for physicians. SIR designates the WCIO 2014 for 22.25 AMA PRA Category 1 Credits™.

In accordance with the ACCME's Standards for Commercial Support of Continuing Medical Education, all faculty and planning partners must disclose any financial relationship(s) or other relationship(s) held within the past 12 months. We have implemented a mechanism to identify and resolve all conflicts of interest prior to delivering the educational activity to learners.

Learning Objectives

Upon completion of the conference, attendees will be able to:

- Utilize new technologies presented to help select the appropriate therapies in the treatment of patients;
- Integrate multi-disciplinary treatment options into a comprehensive patient care program; and
- Apply proven international techniques into current practice.

Who Should Attend?

WCIO 2014 is specifically designed to meet the educational needs of:

- Clinical Researchers
- Diagnostic Radiologists
- Interventional Oncologists
- Interventional Radiologists
- Medical Oncologists
- Radiation Oncologists
- Scientists
- Surgical Oncologists
- Medical Students
- Residents
- Interventional Radiology Nurses
- Interventional Radiology Physician Assistants
- Interventional Oncology Nurses
- Interventional Oncology Physician Assistants
- Oncology Nurses
- Oncology Physician Assistants
- Hepatology Nurses
- Hepatology Physician Assistants
- Liver Transplant Nurses/Coordinators
- Nursing Students

SA-CME — New in 2014!

Marked sessions are provisionally qualified as of April 23, 2014 by the American Board of Radiology in meeting the criteria for self-assessment CME toward the purpose of fulfilling requirements in the ABR Maintenance of Certification Program. Full qualification by the ABR is expected before the SAM is taken.

SA-CME Sessions:

Monday, 12 May, 10:00-11:30

Plenary Session – Primary Liver Cancer

Wednesday, 14 May, 10:00-11:30

Plenary Session – Liver Mets (mCRC, NET)

Allied Health Program Faculty

Matthew Cestone, RT

Memorial Sloan-Kettering Cancer Center
New York, New York, USA

Ginna Deitrick, MSN, CRNP, AOCNP

University of Pennsylvania
Philadelphia, Pennsylvania, USA

Deborah Fleischer, BSN, RN, MA, ACNP-BC

Memorial Sloan-Kettering Cancer Center
New York, New York, USA

Angela Greco, RT

Memorial Sloan-Kettering Cancer Center
New York, New York, USA

Avinash Kambadakone, MD

Massachusetts General Hospital
Boston, Massachusetts, USA

Matthew Kennedy, RN

Memorial Sloan-Kettering Cancer Center
New York, New York, USA

Nicole Kowalewski, NP

Memorial Sloan-Kettering Cancer Center
New York, New York, USA

Eibhlis Murray, NP

Memorial Sloan-Kettering Cancer Center
New York, New York, USA

Piera Robson, NP, CNS

Memorial Sloan-Kettering Cancer Center
New York, New York, USA

Dave Silva, RA, RT

Memorial Sloan-Kettering Cancer Center
New York, New York, USA

Diana Van Houten, MSN, CRNP, CCRN

University of Pennsylvania
Philadelphia, Pennsylvania, USA

Amy Vatanapradit, NP

Memorial Sloan-Kettering Cancer Center
New York, New York, USA

FACULTY

Nadine Abi-Jaoudeh, MD

National Institutes of Health
Bethesda, Maryland, USA

Ghassan K. Abou-Alfa, MD

Memorial Sloan-Kettering Cancer Center
New York, New York, USA

Richard G. Abramson, MD

Vanderbilt-Ingram Cancer Center
Nashville, Tennessee, USA

Muneeb Ahmed, MD

Beth Israel Deaconess Medical Center
Boston, Massachusetts, USA

Yasuaki Arai, MD

National Cancer Center
Tokyo, Japan

Tanios Bekaii-Saab, MD

The Ohio State University College of Medicine
Columbus, Ohio, USA

David Boshell, MBBS

St. Vincent's Hospital
Sydney, Australia

Christopher Brace, PhD

University of Wisconsin
Madison, Wisconsin, USA

David Breen, MD

University Hospital of Southampton
Southampton, Hampshire, United Kingdom

Daniel Brown, MD

Thomas Jefferson University
Philadelphia, Pennsylvania, USA

Michael Brunner, MD, FSIR, FACR

University of Wisconsin School of Medicine
and Public Health
Madison, Wisconsin, USA

Matthew Callstrom, MD, PhD

Mayo Clinic
Rochester, Minnesota, USA

Juan C. Camacho, MD

Emory University School of Medicine
Atlanta, Georgia, USA

Daniel Canter, MD

Urologic Institute of Southeastern Pennsylvania
Elkins Park, Pennsylvania, USA

Andrea Cercek, MD

Memorial Sloan-Kettering Cancer Center
New York, New York, USA

Julius Chapiro, MD

Johns Hopkins University School of Medicine
Baltimore, Maryland, USA

Jonathan Coleman, MD

Memorial Sloan-Kettering Cancer Center
New York, New York, USA

Anne Covey, MD

Memorial Sloan-Kettering Cancer Center
New York, New York, USA

Laura Crocetti, MD, PhD

Pisa University School of Medicine
Pisa, Italy

Thierry De Baere, MD

Institut Gustave Roussy
Villejuif, France

Alban Denys, MD

CHUV University of Lausanne
Lausanne, Switzerland

Frederic Deschamps, MD

Institut Gustave Roussy
Villejuif, France

Robert Dixon, MD

University of North Carolina, Chapel Hill
Chapel Hill, North Carolina, USA

Jeremy Durack, MD

Memorial Sloan-Kettering Cancer Center
New York, New York, USA

Joseph Erinjeri, MD, PhD

Memorial Sloan-Kettering Cancer Center
New York, New York, USA

Francis Facchini, MD

VIROChicago/AngioDynamics
Latham, New Jersey, USA

Aaron M. Fischman, MD

Icahn School of Medicine at Mount Sinai
New York, New York, USA

Raja M. Flores, MD

Icahn School of Medicine at Mount Sinai
New York, New York, USA

Chiara Floridi, MD

Universita di Insubria Varese
Varese, Italy

Shanmugasundaram Ganapathy-Kanniappan, PhD

Johns Hopkins University School of Medicine
Baltimore, Maryland, USA

Afshin Gangi, MD

University Hospital of Strasbourg
Strasbourg, Bas-Rhin, France

Ricardo D. Garcia-Monaco, MD, PhD

Hospital Italiano de Buenos Aires
Buenos Aires, Argentina

David A. Geller, MD

University of Pittsburgh
Pittsburgh, Pennsylvania, USA

Christos Georgiades, MD, PhD

American Medical Center
Nicosia, Cyprus

Debra Gervais, MD

Massachusetts General Hospital
Boston, Massachusetts, USA

Jeffrey Geschwind, MD

Johns Hopkins University School of Medicine
Baltimore, Maryland, USA

S. Nahum Goldberg, MD

Hadassah University Hospital
Jerusalem, Israel

Dana Haddad, MD

Columbia University
New York, New York, USA

Ryan Hickey, MD

Northwestern University
Chicago, Illinois, USA

Kelvin Hong, MD

Johns Hopkins University School of Medicine
Baltimore, Maryland, USA

Tobias Jakobs, MD

Hospital Barmherzige Brueder Munich
Munich, Bavaria, Germany

Alexis Kelekis, MD, PhD, DO

National and Kapodistrian University of Athens
Athens, Greece

Hyun S. "Kevin" Kim, MD

University of Pittsburgh School of Medicine
Pittsburgh, Pennsylvania, USA

Anil "Nick" Kurup, MD

Mayo Clinic
Rochester, Minnesota, USA

Marnix Lam, MD, PhD

University Medical Center Utrecht
Utrecht, Netherlands

Fred Lee Jr., MD

University of Wisconsin
Madison, Wisconsin, USA

Riccardo Lencioni, MD

Pisa University School of Medicine
Pisa, Italy

Robert Lewandowski, MD

Northwestern University
Chicago, Illinois, USA

Katerina Malagari, MD, PhD

University of Athens
Athens, Greece

Majid Maybody, MD

Memorial Sloan-Kettering Cancer Center
New York, New York, USA

Alessandro Napoli, MD, PhD

Sapienza-University of Roma
Rome, Italy

Govindarajan Narayanan, MD

University of Miami Miller School of Medicine
Coral Gables, Florida, USA

Kenneth R. Olivier, MD

Mayo Clinic
Rochester, Minnesota, USA

Jean Palussière, MD

Institut Bergonié
Bordeaux, France

Timothy Pawlik, MD, PhD

Johns Hopkins University School of Medicine
Baltimore, Maryland, USA

Victor Reuter, MD

Memorial Sloan-Kettering Cancer Center
New York, New York, USA

Hyunchul Rhim, MD

Samsung Medical Center
Seoul, Korea

William Rilling, MD

Medical College of Wisconsin
Milwaukee, Wisconsin, USA

Nabil Rizk, MD

Memorial Sloan-Kettering Cancer Center
New York, New York, USA

Kenneth Rosenzweig, MD

Icahn School of Medicine at Mount Sinai
New York, New York, USA

Saurabh Saha, MD, PhD

BioMed Valley Discoveries
Kansas City, Missouri, USA

Riad Salem, MD, MBA

Northwestern University
Chicago, Illinois, USA

Shaun Samuels, MD

Baptist Cardiac and Vascular Institute
Miami, Florida, USA

Ernesto G. Santos Martin, MD

University of Pittsburgh School of Medicine
Pittsburgh, Pennsylvania, USA

Grant Schmit, MD

Mayo Clinic
Rochester, Minnesota, USA

Myron Schwartz, MD

Icahn School of Medicine at Mount Sinai
New York, New York, USA

Constantinos Sofocleous, MD, PhD

Memorial Sloan-Kettering Cancer Center
New York, New York, USA

Luigi Solbiati, MD

General Hospital of Busto Arsizio
Busto Arsizio, Varese, Italy

Stephen Solomon, MD

Memorial Sloan-Kettering Cancer Center
New York, New York, USA

Michael Soulen, MD

University of Pennsylvania
Philadelphia, Pennsylvania, USA

Robert D. Suh, MD

Ronald Reagan UCLA Medical Center
Los Angeles, California, USA

Ashraf Thabet, MD

Massachusetts General Hospital
Boston, Massachusetts, USA

Sean Tutton, MD

Medical College of Wisconsin
Milwaukee, Wisconsin, USA

Thomas J. Vogl, MD

Universtats Klinikum
Frankfurt, Germany

Dan Wassilchick, MHA

University of Pittsburgh Medical Center
Pittsburgh, Pennsylvania, USA

Sarah B. White, MD

Medical College of Wisconsin
Milwaukee, Wisconsin, USA

Roger Williams, DO

Emory University School of Medicine
Atlanta, Georgia, USA

Bradford Wood, MD

National Institutes of Health
Washington, District of Columbia, USA

Abraham Wu, MD

Memorial Sloan-Kettering Cancer Center
New York, New York, USA

Hooman Yarmohammadi, MD

Memorial Sloan-Kettering Cancer Center
New York, New York, USA

ACKNOWLEDGEMENTS

WCIO thanks the following companies for their support:

Sponsors



Exhibitors



Sponsors and exhibitors listed are as of April 2014. For more information about the WCIO Corporate Partner program, please contact Beverlee Galstan at bgalstan@wcioonline.org.

Corporate Partners

Platinum



Gold



Partners



INDUSTRY SYMPOSIA INFORMATION

Industry Symposia Information

Sunday, 11 May, 12:30 – 13:10

East Ballroom

Industry Symposium

presented by NeuWave Medical, Inc.



Growing Your Practice with Microwave Ablation

Speakers: Matthew Callstrom, MD, PhD;
J. Louis Hinshaw, MD; Stephen Solomon, MD
Moderator: Fred Lee Jr., MD

Sunday, 11 May, 13:10 – 13:50

East Ballroom

Industry Symposium

presented by Siemens Medical Solutions

SIEMENS

syngo DynaCT – Staying a Step Ahead in Sound Tumor Treatment

Speakers: Robert Lewandowski, MD,
Sandeep Bagla, MD
Moderator: Riad Salem, MD, MBA

Sunday, 11 May, 18:00 – 19:15

West Ballroom

Industry Symposium presented by Covidien



Evolution of Embolization: The Columbia Experience with Fully Retrievable Coil Technology

Speaker: Jonathan Susman, MD

Tuesday, 13 May, 12:30 – 13:10

East Ballroom

Industry Symposium presented by GE Healthcare



3D Applications in the Angio Suite: Gadgets or Must-Have? A Case Review

Speakers: Thierry De Baere, MD;
Maxime Ronot, MD; Stephen Solomon, MD

Tuesday, 13 May, 13:10 – 13:50

East Ballroom

Industry Symposium presented by Covidien



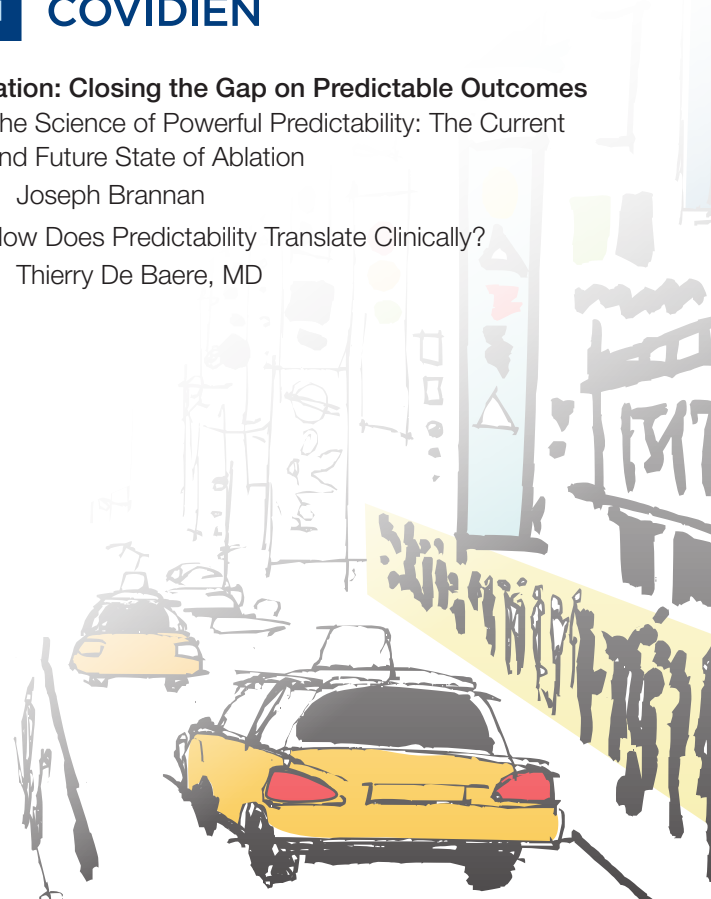
Ablation: Closing the Gap on Predictable Outcomes

The Science of Powerful Predictability: The Current and Future State of Ablation

Joseph Brannan

How Does Predictability Translate Clinically?

Thierry De Baere, MD



SCIENTIFIC PROGRAM

* Schedule subject to change.

Sunday, 11 May 2014


8:50-9:00		Welcome and General Session	
IO Primer for Early Career		Advanced IO Techniques and Applications	
Time	East Ballroom	Time	West Ballroom
9:00-10:30		9:00-10:30	
IO Fundamentals – Part 1 <i>Moderators: Michael Soulen, MD; Constantinos Sofocleous, MD, PhD</i>		Imaging, Therapy Planning, and Guidance <i>Moderators: Daniel Brown, MD; Luigi Solbiati, MD</i>	
9:00-9:20	Assessment and Triage of the IO Patient, Part 1 – What You Need to Know <i>Ryan Hickey, MD</i>	9:00-9:15	Advanced Imaging Techniques for Response Evaluation Following Locoregional Therapy <i>Rick Abramson, MD</i>
9:20-9:40	Assessment & Triage of the IO Patient, Part 2 – Establishing Credibility in Tumor Boards <i>Michael Soulen, MD</i>	9:15-9:30	Therapy Planning, Guidance, and Endpoint Determination for Tumor Ablation <i>Grant Schmit, MD</i>
9:40-10:00	Taking Ownership of Imaging Before and After IO Therapy - What the Referring Docs Aren't Telling You <i>Debra Gervais, MD</i>	9:30-9:45	Guidance, Advanced Techniques, and Endpoint Determination for Chemoembolization <i>Jeff Geschwind, MD</i>
10:00-10:30	Audience Response Case Based Review – Assessment Triage and Imaging <i>Michael Soulen, MD</i>	9:45-10:00	Therapy Planning and Dosimetry for Radioembolization <i>Mamix Lam, MD, PhD</i>
		10:00-10:15	New Concepts in Y90 Dosimetry, Radiation Segmentectomy and Beyond <i>Robert Lewandowski, MD</i>
		10:15-10:30	Panel Discussion
10:30-11:00		Break with Exhibitors	
11:00-12:30		11:00-12:30	
IO Fundamentals – Part 2 <i>Moderators: Michael Soulen, MD; Constantinos Sofocleous, MD, PhD</i>		Update on New Therapeutic Modalities <i>Moderator: Stephen Solomon, MD; Michael Brunner, MD, FSIR, FACR</i>	
11:00-11:15	Common Systemic Therapies - What Your Oncologists and Patients Expect You to Know <i>Andrea Cercek, MD</i>	11:00-11:15	Microwave Ablation: Breaking the 3CM Barrier? <i>Chris Brace, PhD</i>
11:15-11:30	Essential Palliative Skills in IO, Part 1 - Pain Management <i>Ashraf Thabet, MD</i>	11:15-11:30	Where Does IRE Fit In? <i>S. Nahum Goldberg, MD</i>
11:30-11:45	Essential Palliative Skills in IO, Part 2 - Management of Ascites and Effusions <i>Hooman Yarmohammadi, MD</i>	11:30-11:45	HIFU Update: Current and Future Applications <i>Alessandro Napoli, MD, PhD</i>
11:45-12:00	Establishing Trust and Communicating With the Difficult Patient and Family <i>Majid Maybody, MD</i>	11:45-12:00	Novel Locoregional Drug Delivery: New Drugs and Targets <i>Riccardo Lencioni, MD</i>
12:00-12:30	Audience Response Case Based Review - My Greatest Saves Through Integrated Care <i>Constantinos Sofocleous, MD</i>	12:00-12:15	Biosurgery for the Treatment of Cancer <i>Saurabh Saha, MD, PhD</i>
		12:15-12:30	Virus <i>Dana Haddad, MD</i>
12:30-13:10	Lunch Symposium (Presented by NeuWave Medical, Inc.): Growing Your Practice with Microwave Ablation		
13:10-13:50	Lunch Symposium (Presented by Siemens Medical Solutions): syngo DynaCT – Staying a Step Ahead on Sound Tumor Treatment		
13:50-14:15 Break with Exhibitors			
14:15-15:30		14:15-15:30	
IO Practice Development – Part 1 <i>Moderators: Hyun S. "Kevin" Kim, MD; William Rilling, MD</i>		Case-Based Review of Advanced IO Techniques – Part 1 <i>Moderator: Fred Lee, MD; Riad Salem, MD</i>	
14:15-14:30	IO Clinical Practice Models: What Works and What Doesn't <i>Hyun S. "Kevin" Kim, MD</i>	14:15-14:45	Panel Discussion: Liver Tumor Ablation <i>Fred Lee, MD; Stephen Solomon, MD; Riccardo Lencioni, MD; Luigi Solbiati, MD</i>
14:30-14:45	IO Clinic Models: Personnel and Finances <i>Sarah White, MD</i>		
14:45-15:00	Finances, Performa, and Business Plan of IO <i>Dan Wassilchuk, MHA</i>	14:45-15:30	Panel Discussion: TACE and Y90 <i>Riad Salem, MD, MBA; Yasuaki Arai, MD; Katerina Malagari, MD, PhD, EBIR; Anne Covey, MD</i>
15:00-15:30	The Evolving Coding and Payment Landscape for IO Therapies <i>Sean Tutton, MD</i>		
15:30-16:00 Break with Exhibitors			

Sunday, 11 May 2014 (continued)

IO Primer for Early Career		Advanced IO Techniques and Applications	
Time	East Ballroom	Time	West Ballroom
16:00-18:00	IO Practice Development – Part 2 <i>Moderators: Riad Salem, MD, MBA; Hyun S. “Kevin” Kim, MD; William Rilling, MD</i>	16:00-18:00	Case-Based Review of Advanced IO Techniques – Part 2 <i>Moderators: Matthew Callstrom, MD, PhD; Thierry De Baere, MD</i>
	16:00-16:15 Integration in the Cancer Center – Why and How <i>William Rilling, MD</i>	16:00-17:00	Panel Discussion: Advanced MSK Techniques <i>Alexis Kelekis, MD, PhD, DO, EBIR; Matthew Callstrom, MD, PhD; Sean Tutton, MD</i>
	16:15-16:30 Value of IO to the Cancer Center <i>Govindarajan Narayanan, MD</i>		
	16:30-16:45 Modern Marketing of IO – Web, Social Media, and Patient Advocacy, etc. <i>Francis Facchini, MD</i>		
	16:45-17:00 Value of Research/Clinical Trials in IO <i>Jeff Geschwind, MD</i>		
	17:00-17:15 Developing Quality Metrics in IO <i>Ryan Hickey, MD</i>	17:00-18:00	Panel Discussion: Lung and Renal Ablation <i>David Breen, MD; Christos Georgiades, MD, PhD; Thierry De Baere, MD</i>
	17:15-17:30 No Transplant Center, No Problem: Building IO in Private Practice <i>Shaun Samuels, MD</i>		
	17:30-18:00 Panel Discussion		
18:00-19:30	Fellows' Program – East Ballroom	18:00-19:15	Symposium (Presented by Covidien): Evolution of Embolization: The Columbia Experience with Fully Retrievable Coil Technology

11

Monday, 12 May 2014

Time	General Session – East Ballroom	Time	West Ballroom
8:00-9:30	Workshop: Tumor Embolization (Bland, cTACE, DEB TACE) <i>Katerina Malagari, MD, PhD; Yasuaki Arai, MD; Ricardo D. Garcia-Monaco, MD, PhD</i>	8:00-9:30	Scientific Abstracts: HCC
9:30-10:00	Break with Exhibitors		
10:00-11:30	Plenary Sessions - Primary Liver Cancer (SA-CME Credit Available) <i>Moderators: William Rilling, MD; Yasuaki Arai, MD</i>	10:00-13:10	Allied Health Program
	10:00-10:15 Trends in Treatment Allocation for Early Stage HCC: Transplant, Resection, Ablation <i>Timothy Pawlik, MD, PhD</i>		
	10:15-10:30 Percutaneous Ablation for HCC: Patient Selection and Results in 2014 <i>Riccardo Lencioni, MD</i>		
	10:30-10:45 Chemoembolization for HCC: Best Evidence and Practice <i>William Rilling, MD</i>		
	10:45-11:00 Current Role of Radioembolization for HCC <i>Robert Lewandowski, MD</i>		
	11:00-11:15 Combination Therapies for HCC: Why, When, and How <i>Jeff Geschwind, MD</i>		
	11:15-11:30 Debate: Locoregional Therapy Should Be Offered to BCLC C Patients (Pro and Con) <i>Yasuaki Arai, MD vs. Ghassan Abou-Alfa, MD</i>		
11:30-12:30	Plenary Sessions – HCC Tumor Board <i>Moderators: Jeff Geschwind, MD; Riccardo Lencioni, MD</i> <i>Panel: Timothy Pawlik, MD, PhD; Riccardo Lencioni, MD; William Rilling, MD; Robert Lewandowski, MD; Jeffrey F. Geschwind, MD; Ghassan Abou-Alfa, MD; Myron Schwartz, MD</i>		
12:30-13:45	Lunch Symposium: Global Evolution of Techniques and Guidelines for HCC Treatment*		
13:50-14:15	Break with Exhibitors		

*Supported by an educational grant from BTG and Guerbet

SCIENTIFIC PROGRAM

Monday, 12 May 2014 (continued)

Time	General Session — East Ballroom	Time	West Ballroom	Trianon
14:15-15:00	Plenary Sessions - MSK, Pain Palliations <i>Moderators: Matthew Callstrom, MD, PhD; Afshin Gangi, MD</i>			
14:15-14:25	Ablation Techniques and Outcomes in the Spine <i>Afshin Gangi, MD</i>			
14:25-14:35	Ablation, Cement and Hardware in the Pelvis <i>Sean Tutton, MD</i>			
14:35-14:45	SBRT Treatment of Focal Bone Metastases <i>Kenneth Olivier, MD</i>			
14:45-14:55	MSK Ablation — Palliation and Local Control <i>Matthew Callstrom, MD, PhD</i>			
14:55-15:00	Safety and Efficacy of Chemoembolization in Patients with Tumor Arteriovenous Shunting			
15:00-15:30	MSK Tumor Board <i>Moderator: Anil "Nick" Kurup, MD;</i> <i>Panel: Afshin Gangi, MD; Sean Tutton, MD; Kenneth Olivier, MD; Matthew Callstrom, MD, PhD</i>			
15:30-16:00	Break with Exhibitors			
		16:00- 17:30	Scientific Abstracts: Palliative Care and Radioembolization	Hands-on Workshop: Bone, Spine, Soft Tissue, and Palliative Care Therapies <i>Alexis Kelekis, MD, PhD, DO, EBIR; Roger Williams, MD; Ernesto Santos, MD</i>
17:30-18:00	Poster Presentations – America's Hall 1			
18:00-19:00	Reception in Exhibit Hall			

Tuesday, 13 May 2014

Time	General Session — East Ballroom	Time	West Ballroom
8:00-9:30	Workshop: Kidney and Lung Ablation <i>Robert Suh, MD; Jean Palusciare, MD; Thomas Vogl, MD; Christos Georgiades, MD, PhD</i>	8:00-9:30	Scientific Abstracts: Pre-Clinical Research: Ablations and TACE
9:30-10:00	Break with Exhibitors		
10:00-11:00	Plenary Sessions - Molecular Oncology <i>Moderators: Jeffrey F. Geschwind, MD; Riccardo Lencioni, MD, PhD</i>	10:00-13:10	Allied Health Program
10:00-10:10	Oncogenic Pathways and Their Relevance to Interventional Oncology <i>S. Nahum Goldberg, MD</i>		
10:10-10:20	Tumor Hypoxia <i>Bradford Wood, MD</i>		
10:20-10:30	Angiogenesis <i>Julius Chapiro, MD</i>		
10:30-10:40	Glycolysis and Its Importance in Cancer <i>Jeffrey F. Geschwind, MD</i>		
10:40-10:50	Cancer Stem Cells <i>Shanmugasundaram Ganapathy-Kanniappan, PhD</i>		
10:50-11:00	Panel Discussion		



Tuesday, 13 May 2014 (continued)

Time	General Session — East Ballroom	Time	West Ballroom	Trianon
11:00-12:30	Plenary Sessions - Renal <i>Moderators: David Breen, MD; Jeremy Durack, MD</i>	10:00-13:10	Allied Health Program	Hands-on Workshop: Guidance, Targeting, Monitoring, and Assessment <i>Nadine Abi-Jaouden, MD; Afshin Gangi, MD; Juan Camacho, MD; Frederic Deschamps, MD</i>
	11:00-11:12 "Indolent" Renal Neoplasms: The Pathologist's Perspective <i>Victor Reuter, MD</i>			
	11:12-11:24 Renal Mass Surveillance: How Often, What Modality, and Thresholds for Intervention? <i>Daniel Canter, MD</i>			
	11:24-11:36 Cental Renal Masses: Hot, Cold, or Resection? <i>Debra Gervais, MD</i>			
	11:36-11:48 Partial Nephrectomy and Ischemic Injury: What's Happening? <i>Jonathan Coleman, MD</i>			
	11:48-12:00 Best Ablation Modality for RCC: Achieving Outcomes in Equipose with Resection <i>Aaron Fischman, MD</i>			
12:00-12:30 Renal Tumor Board <i>Moderator: Jeremy Durack, MD</i> <i>Panel: Victor Reuter, MD; Daniel Canter, MD; Jonathan Coleman, MD; Aaron Fischman, MD; Debra Gervais, MD; David Breen, MD</i>				
12:30-13:10	Lunch Symposium (Presented by GE Healthcare): <i>3D Applications in the Angio Suite: Gadgets or Must Have? A Case Review</i>			
13:10-13:50	Lunch Symposium (Presented by Covidien): <i>Closing the Gap on Predictable Outcomes</i>			
13:50- 14:15	Break with Exhibitors			
14:15-15:55	Plenary Sessions — Lung <i>Moderators: Constantinos Sofocleous, MD, PhD; Thierry De Baere, MD</i>	14:15-15:55	Workshop: Liver Ablation <i>Laura Crocetti, MD, PhD; Robert Dixon, MD; Alban Denys, MD; Hyunchul Rhim, MD</i>	
	14:15-14:25 Which Patients with Primary Lung Cancer Should Receive Which Resection? <i>Raja Flores, MD</i>			
	14:25-14:35 Which Patients with Primary Lung Cancer Should Receive Which Radiation Therapy? <i>Andreas Rimmer, MD</i>			
	14:35-14:45 Which Patients with Primary Lung Cancer Should Receive Which Abalation? <i>Robert Suh, MD</i>			
	14:45-14:55 Surgery: Is It the Best Option for All Pulmonary Metastases? <i>Robert Downey, MD</i>			
	14:55-15:05 In Which Patients SBRT Can Replace Surgery for Treatment of Pulmonary Metastases? <i>Kenneth Rozenzweig, MD</i>			
	15:05-15:15 Is Ablation a First Line Therapy for Pulmonary Metastases? <i>Thierry De Baere, MD</i>			
	15:15-15:55 Lung Tumor Board <i>Moderator: Costantinas Sofocleous, MD</i> <i>Co-Moderators: Joseph Erinjeri, MD; Kelvin Hong, MD</i> <i>Panel: Giampaolo Carrafiello, MD, PhD; Thierry De Baere, MD; Stephen Solomon, MD; Robert Downey, MD; Kenneth Rozenzweig, MD; Raja Flores, MD; Andreas Rimmer, MD; Robert Suh, MD</i>			
16:00-16:30	Break with Exhibitors			
16:30-18:00	Case of the Week: Live! <i>America's Hall 1</i> This interactive roundtable is the opportunity to explore a case and discuss with colleagues and experts.	16:30-18:00	Scientific Abstracts: Image Guidance and Follow-Up	Hands-on Workshop: RFA, MW, and Cryoablation <i>Muneeb Ahmed, MD; Kelvin Hong, MD</i>
18:00-19:30	Corporate Advisory Council Reception (invitation only) – 44th Floor Executive Lounge			

SCIENTIFIC PROGRAM

Wednesday, 14 May 2014

Time	General Session — East Ballroom	Time	West Ballroom
8:00-9:30	Workshop: Y90 Radioembolization <i>David Boshell, MD; Tobias Jakobs, MD; Hyun S. "Kevin" Kim, MD</i>	8:00-9:30	Scientific Abstracts: Ablation
9:30-10:00	Break with Exhibitors		
10:00-12:30	Plenary Sessions - Liver Mets (mCRC, NET) - (SA-CME Credit Available) <i>Moderators: Hyun S. "Kevin" Kim, MD; Tobias Jakobs, MD</i>		
10:00-10:10	Imaging for mCRC and NET (Diagnosis and LRT Assessment) <i>Alban Denys, MD</i>		
10:10-10:20	Systemic Therapy for mCRC <i>Tanios Bekaii-Saab, MD</i>		
10:20-10:30	Metastectomy for mCRC <i>David H. Geller, MD</i>		
10:30-10:40	Ablation for mCRC <i>Fred Lee, MD</i>		
10:40-10:50	TACE and DEB Therapy for mCRC <i>Thomas J. Vogl, MD</i>		
10:50-11:00	Y90 Therapy for mCRC <i>Tobias Jakobs, MD</i>		
11:00-11:10	Systemic Therapy for NET <i>Tanios Bekaii-Saab, MD</i>		
11:10-11:20	LRT Therapy for NET <i>Ricardo D. Garcia-Monaco, MD, PhD</i>		
11:20-11:30	Systemic and LRT - Future Direction <i>Hyun S. "Kevin" Kim, MD</i>		
11:30-12:30	Liver Mets Tumor Board <i>All Faculty</i> <i>Moderators: Hyun S. "Kevin" Kim, MD; Tobias Jakobs, MD</i> <i>Panel: Tanios Bekaii-Saab, MD; Riccardo D. Garcia-Monaco, MD, PhD; David H. Geller, MD; Fred Lee, MD; Thomas J. Vogl, MD; Alban Denys, MD</i>		



STAY CONNECTED



Follow @WCIO and use hashtag #WCIO2014



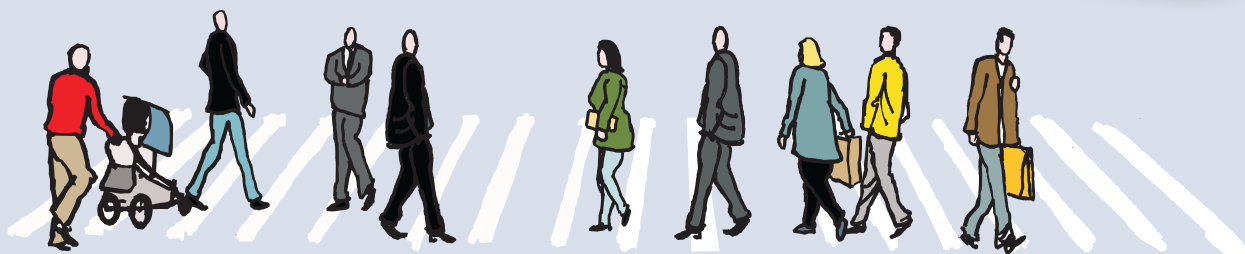
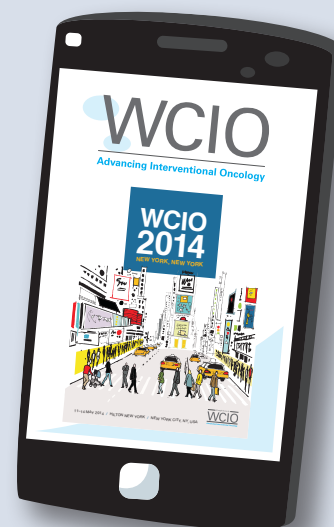
Join the **WCIO: Advancing Interventional Oncology** group to connect with colleagues leading up to the conference

WCIO 2014 Mobile App

We are pleased to once again feature the WCIO 2014 smartphone app, available this spring. Stay up-to-date with the latest information on the conference program, updates, speakers, abstracts, and exhibitor and sponsor details.

Features include the following:

- Sync your personalized schedule with your mobile calendar using "My Schedule" tool
- Quickly view logistics of meeting including times and locations in real time
- Sort by speaker and view all sessions he/she is presenting in one place
- Access the exhibitor listing with an interactive map of the exhibit hall



ALLIED HEALTH PROGRAM

West Ballroom

Monday, 12 May

10:00-10:45	Vena Cava Filters and Venous Access: Potential Nightmares (case discussions) <i>Dave Silva, RA, RT</i>
10:45-11:15	Kyphoplasty: Procedure Overview and Patient Impact <i>Angela Greco, RT</i>
11:15-12:00	Sepsis in the IO Patient <i>Nicole Kowalewski, NP & Deborah Fleischer, NP</i>
12:00-13:00	Y90: Beginnings, Present Practice and Future Directions <i>Ginna Deitrick, MSN, CRNP, AOCNP & Diana Van Houten, MSN, CRNP</i>

Tuesday, 13 May

10:00-10:30	Assessment and Triage of mNet <i>Ginna Deitrick, MSN, CRNP, AOCNP</i>
10:30-11:00	Advance Imaging in the Interventional Radiology Environment <i>Matthew Cestone, RT</i>
11:00-11:45	Malignant Ascites <i>Amy Vatanapradit, NP & Eibhlis Murray, NP</i>
11:45-12:30	IO-Biliary Interventions <i>Piera Robson, NP, CNS</i>
12:30-13:00	Pain Control Procedures in Interventional Oncology: Celiac Plexus Neurolysis <i>Avinash Kambaolakone, MD</i>

15

Get the Latest Interventional Oncology News with

IO Insights



www.IO-Central.org

Brought to you by

WCIO

Advancing Interventional Oncology

AngioDynamics

Booth 401

14 Plaza Drive
Latham, New York 12110 USA
www.angiodynamics.com

Bard Biopsy

1415 West 3rd Street, Suite 109
Tempe, Arizona 85281 USA

Boston Scientific

Booth 108

1 Boston Scientific Place
Natick, MA 01760 USA
www.bostonscientific.com

BTG

Booth 105

115 Hurley Road, Building 3
Oxford, Connecticut 06478 USA
www.biocompatibles.com

CareFusion

Booth 301

75 North Fairway Drive
Vernon Hills, Illinois 60061 USA
www.carefusion.com

CeloNova Biosciences, Inc.

Booth 305

18615 Tuscan Stone, Suite 100
San Antonio, Texas 78258 USA
www.celonova.com

Celsion Corporation

Booth 111

997 Lenox Drive, Suite 100
Lawrenceville, New Jersey 08648 USA
www.celsion.com

Cook Medical

Booth 302

750 Daniels Way
Bloomington, Indiana 47402 USA

Covidien

Booth 104

5920 Longbow Drive
Boulder, Colorado 80301 USA
www.covidien.com

DFINE, Inc.

Booth 502

3047 Orchard Parkway
San Jose, California 95134 USA
www.dfineinc.com

EDDA Technology

Booth 605

5 Independence Way
Princeton, NJ 08540 USA
www.eddatech.com

Endocare, Inc.

Booth 201

9825 Spectrum Drive, Building 3
Austin, Texas 78717 USA
www.heathtronics.com

Galil Medical

Booth 602

4364 Round Lake Road West
Arden Hills, Minnesota 55115 USA
www.galilmedical.com

Guerbet, LLC

Booth 113

120 West 7th Avenue, Suite 108
Bloomington, Indiana USA
www.guerbet-group.com

HS Medical Inc.

Booth 501

4521 North Dixie Highway
Boca Raton, Florida 33431 USA
www.hsmedicalinc.com

Interventional News

Booth 100

526 Fulham Road
Fulham, London, SW6 5NR England
www.interventionalnews.com

Medtronic Spinal

2600 Sofamor Danek Drive
Memphis, Tennessee 38132 USA

Merit Medical, Inc.

Booth 603

1600 West Merit Parkway
South Jordan, UT 84095 USA
www.merit.com

NeuWave Medical Inc.

Booth 601

3529 Anderson Street
Madison, Wisconsin 53704 USA
www.neuwave.com

Onyx Pharmaceuticals/Bayer Healthcare

Booth 103

249 East Grand Avenue
South San Francisco, California 94080 USA
www.onyx.com
www.healthcare.bayer.com

Philips Healthcare

22100 Bothell Everett Highway
Bothell, Washington 98021 USA
www.philips.com

Sirtex Medical Inc.

Booth 403

300 Unicorn Park Drive
Woburn, Massachusetts 01801 USA
www.sirtex.com

The best of WCIO 2014

Buenos Aires, Argentina

BUENOS AIRES

World Conference Interventional Oncology

October 16 | 17 2014

Sheraton Hotel & Convention Center

International Invited Faculty

T. de Baere
*Institut de Cancérologie
Gustave Roussy
Villejuif, France*

J. F. Geschwind
*Johns Hopkins Hospital
Baltimore, Maryland, USA*

R. A. Lencioni
*University of Pisa
Pisa, Italy*

D. Liu
*University of British Columbia
Vancouver, Canada*

G. Narayanan
*University of Miami,
Miller School of Medicine
Miami, Florida, USA*

C. Sofocleous
*Memorial Sloan-Kettering
Cancer Center
New York, New York, USA*

M. C. Soulen
*Hospital of the University
of Pennsylvania
Philadelphia, Pennsylvania, USA*

Topics

- Interventional oncology
- Multidisciplinary approach
- Hepatic tumors:
 - Hepatocarcinoma
 - Cholangiocarcinoma
 - Neuroendocrine tumors
 - Colorectal metastases
- Lung cancer
- Kidney tumors
- Musculoskeletal tumors

Contact

info@wcioargentina.com
Tel/Fax + 54 11 4959-0595
www.wcioargentina.com

Brought to you by

WCIO

Advancing Interventional Oncology



World Conference on Interventional Oncology (WCIO) 2014

May 11-14, 2014, New York, New York

Paper 1: Definitive Locoregional Therapy versus Neoadjuvant Locoregional Therapy and Transplant for Unresectable Very Small Hepatocellular Carcinoma

S. Hunt, T. Bitterman, M. Hoteit, G. Nadolski

Objectives: Unresectable very small HCC (vsHCC, <2cm) can be treated with either definitive locoregional therapy (dLRT) at diagnosis or liver transplant listing (TXP) and delayed neoadjuvant LRT (naLRT) when the tumor demonstrates growth or exceeds 2 cm, as dictated by transplant exception point rules. The current study compares the intention to treat survival of patients with unresectable vsHCC treated with each treatment strategy.

Methods: Retrospective review of patients with vsHCC evaluated in multidisciplinary liver tumor clinic between 2003-11 were examined. Tumor size, time to treatment, severity of liver disease, recurrence and survival from time of detection were reviewed. Sample size was of sufficient power to detect a 10% difference in survival with type I error of 0.05.

Results: Eighty-one patients were evaluated; 19 received dLRT (Group 1) and 62 were treated with TXP and naLRT (Group 2). Results are summarized in Table 1. Median length of follow up was 1235 days. In group 1, all received dLRT (10 TACE, 9 RFA). In Group 2, 34/62(55%) received naLRT (32 TACE, 2 RFA), and 46/62(74%) underwent TXP. Twelve listed patients did not undergo TXP because of tumor progression (2), medical illness (3), or death (7). Four patients were alive on the TXP waiting list at last follow-up. Time from diagnosis to LRT was significantly less in the dLRT group (Table 1). Recurrence rate in patients receiving a transplant was lower than after dLRT (Table 1), however the 4-year intention to treat survival from diagnosis was not different between the two groups (p=0.77).

Conclusions: Despite higher rates of tumor recurrence, the 4-year intention to treat survival of patients with unresectable vsHCC treated with definitive LRT is not significantly different from those patients receiving neoadjuvant LRT and TXP. Continued follow up is needed to compare long-term survival of patients receiving these two treatment strategies.

	Median Age (years)	Male Gender	Calculated MELD at the time of diagnosis	Tumor diameter @ diagnosis (mm)	Tumor diameter @ LRT (mm)	Median time from diagnosis to LRT (days)	Tumor Recurrence	Overall survival @ 4 years (95% CI)
Definitive LRT (Group 1, N=19)	71+/-10	10 (53%)	11.1+/-4	17.1+/-3.4	19.4+/-4.8	74+/-203	9 (47.4%)	66.7% (34.5 - 85.7)
Neoadjuvant LRT and TXP (Group 2, N=62)	59+/-6	49 (79%)	11.7+/-4.4	13.5+/-2.8	22.9+/-8	225+/-184	3 (6.5%)	70.5% (56.7 - 80.70)
p value	<0.01	0.04	0.59	<0.01	0.054	0.02	<0.01	0.77

Paper 2: Repeated Hepatic Resection versus Radiofrequency Ablation for Recurrent Hepatocellular Carcinoma after Hepatic Resection

K. Song, H. Lim, H. Rhim, M. Lee

Objectives: To compare the long-term outcomes between repeated-hepatic resection (rHR) and radiofrequency ablation (RFA) for recurrent hepatocellular carcinoma (HCC) after initial HR for HCC using propensity score matching

Methods: Out of 2387 patients who underwent HR for initial HCC, 40 patients and 185 patients who received rHR and RFA for recurrent HCC were included. A 1:2 rHR group-RFA group matching was done using propensity score matching. The cumulative overall survival (OS) and disease-free survival (DFS) rates were compared before and after matching. Complication rates were also compared between both groups.

Results: Before matching, the OS rates at 1, 3, 5, 8 years were 89.2%, 85.8%, 80.8% and 54.5% for rHR, and 97.8%, 80.1%, 69.5% and 54.3% for RFA. The DFS rates at 1, 3, 5 years were 66.4%, 49.6%, 44.6% for rHR, and 68.1%, 40.1%, 30.5% for RFA. Both OS and DFS were not significantly different (p = 0.643, p = 0.337, respectively). After matching, The OS rates at 1, 3, 5, 8 years were 97.5%, 76.9%, 72.5, and 69.3% in RFA group (n=80). The DFS rates at 1, 3, 5 years were 65.0%, 40.1%, and 36.1%. Both OS and DFS rates were still not significantly different (p = 0.696, p = 0.498, respectively). Post-operative mortality rates were 5.0% in rHR group and 0% in RFA group, respectively.

Conclusions: OS rate was not significantly different between rHR and RFA for patients with recurrent HCC after HR. Although rHR tended to yield better DFS than RFA, it was not significantly different. In clinical practice, resorting to RFA for recurrent HCC after HR can be considered reasonable due to lower procedure-related mortality.

Paper 3: Safety and Efficacy of Chemoembolization in Patients with Tumor Arteriovenous Shunting

Y. Amir, A. Patel, E. Kim, R. Patel, F. Nowakowski, R.A. Lookstein, A. Fischman

Objectives: Primary and secondary hepatic malignancies, particularly hepatocellular carcinoma (HCC), are known to cause arteriovenous shunting. If great enough, such shunting can result in non-target embolization of transarterial therapies, thereby rendering them ineffective and possibly increasing patient morbidity from lung toxicity. The purpose of this study is to examine the safety and efficacy of transarterial chemoembolization (TACE) in patients with proven tumor arteriovenous shunting.

Methods: A retrospective single center review was conducted on 834 patients who had intra-arterial injection of Technitium-99m macroaggregated albumin (Tc99m-MAA) prior to 90Yttrium (Y90) selective internal radiotherapy (SIRT) from February 2004 to August 2013. Excessive pulmonary shunting, as defined by greater than 20% tracer uptake in the pulmonary vasculature on the MAA study, was detected in 30/834 (3.6%) patients. 14/30 (46.7%) had subsequent chemoembolization. 7/14 (50%) patients had target lesions suitable for mRECIST evaluation [1 (14.2%) female and 6 (85.7%) males; mean age: 66.6±15.9 years; all had HCC; pulmonary shunt 41.7±19.3% (range 20.5–71.0)]. Follow-up CT or MR was obtained 1 month post-procedure. Analysis included embolization technique, procedural technical success, adverse events, and tumor response according to mRECIST imaging criteria.

Results: All procedures were technically successful and without intraprocedural complication. 1 (14.2%) patient had a symptomatic hepatic abscess on the 1 month follow-up MRI which required percutaneous drainage. 5 (71.4%) patients were treated with drug-eluting bead TACE (DEB-TACE) and 2 (28.6%) patients were treated with conventional TACE. After chemoembolization, 2/7 (28.5%) patients had stable disease, 3/7 (42.9%) patients had partial response, and 2/7 (28.5%) patients had complete response. No patients had progression of disease.

Conclusions: Transarterial chemoembolization appears safe and effective as a locoregional therapy in patients with significant arteriovenous shunting.

Paper 4: Predicting Survival after TACE: A Systematic Comparison of Available Tumor Response Criteria with a New 3D Quantitative Approach in Patients with HCC

V. Tacher, M. Lin, N. Bhagat, C. Frangakis, H. Yarmohammadi, R. Duran, Z. Wang, R. Chen, J. Chapiro, J. Geschwind

Objectives: Tumor response in patients with hepatocellular carcinoma (HCC) treated by transarterial chemoembolization (TACE) is currently assessed using uni- or bi-dimensional measurement criteria such as Response Evaluation Criteria in Solid Tumor (RECIST), modified RECIST (mRECIST), and European Association for the Study of the Liver (EASL). Previous studies have confirmed the potential of 3D quantitative

methodologies such as volumetric RECIST (vRECIST) and quantitative EASL (qEASL) to assess tumor response. This study was therefore designed to compare the ability of 2D- and 3D methodologies to assess primary tumor response, targeted tumor (TT) response and overall response (OR) from the standpoint of variability, reproducibility and survival predictability after TACE of these five methods at an early endpoint.

Methods: This was a single institution prospective study but the data analysis was done retrospectively. This study included eighty-four patients with unresectable HCC, treated with a first TACE. Primary tumor response, TT response and OR were assessed by three radiologists using pre- and post-TACE contrast-enhanced MRI (CE-MRI). OR was based on the assessment of the primary TT response, non-TT response and the appearance of new lesions. Based on all five assessment methods, the patient cohort was stratified into two groups: responders (R) and non-responders (NR). Survival analysis was performed using the Kaplan-Meier and Cox proportional hazard ratios, by a univariate and a multivariate analysis. Variability and reproducibility of readers' tumor measurements were assessed using the coefficient of variation (COV), and the concordance correlation coefficient (CCC), respectively.

Results: All TACE procedures were technically successful. A total of 131 TT, 32 non-TT and 9 new lesions were evaluated. 114 out of these 128 target lesions were treated during the first TACE session. The mean target tumor length decreased significantly from 6.3 ± 3.7 cm to 6 ± 3.5 cm ($P=.001$), the mean tumor enhancement size decreased significantly from 5.6 ± 3.4 cm to 4.6 ± 3.3 cm ($P<.001$), the mean tumor enhancement area decreased significantly from 30.6 ± 37.7 cm² to 20.4 ± 32.8 cm² ($P<.001$), the mean tumor volume changed from 235 ± 477 cm³ to 224 ± 412 cm³ ($P=.344$), and the mean enhancing tumor volume decreased significantly from 119 ± 250 cm³ to 95 ± 200 cm³ ($P<.001$). The median survival was 15 months [1-125]. Within univariate analysis, mRECIST and qEASL showed a statistically significant ability to classify TACE R and NR for all response measurements ($P<.05$). EASL showed statistical significance only for primary index lesion response and overall survival, and vRECIST showed significance only for overall survival. RECIST did not show any R for all response measurements. Multivariate analysis showed that treatment response based on primary index lesion response, TT response and OR according to mRECIST, EASL and qEASL were reliable independent factors to predict survival ($P<.05$). EASL measurements had higher variability (COV=79% for EASL, and 22% and 39% for mRECIST, and qEASL, respectively, $P<.05$) and lower reproducibility than mRECIST and qEASL (CCC=0.35 for EASL, and 0.93 and 0.92 for mRECIST and qEASL, respectively). **Conclusions:** Both mRECIST and qEASL are capable of predicting patient survival with low variability and high reproducibility in HCC after the first TACE procedure. In addition, qEASL provides a complete 3D-tumor assessment.

Paper 5: Feasibility of Combining Capecitabine and Temozolomide with Yttrium 90 Radioembolization (CapTemY90) for Intermediate-Grade Metastatic Neuroendocrine Tumors

M.C. Soulen, G. Deitrick, D. van Houten, J.I. Mondschein, S. Stavropoulos, B. Giantonio, U. Teitelbaum

Objectives: Grade 2 neuroendocrine tumors (NET) have an intermediate proliferative rate and progress more aggressively than low-grade NETs. The combination of capecitabine and temozolomide (CapTem) has been shown to achieve response rates of 61% in this population. Capecitabine is synergistic with radiation and often used concurrently in other malignancies. We investigated the safety and tolerability of combining CapTem with Y90 radioembolization for progressive Grade 2 NETs with liver-dominant metastases.

Methods: Patients with liver dominant G2 NET were treated with capecitabine 600 mg/m² twice daily for 14 days and temozolomide 150-200 mg/m² in two divided doses on Days 10-14, with 14 days between cycles. Simulation angiography and MAA scan for Y90 planning were performed during the first cycle of chemotherapy. During the second cycle, Y90 radioembolization with resin microspheres was performed to one lobe on Day 7. The other lobe was treated if needed on Day 7 of the 4th cycle. CapTem was continued monthly. Clinical and laboratory toxicities were assessed monthly. Imaging was performed 3 months after the first radioembolization, then every 3 months. This retrospective analysis was IRB approved.

Results: 10 patients with Grade 2 liver-dominant metastases were treated. Primary NETs were pancreatic (5), bronchial (2), rectal (2), and duodenal. 9/10 patients completed the prescribed combination of oral chemotherapy and radioembolization. One heavily pre-treated patient developed Grade 2 hyperbilirubinemia after the first radioembolization and did not have the other lobe treated. One patient stopped CapTem on Cycle 3 for Grade 4 thrombocytopenia. One patient required dose interruption for ITP which responded to steroids. One patient required dose reduction of CapTem for Grade 3 fatigue. Six patients have had 3-month imaging, with 4 PR, 1 SD, and 1 PD.

Conclusions: CapTemY90 is a tolerable regimen with toxicities similar to those reported for CapTem alone. Early responses are encouraging and supports further evaluation in a formal Phase 2 trial.

Paper 6: Left Hepatic Atrophy Following Hepatic Arterial Infusion (HAI) FUDR Chemotherapy: Incidence and Predisposing Factors

H.B. Suchy, A.M. Covey, G.I. Getrajdman, J.P. Erinjeri, M. Silk, R. Do, N. Kemeny, K.T. Brown

Objectives: Patients receiving HAI FUDR chemotherapy via a surgically implanted pump have been noted to develop left hepatic lobar atrophy. This study was undertaken to determine the frequency with which this occurs, and examine clinical/anatomical characteristics that may predispose to this outcome.

Methods: Fifty consecutive patients with HAI pumps placed for FUDR infusion without concomitant hepatic resection in 2010 were identified in a prospectively maintained HAI database. Pre-operative arterial anatomy was assessed on a baseline scan prior to the start of HAI therapy. CT volumetry was performed using this scan and either the most recent scan available, or the scan obtained immediately before hepatic resection for patients rendered resectable. Total liver volume (TLV) was measured and the liver was split to obtain volumes of the right and left hemi-livers. Clinical data was obtained by review of both the HAI database and the electronic medical record. Chi-square test was used to assess difference between patients with and without atrophy.

Results: Left lobar atrophy developed in 10 of the 50 patients evaluated (20%) at a median follow-up of 27.9 months. An accessory left hepatic artery (ALHA) or LHA was ligated in 4 of the 10 patients who subsequently developed left liver atrophy. In the group of 40 patients without atrophy, 4 patients underwent ligation of ALHA or LHA. There was a significantly higher rate of atrophy in the group of patients who had ALHA or LHA ligation compared to patients who did not ($p<0.02$).

Conclusions: One fifth of patients receiving HAI chemotherapy with FUDR from a surgically implanted pump go on to develop left hepatic atrophy and 40% of those patients have had ligation of an ALHA or LHA. This may have implications for patients receiving HAI chemotherapy delivered by ports placed percutaneously, particularly if they undergo coil embolization of a ALHA or LHA in order to redistribute hepatic arterial flow.

Paper 7: Transarterial Embolization for Hepatocellular Carcinoma with and without Extrahepatic Spread

J.N. Leal, M. Gonen, A.M. Covey, G.I. Getrajdman, C.T. Sofocleous, J.P. Erinjeri, R. Thornton, P. Kingham, M. D'Angelica, P.J. Allen, R.P. DeMatteo, Y. Fong, W.R. Jarnagin, K.T. Brown

Objectives: Locoregional therapy is effective treatment for unresectable hepatocellular carcinoma (HCC) but its use in patients with extrahepatic disease is controversial. The current study sought to analyze the use of hepatic artery embolization in patients with advanced HCC with and without extrahepatic spread and to evaluate its impact on disease progression and survival.

Methods: All patients who underwent initial hepatic artery embolization between January 2008 and August 2013 for treatment of HCC were identified from institutional and service specific databases. Patients were categorized into groups based on the presence or absence of extrahepatic disease (EHD) at the time of initial embolization. Clinicopathologic and embolization characteristics were recorded and compared between groups using Chi-square and independent T-tests. Survival and progression were assessed using the Kaplan-Meier method. Univariate and multivariate analysis was completed using logrank test and Cox proportional hazards, respectively.

Results: 224 patients were identified, 37 (16.5%) had radiologic evidence of EHD at presentation compared to 187 (83.4%) who did not. Baseline demographics, target lesion features, and embolization characteristics (type/number) were not different between groups. Overall 75% of patients had disease progression (73.8% in the no EHD group and 81.0% in the EHD group). Time to progression in the liver was shorter than time to progression at extrahepatic sites (6.0 vs. 9.8 months, $p<0.001$). Progression free survival (PFS) was 12.0 +/-2.0 months in patients with EHD compared to 18 +/-1.7 months in those with no EHD, $p=0.018$ (Figure 1). Overall survival (OS) was significantly lower in patients with EHD compared to those with no EHD (13 +/- 4.7 vs. 25 +/- 2.6 months, $p=0.007$) (Figure 2). In patients with EHD at initial presentation, post embolization treatment in the form of repeat local therapy and/or systemic therapy was associated with improved PFS (8 +/- 2.1 vs. 24 +/- 6.92 months, $p=0.009$) and OS (8 +/- 2.65 vs. 24 +/- 7.9 months, $p=0.05$).

Conclusions: In this population of patients undergoing embolization for advanced HCC, the presence of EHD at presentation significantly reduced PFS compared to liver only disease. Similarly, OS was lower in patients with EHD but was comparable to that reported in recent trials of systemic therapy alone. These findings suggest that in patients with EHD multi-modal treatment, including transarterial embolization, is warranted and clinical trials of multimodal therapy in this subgroup are necessary.

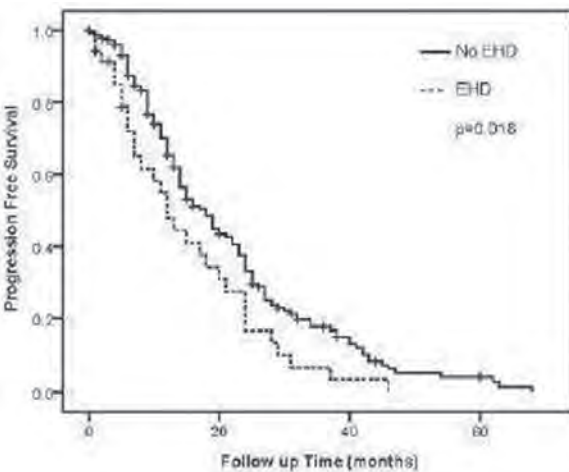


Figure 1: Progression Free Survival in patients with (--- EHD) and without extrahepatic disease (— no EHD) at initial embolization

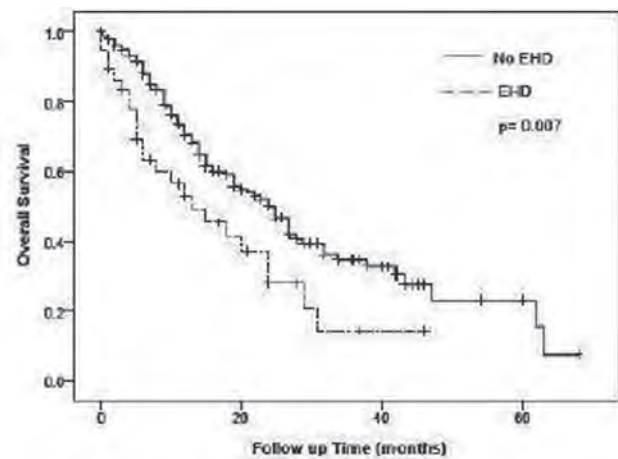


Figure 2: Overall Survival in patients with (--- EHD) and without extrahepatic disease (— no EHD) at initial embolization

Paper 8: Survival Correlation of Pre-treatment Magnetic Resonance Imaging Biomarkers with Tumor Response after Doxorubicin Drug Eluting Beads Trans-arterial Chemoembolization (DEB TACE) in Patients with Unresectable Hepatocellular Carcinoma (HCC)

H.J. Prajapati, J.C. Camacho, H.S. Kim

Objectives: To evaluate survival correlation between pre-treatment MRI biomarkers and imaging tumor response after DEB TACE in patients (pts) with unresectable HCC. **Methods:** Pts with unresectable HCC, who underwent DEB TACE and who had pre and 1-2 months (m) post DEBTACE dynamic contrast-enhanced MRI at our institute, during period of 2006 to 2011, were studied. Pre and post treatment MRI imaging findings of HCCs were investigated. The pts were excluded from the study if MRI features were suggestive of infiltrative-type HCC or who received the liver transplantation after DEB TACE. Modified Response Evaluation Criteria in Solid Tumors (mRECIST) and European Association for Study of the Liver (EASL) imaging response guidelines were used to assess target post DEB TACE response. Median periods between pre-treatment MRI and DEB TACE, and between the DEB TACE and post-treatment assessment MRI were 36.8 and 37.4 days respectively. Median follow up time after 1st DEB TACE was 44.7 months. Portal hypertension (PHT) was defined by dilated collateral veins of portal-systemic pathways with splenomegaly on MRI. Kaplan Meier estimator with log rank test was used to analyze survival. Multivariate analysis (MVA) was performed

with Cox proportional model after including imaging parameters, child Pugh class and BCLC staging.

Results: 105 pts (mean 62.5 years, SD 10.4) had an overall median survival (OS) of 21 m. Child Pugh class A, B and C pts were present in 60%, 33.3 % and 6.7% with OSs of 28.4, 12.9 and 7.4 m accordingly (p=0.0001). BCLC A (13.3%), B (18.1%), C (62.9%) and D (5.7%) stage pts had OSs of 37.1, 28.4, 15.8 and 5.4 m accordingly (p=0.04). OS of pts with hyperintense HCC on T2 weighted images (T2WI), in 76.2%) was 28 m versus (vs) 9 m in pts with isointense HCC on T2WI (p<0.0001). Portal vein thrombosis (PVT) was present in 19% of pts with an OS of 13.4 vs 23.7 m in pts with no PVT (p=0.01). Imaging findings of PHT were present in 65.7% pts with an OS of 16.6 m vs 30.8 m in pts with no PHT (p=0.003). Per mRECIST and EASL criteria, target response rates were 72.4% and 56.1% with corresponding survivals were 28 m and 30.3 m respectively (p<0.0001). The survival correlation of pre-treatment MRI biomarkers and imaging tumor response is shown in table 1. Other MRI features failed to show survival correlation with imaging response. Baseline T2 intensity of HCC and mRECIST target imaging tumor response were significant prognostic indicators of survival on MVA (Tables 2).

Conclusions: Baseline T2 hyperintense HCC, objective hyperenhancement of HCC and absence of MR findings of PHT had significantly higher OS and imaging response according to mRECIST and EASL criteria. Baseline T2 intensity of HCC and mRECIST target imaging tumor response were significant independent determinants of survival by MVA.

Table 1 Survival correlation of pre-treatment MRI biomarkers with tumor response by imaging

MRI biomarkers of HCC	mRECIST		P value	EASL		P value
	Responded OS ^a (m) / (%)	Non responded OS (m) / (%)		Responded OS (m) / (%)	Non responded OS (m) / (%)	
T2 Hyperintense	30 (78.7%)	12.1 (21.3%)	<0.0001	34 (61.3%)	15.9 (38.7%)	<0.0001
T2 Isointense	10.1 (52.2%)	5.4 (47.8%)		10.1 (40%)	8.1 (60%)	
Hyper enhancing	28.4 (84.2%)	7.4 (15.8%)	<0.0001	34 (58.3%)	15.2 (41.7%)	0.001
Hypo enhancing HCC	24.2 (57.1%)	10.5 (42.9%)		28.4 (47.6%)	7.4 (52.4%)	
Portal hypertension present	22.9 (71.1%)	7.4 (28.9%)	<0.0001	27.6 (52.2%)	10.5 (47.8%)	0.001
Portal hypertension absent	37.3 (75%)	12.9 (25%)		40.4 (63.9%)	12.9 (32.1%)	

Table 2 Multivariate analysis

Parameters	P value	Hazard Ratio (HR)	95.0% CI for HR - Lower	95.0% CI for HR - upper
T2imaging of the index lesion 1- Isointense 2-Hyperintense (reference)	0.036	2.1	1.05	4.3
mRECIST target response 0-non responder 1-responder (reference)	0.042	1.9	1.08	4.2
EASL target response 0-non responder 1-responder (reference)	0.06	1.4	0.95	2.8

Paper 9: Bridging Locoregional Therapy Long-Term Survival Trends in Hepatocellular Carcinoma Patients Listed for Liver Transplant Within the Milan Criteria: a 15-year experience

M. Xing, S. Sakaria, R. Dhanasekaran, N. Kokabi, J.C. Camacho, S. Parekh, J. Spivey, H.S. Kim

Objectives: 1. To evaluate the long-term survival benefit of bridging locoregional therapy (LRT) prior to orthotopic liver transplant (OLT) in patients with hepatocellular carcinoma (HCC), within the Milan Criteria and listed for OLT. 2. To evaluate long-term survival benefit of LRT in patients within the Milan Criteria and listed for OLT but did not receive OLT.

Methods: Under IRB approval, our transplant center registry was queried for all HCC patients within the Milan Criteria who were listed for OLT from June 1998 to August 2013. Baseline clinical characteristics, median overall survival (OS) from HCC diagnosis and median OS from OLT were calculated and stratified by LRT and OLT status. Survival analysis was conducted using Kaplan-Meier estimation and log-rank test.

Results: A total of 265 HCC patients were listed for OLT - 205 underwent OLT and 60 did not. Mean follow-up duration from HCC diagnosis was 7.6 years. Of the 205 transplanted patients, 111 received LRT prior to OLT (Group A), and 94 did not receive LRT (Group B). Both groups were similar for age at diagnosis, gender, race, lobar involvement, HCC etiology and mean largest tumor size (p>0.05). Median OS from HCC diagnosis for Groups A and B were 87.3 months and 74.3 months, respectively (p=0.01). Median OS from OLT for Groups A and B were 79.6 months and 64.9 months, respectively (p=0.03). Interval survival rates from HCC diagnosis for Group A vs. B were: 91% vs. 76% (1 year), 85% vs. 65% (2 years), 72% vs. 53% (5 years, p=0.02). Of 60 patients who were listed but did not undergo transplant, 44 received LRT (Group C) and 16 received best supportive care (Group D). Median OS from HCC diagnosis for Groups C and D were 37.1 months and 24.8 months (p=0.03), respec-

tively. Interval survival rates from HCC diagnosis for Group C vs. D were: 48% vs. 31% (1 year), 39% vs. 25% (2 years) and 18% vs. 6% (5 years, $p=0.005$).

Conclusions: Bridging locoregional therapy prior to OLT in patients with HCC within the Milan Criteria demonstrated significantly greater median OS and 5-year survival rates compared to those who did not receive LRT as a bridge to transplantation.



	Group A (LRT; OLT) n=111	Group B (No LRT; OLT) n=94	p-value, Group A vs. B	Group C (LRT; No OLT) n=44	Group D (No LRT; No OLT) n=16	p-value, Group C vs. D
Median Survival from HCC diagnosis (months)	87.3	74.3	$p=0.01$	37.1	24.8	$p=0.03$
Median Survival from OLT (months)	79.6	64.9	$p=0.03$	N/A	N/A	N/A
5-year survival	72%	53%	$p=0.02$	18%	6%	$p=0.005$

Paper 10: Ultrasound-guided Percutaneous Microwave Ablation versus Open Radical Nephrectomy for Small Renal Cell Carcinoma: Intermediate-Term Results

P. Liang, J. Yu

Objectives: To review the intermediate-term (median follow-up between 12 and 24 months) clinical outcomes of microwave ablation (MWA) compared to those after open radical nephrectomy (ORN) in patients with small renal cell carcinoma (RCC) and identify prognostic factors associated with using two techniques

Methods: Our retrospective study was approved by our Institutional Review Board. A total of 163 patients (mean age 56.7±15.9 years, range 6-87 years) with small RCC measuring ≤4 cm were included from April 2006 to March 2012. There were 127 males (mean age 58.6±14.4 years, range 29-87 years) and 36 females (mean age 50.1±19.1 years, range 6-81 years). 65 patients underwent MWA and 98 patients ORN. The survival, recurrence and renal function changes were compared between the two treatments. The effect of changes in key parameters (including overall survival, RCC-related survival and metastasis-free survival) was statistically analyzed by using the log-rank test

Results: Although overall survival after MWA (67.3% at 5 years) was lower than those after ORN (97.8% at 5 years, $p = 0.002$), the RCC-related survival (97.1% at 5 years) was comparable to those following ORN (97.8% at 5 years, $p = 0.78$). The P values were both obtained from the log-rank test for the entire curves. There was one local tumor recurrence 32 months after MWA and none occurred after ORN. The major complication rates was comparable ($p = 0.81$) between two techniques (2.5% in MWA vs 3.1% in ORN). The MWA group needed less operative time ($p < 0.0001$), estimated blood loss ($p < 0.001$), postoperative hospitalization ($p < 0.0001$). The multivariate analysis showed age ($P=0.014$), tumor type ($P=0.003$), postoperative urea nitrogen ($P=0.042$), co-morbid disease ($P=0.005$) and treatment modality ($P<0.001$) may become predictors related to the survival rate

Conclusions: In the intermediate term, ultrasound-guided percutaneous MWA and ORN provide comparable results in oncologic outcomes. MWA appears to be a safe and effective technique for the management of small RCC patients with little loss of renal function

Paper 11: Percutaneous Microwave Ablation of Hepatocellular Carcinoma: Clinical Results with 118 Tumors Treated Over 3 Years

T. Ziemlewicz, J.L. Hinshaw, M.G. Lubner, D.R. Kitchin, C.L. Brace, M. Alexander, P. Agarwal, F.T. Lee

Objectives: Microwave (MW) ablation is a promising technology that offers several advantages over radiofrequency (RF) ablation. However, clinical evaluation of microwave ablation is limited currently. The purpose of this study was to retrospectively review the results in the first 79 patients with hepatocellular carcinoma (HCC) treated with a high-power, gas-cooled MW device at a single center.

Methods: Between December 2010 and November 2013 we treated 118 hepatocellular carcinomas in 85 sessions in 79 BCLC stage A patients via a percutaneous approach utilizing US and/or CT guidance. There were 64 male and 15 female patients with mean age of 60.5 years (range 44-82). All procedures were performed with a high-powered, gas-cooled microwave system (Certus 140, Neuwave Medical, Madison, WI). Complications were recorded according to the Clavien-Dindo classification. Follow-up with contrast-enhanced CT or MR was planned at 1, 3, 6, 12, 18, 24, 30, and 36 months post-procedure.

Results: Tumors ranged in size from 0.5 to 4.2 cm (mean 2.1 cm) and median follow-up was 12 months (range 1-35). All treatments were completed in a single session and considered technically successful with no evidence of residual tumor at immediate post-procedure CECT. Mean power was 73 Watts (range 30-140 Watts) and mean ablation time was 5.1 minutes (range 1-11.5 minutes). Primary treatment effectiveness by imaging was 93.2% (110/118), 93.1% (95/102) for tumors < 3 cm, 100% (14/14) for tumors 3-4 cm, and 50% (1/2) for tumors > 4 cm. Of the 8 tumor progressions, 2 were treated with repeat ablation, 2 were noted at explant pathology, and 4 were treated with intra-arterial therapy as they were abutting an adjacent critical structure, precluding more aggressive ablation, or multifocal HCC had developed in the interval. Distant intrahepatic progression occurred in 20.2% of patients during the follow-up period with 5 patients undergoing repeat ablation and the other 11 developing multifocal disease treated with intra-arterial or systemic therapy. A single Grade II complication occurred (1.2%), a main portal vein thrombus following ablation of a caudate lobe lesion, which was noted at 1-month follow-up and resolved with low dose anti-coagulation (target INR 1.5-2.0). There were no Grade III or higher complications. There was no procedure related mortality. Overall survival is 78.8% with most deaths related to end stage liver disease (n=8) or multifocal HCC (n=5).

Conclusions: Treating hepatocellular carcinoma using percutaneous microwave ablation is safe, and in our experience is as effective with small (<3 cm) tumors, but more effective with larger tumors (excellent efficacy maintained up to 4 cm) as compared to other more established ablation modalities.

Treatment Results by Tumor Size

Size	< 2 cm	2-3 cm	3-4 cm	> 4 cm
Number of type	51	51	14	2
Mean Diameter (range)	1.4 cm (0.5-1.9 cm)	2.4 cm (2.0-2.9 cm)	3.4 cm (3.0-3.9 cm)	4.2 cm (both 4.2 cm)
Treatment Time	4.3 minutes (1-9 minutes)	5.4 minutes (1.5-10 minutes)	5.8 minutes (4-11.5 minutes)	8.8 minutes (7.5-10 minutes)
Maximum Treatment Power	73.6 Watts (35-140 Watts)	73.4 Watts (40-140 Watts)	64.7 Watts (55-95 Watts)	87.5 Watts (80-95 Watts)
Primary Effectiveness	94.1% (48/51)	92.2% (47/51)	100% (14/14)	50% (1/2)
Median Follow-up	11.0 months	12.0 months	15.0 months	26.5 months

Paper 12: Percutaneous Radiofrequency Ablation for Children with Small Lung Metastases

F. Deschamps, T. de Baere

Objectives: Despite percutaneous radiofrequency ablation (RFA) have been proven safe and effective for small lung metastases (LM), thoracotomy remains the gold standard for cancer children.

Methods: We prospectively analyzed all the children referred for RFA of LM in our institute. Indications and feasibility were discussed at multidisciplinary meeting. The goal was to treat all the LM using RFA in order to avoid thoracotomy. All the procedures were performed under general anesthesia by an interventional radiologist under CT guidance. Two procedures were performed if LM were bilateral. The follow-up included a chest CT at 1 month and then, every 3 months. We report the patients' (gender, age, primary tumor and number of previous thoracotomy(ies)) and metastases' characteristics (number, bilateral, size, treatability by RFA), the procedure details (duration, number of LM treated per procedure, complication rate, duration of hospital stay), the rate of complete treatment per LM and the occurrence of new LM.

Results: 11 patients (5 males, 6 females, mean=12 years old, 3.3 to 18) suffering from osteosarcoma (n=7), hepatoblastoma (n=2) and Ewing sarcoma (n=2) were referred for RFA of 38 LM between October 2011 and August 2013. Ten patients had previous surgical resection of LM (mean thoracotomies= 2.4, 0 to 5). The LM were bilateral in 3 patients. The mean diameter was 5 mm (2 to 14). One LM was contraindicated for RFA because it was too close to the hilum and was referred for surgical resection. Thirty-seven LM were successfully treated in 13 procedures (mean LM treated per procedure= 2, 1 to 7). We experienced 6 pneumothorax, including 2 that required chest

tube drainage. We didn't experience any pain or dyspnea. The mean hospital stay was 3 days after the procedure (1 to 8). After a median follow-up of 482 days (28 to 624), the complete treatment was 100% per LM. Seventy-one percent of the patients with osteosarcoma are still in complete remission after a mean follow-up of 443 days (28 to 624).

Conclusions: RFA is a safe and effective alternative to thoracotomy, even in children, and must be taking into account in the management of small, and potentially iterative, lung metastases.

Paper 13: Impact of Location on Local Tumor Control after RFA of Colon Cancer Hepatic Metastases

W. Shady, E.N. Petre, M. Gonen, J.P. Erinjeri, K.T. Brown, W. Alago, L. Brody, R.H. Siegelbaum, J.C. Durack, R. Thornton, M. Maybody, W.R. Jarnagin, M. D'Angelica, S.B. Solomon, N. Kemeny, C.T. Sofocleous

Objectives: To evaluate the association between lesion location and local tumor progression (LTP)-free survival after RFA of colorectal liver metastases (CLM).

Methods: We performed an Institutional Review Board approved retrospective review of a prospectively created and maintained HIPAA compliant clinical ablation database. The study included patients with up to 3 CLM treated with percutaneous RFA for the period between December 2002 and March 2012. We excluded lesions for which ablation margin could not be measured on the 1st post procedural CT. Technique effectiveness was defined as the ablation zone encompassing the target CLM, with no radiological evidence of residual tumor on a dynamic CT 4-8 weeks post RFA. Lesions were classified into 2 categories according to location: "central" (n=57) and "sub-capsular" (within 1 cm of capsule, n=78). The ablative margin, measured using anatomic landmarks on the 1st post RFA CT, was classified into 2 groups: ≤ 5 mm, and > 5 mm. The lesion size was classified into 2 groups: ≤ 3 cm, > 3 cm. Kaplan Meier methodology was used to calculate time to LTP. The following clinical factors were evaluated as predictors of LTP-free survival: age, sex, node positive primary, synchronous liver metastases, prior liver resection, number of liver tumors, lesion size, margin size, and lesion location. Cox-regression model adjusted for effect of clustering was used for uni-variate and multivariate analysis, since some patients had more than one ablated tumor.

Results: We treated 135 lesions in 98 patients; 55 males (56%) and 43 females (44%) with a median age of 59 years, and a median lesion size of 1.8 (range; 0.5-4) cm. The mean lesion size according to location was: 1.7 cm for "central" and 2.1 cm for "sub-capsular" lesions (P=0.001). In 72 patients, RFA was used to treat recurrence after a prior liver resection (73%). Sixty-one patients presented with synchronous liver metastases (62%). Technique effectiveness was documented in 132/135 lesions (98%). The median LTP-free survival for the group was 24 months. The median LTP free survival for "Central" and "Sub-capsular" lesions were 27 and 20 months respectively (P=0.2). On uni-variate analysis; size > 3 cm (P=0.05), margin < 5 mm (P<0.001), node positive primary (P=0.06), and male sex (P=0.05) were predictors of shorter LTP-free survival. On multivariate analysis only size > 3 cm (P=0.03) (HR: 2.3; 95% CI: 1.1-4.9), and margin < 5 mm (P=0.001) (HR: 3.7; 95% CI: 2.0-6.8) were independent predictors of shorter LTP-free survival. Complications were observed in 5 patients: pneumothorax requiring thoracostomy (n=3), biloma (n=1), pulmonary embolus in a heart disease patient (n=1).

Conclusions: Large lesion size and smaller ablation margins, but not lesion location, were predictors of shorter local tumor progression-free survival after radiofrequency ablation of colorectal metastasis.

Paper 14: The Clinical Value of Ultrasound-guided High Intensity Focused Ultrasound Treatment in Advanced Pancreatic Cancer

J. Wang, Q. Wang, W. Ren, R. Xu, T. Li, H. Zhang, D. Fan

Objectives: The surgical resection rate of pancreatic cancer was only 20%, and the 5-years survival rate of these patients was only 5%. In various nonesurgical therapy, The chemotherapy and radiotherapy had not good results. This study was to evaluate the clinical value of ultrasound-guided high intensity focused ultrasound (HIFU) treatment in advanced pancreatic cancer.

Methods: 158 patients with advanced pancreatic cancer whom could not get surgery were treated by HIFU from December 2006 to July 2010. Among them 15 patients were lost follow-up and 4 patients hadn't complete clinical data, 139 patients were included in this study actually. There are 91 males and 48 females, the median age was 52.4 years old. The JC-1 mode HIFU system (Chongqing, China) was used under the ultrasonographic guided and it had got a three dimensional conformal tumour ablation through the three dimensional movements of the therapeutic probe under the computers control. HIFU ablation was mainly intratumour from point ablation to make a linear ablation and to volume ablation which should be overrun the tumour volume. All patients had prone position and got a general anesthesia during the HIFU therapy. The clinical symptom, the serum ca19-9 levels and CECT or CEMRI of these patients in pre-treatment and post-treatment were evaluated closely.

Results: The pancreatic tumor size was 2.0 to 5.7cm and the average tumor size was 3.4cm. The tumor location in pancreatic head were 93 cases and in pancreatic body and tail were 46 cases. The tumour echogenicity were enhanced immediately during HIFU in 122 cases (87.8%), enhanced after HIFU in 6 cases (4.3%) and no enhancement in 11 cases. The 22.7% patients (27/139) got complete response (CR), the 64.0% patients (89/139) got partial response (PR) and the 16.5% patients (23/139) had no responses after HIFU. So the HIFU treatment efficiency in advanced pancreatic cancer was 86.6%. Among the 136 patients with clinical symptom, the pain symptom had got disappeared in 31 patients, the pain had abated in 91 cases and no response in 14 patients after HIFU. The patient survival period was 1 month to 35 month in 139 cases, the median survival period was 11.6 months. The complications occurred in 15 cases including 7 cases with acute gastric mucosal damage, 4 cases with slight abdominal skin burn, 2 cases with gastric ulcer and one gastric perforation. No major complications occurred.

Conclusions: Ultrasound-guided HIFU is a new therapy method in advanced pancreatic cancer. As one of the methods in pancreatic cancer polytherapy, it is a considerably safe and effective and need more clinical studies.

Paper 15: Percutaneous Cryoablation for Stage IV Lung Cancer: A Retrospective Analysis

L. Haibo

Objectives: The aim of this study was to investigate the therapeutic effect of cryoablation treatment and palliative treatment in stage IV lung cancer.

Methods: Fifty-four patients were enrolled into the study. Thirty-one patients received cryoablation treatment (including intra- and extrapulmonary tumors), and 23 patients had palliative treatment (no cryoablation). Both the safety of the procedure and overall survival (OS) for stage IV lung cancer were assessed during a 6.5 year follow-up period. The OS of patients in both groups and the effects of treatment timing and frequency were compared.

Results: The OS in the cryoablation group was significantly longer than in the palliative group (median OS: 14 months vs. 7 months, P = 0.0009). The OS of those who received delayed cryoablation treatment was longer than that observed for those who received timely treatment (median OS: 18.5 months vs. 10 months, P = 0.0485), but this was not observed in those who received palliative treatment (median OS: 7 months vs. 7.5 months, P = 0.9814). Multiple treatments played an important role in improving the OS of patients who received cryoablation treatment (median OS: 18 months vs. 14 months, P = 0.0376).

Conclusions: There was a significant difference between cryoablation and palliative treatment, in terms of OS. In addition, multiple cryoablation treatments may have an advantage over single treatments.

Paper 16: Percutaneous Microwave Ablation of Hepatic Metastases with High-Powered, Gas-Cooled Antennas: An update on a 3 year experience

L. Hinshaw, T. Ziemlewicz, M.G. Lubner, C.L. Brace, M. Alexander, F.T. Lee

Objectives: Oligometastatic disease is a leading indication for thermal ablation. Microwave (MW) ablation offers several advantages over radiofrequency (RF) ablation that make it well suited for this indication including: faster heating, higher (more lethal) tissue temperatures, improved consistency in different tissue types, and potentially larger ablation zone sizes. The purpose of this study was to retrospectively review the results in the first 47 patients with hepatic metastatic disease treated with a high-power, gas-cooled MW device at a single center.

Methods: Between December 2010 and December 2013 we treated 83 hepatic metastases (Primary: 31 colon, 14 carcinoma, 11 melanoma, 8 sarcoma, 4 breast cancer, 3 renal cell carcinoma, 6 neuroendocrine tumor, 2 ovarian cancer and 1 each endometrial cancer, pancreatic cancer, gastrointestinal stromal tumor and squamous cell carcinoma from lung) in 47 patients via a percutaneous approach utilizing US and/or CT guidance. There were 30 male and 17 female patients with mean age of 61 years (range 35-84). All procedures were performed with a high-powered, gas-cooled microwave system (Certus 140, Neuwave Medical, Madison, WI) utilizing 1-3 (average 2.3 \pm 0.7) 17-gauge antennas. Antenna power and ablation time was determined by the performing physician based on lesion size, location, and monitoring findings. Follow-up imaging was performed immediately post-ablation and at 1, 3, 6, 9, and 12, 18, 24, 36 months with contrast-enhanced CT or MRI.

Results: Tumors ranged in size from 0.5 to 6.0 cm (mean 2.2 cm). Mean imaging follow-up was 12.6 months and median imaging follow up was 11.9 months. Mean clinical follow up was 13.8 months. All treatments were considered technically successful with no evidence of residual tumor at immediate post-procedure CECT. Local tumor progression occurred in 9.6% of tumors (8/83), with a rate of 60% (3/5) for lesions > 4 cm, 9.1% for tumors between 3 and 4 cm (1/11) and 5.9% (4/67) for tumors < 3 cm. All but one patient with LTP had either synchronous systemic metastatic disease or other sites of disease already known at the time of the ablation, and thus, only 1 was re-treated (successfully). Two major complications were reported (4.2%): pulmonary embolus two days post-procedure (successfully treated with anticoagulation) and a

pleural effusion within one week of the procedure (requiring thoracentesis x 2). No minor complications other than post-procedural pain were encountered. There were no procedure related mortalities. Four patients have died of progressive metastatic disease giving an overall survival of 91.5%, at a mean f/u of 13.8 months. 34% (16/47) of patients have no evidence of disease with a mean follow up in those patients of 10.2 months. Note that 14.9% (7/47) of patients were treated with palliative intent and had other sites of known disease at the time of the ablation, meaning that 40% (16/40) of patients treated with curative intent remain without evidence of disease. Both intra-hepatic and systemic metastatic disease were common patterns of failure of therapy. Mean power was 75 W (range, 25-140 W) and mean ablation time was 6.3 minutes (range, 1-19 minutes).

Conclusions: A 3 year experience treating hepatic metastases with a high-powered, gas-cooled microwave ablation system shows that MW is safe and effective with local control rates and patient survival that is comparable to, and potentially even slightly better than other ablation modalities. Continued study is warranted to determine efficacy and survival with longer-term follow-up.

Paper 17: Safety of Hydroinfusion in Percutaneous Thermal Ablation of Hepatic Malignancies

A.N. Plotnik, D. Lu, E.Y. Sako, S. Raman, N. Tan, S. Siripongsakun, J.P. McWilliams

Objectives: Hydroinfusion is a commonly used ancillary procedure during percutaneous thermal ablation of the liver, to separate and protect sensitive structures from the ablation zone. However, risks of hydroinfusion have not been systematically studied. The purpose of this study was to systematically examine the frequency and severity of local and systemic complications related to hydroinfusion.

Methods: From January 2009 to April 2012, 410 consecutive patients underwent percutaneous thermal hepatic tumor ablation. 150 patients in the study group underwent hydroinfusion while 260 patients in the control group did not. We reviewed patient charts and imaging studies of both groups to compare the incidence of complications which could potentially be caused by hydroinfusion, including pleural effusion, bowel injury, infection, electrolyte imbalance, and hyperglycemia.

Results: Pleural effusions were found to occur more commonly in the hydroinfusion group (45.3%) than in controls (16.5%). Pleural effusions were significantly larger ($p < 0.001$) and more likely to be symptomatic (6/150 patients; $p = 0.006$) in the hydroinfusion group than in controls (1/260 patients). Multiple patient and tumor characteristics were analyzed for association with development of major hydroinfusion-type complications (requiring therapy or extended/repeat hospitalization). Subcapsular location of tumor was the only variable to reach statistical significance ($p = 0.009$), with all major hydroinfusion-type complications (10/10) occurring in patients with subcapsular tumors.

Conclusions: Hydroinfusion is overall a safe procedure. However, pleural effusions occur commonly after hydroinfusion, tend to be moderate or large in size, and are occasionally symptomatic.

Paper 18: Hepatic Microwave Ablation Adjacent to the Diaphragm: Safety and Efficacy

A. Smolock, T. Ziemlewicz, D. Kitchin, M.G. Lubner, J.L. Hinshaw, C.L. Brace, F.T. Lee

Objectives: Thermal injury to the diaphragm has been reported with radiofrequency (RF) ablation performed at the hepatic dome. Given the larger and hotter ablation zones associated with microwave (MW) ablation, diaphragm injury may be expected to be frequent. Artificial ascites is a thermoprotective measure to minimize diaphragm injury. The objective of our study was to determine the incidence of clinically-relevant diaphragm injuries after MW of peri-diaphragmatic hepatic tumors controlled for placement of artificial ascites.

Methods: This study was IRB-approved and HIPAA compliant. Our clinical MW database was reviewed for ablations within 5 mm of the diaphragm. Because only a subset of our patients received artificial ascites and the ability of injected fluid to achieve separation between the liver and diaphragm was variable, study patients were subdivided in two ways for comparisons with controls: 1) Was artificial ascites used? (Fluid vs. No Fluid) and 2) Was liver separated from diaphragm by fluid? (Displaced vs. Non-Displaced). Study subjects were compared to centrally located controls (Control). Pre- and post-ablation CT or MRI were used to measure anatomic parameters. Pain scores were obtained from the patient EMR.

Results: Differences between groups in tumor size, ablation zone size, ablation time, and ablation power were not statistically significant. There were no cases of diaphragmatic hernia in either control or study groups. Diaphragm thickness, which was used as an additional measure of diaphragm injury, was not statistically significantly different between groups. There was also no statistically significant difference between groups for surrogate markers of diaphragm injury. However, the incidence of shoulder pain trended higher in the study groups. Similarly, local tumor progression was not statistically significantly different between groups although there was a higher rate in the study groups than in the control group. See Tables 1 and 2.

Conclusions: MW of hepatic tumors adjacent to the diaphragm was not associated with diaphragmatic hernias or substantial increases in post-procedure pain. The incidence of shoulder pain and local tumor progression were both slightly higher with peri-diaphragmatic tumors compared to controls, but this difference was not statistically significant.

Table 1

	Non-Displaced	Displaced	Control	
n	30	25	14	
Tumor Size (cm)	2.5+/-1.5	2.6+/-1.2	2.5+/-1	P=0.6
Ablation Zone Size (cm)	4.5+/-1.3	4.1+/-1.2	3.6+/-0.8	P=0.1
# Diaphragmatic Hernia	0	0	0	
Diaphragm Thickness Immediately Post-Ablation (mm)	3.6+/-1.3	4.4+/-2.4	3.1+/-0.5	P=0.3
# Shoulder Pain	5 (16.7%)	5 (20%)	0 (0%)	P=0.2
Mean Pain Score	3.1+/-2.2	2.5+/-1.8	2.4+/-1.2	P=0.4
Local Tumor Progression	2 (6.7%)	1 (4%)	0 (0%)	P=1
Imaging Follow-up (mo)	10.6+/-6.6	11.6+/-9.4	15+/-8	P=0.2

Table 2

	No Fluid	Fluid	Control	
n	18	37	14	
Tumor Size (cm)	2.5+/-1.7	2.6+/-1.3	2.5+/-1	P=0.7
Ablation Zone Size (cm)	4.4+/-1.4	4.3+/-1.2	3.6+/-0.8	P=0.1
# Diaphragmatic Hernia	0	0	0	
Diaphragm Thickness Immediately Post-Ablation (mm)	3.7+/-1.3	4.1+/-2.1	3.1+/-0.5	P=0.5
# Shoulder Pain	3 (16.7%)	7 (18.9%)	0 (0%)	P=0.3
Mean Pain Score	3+/-2.3	2.8+/-2	2.4+/-1.2	P=0.7
Local Tumor Progression	1 (5.6%)	2 (5.4%)	0 (0%)	P=1
Imaging Follow-up (mo)	11.8+/-7.4	10.8+/-8.3	15+/-7.9	P=0.2

Paper 19: Chemical-Shift MRI of Lipiodol Delivery to Liver Tumors following TACE

A.C. Gordon, W. Li, S. Giri, S. Brinckerhoff, X. Zhong, S. Kannengiesser, E. Gonda, R.J. Lewandowski, F. Miller, R. Salem, A.C. Larson

Objectives: To accurately predict outcomes, functional monitoring during transarterial chemoembolization (TACE) should include quantitative measurements of lipiodol delivery to targeted tumor tissues. The objective of this prospective study was to demonstrate the feasibility of using chemical shift fat/water quantification magnetic resonance imaging (MRI) methods to visualize and quantify intrahepatic lipiodol distributions and delivery to liver tumors following TACE.

Methods: Studies were IRB-approved with informed consent obtained from each participant. Two patients with hepatocellular carcinoma (HCC), treated with TACE at our institution, were prospectively evaluated with 1mo follow-up chemical-shift MRI using a six-echo multiple gradient-recalled echo (MGRE) pulse sequence. Scan parameters included: TR=11.5ms, minimum TE=2.4ms, ΔTE=1.5ms, 256x192 matrix, 4mm slice thickness. Each patient also received our institutional standard-of-care follow-up imaging with pre- and post-contrast MRI sequences as well as non-contrast computed tomography (CT) for assessment of lipiodol accumulation after TACE cycles.

Results: Follow-up MRI enabled evaluation of tumor size, perfusion, and lipiodol content during a single study in each patient. At the time of MRI, one patient had received three TACE cycles to three unique treatment sites and the second patient had received one treatment cycle. Lipiodol was readily visualized with chemical-shift MRI in a segment VIII tumor 14mo after treatment with minimal attenuation on CT at 13mo. However, recent (1mo) parenchymal lipiodol accumulation (identified on non-contrast CT; Figure 1, late CT) in this same patient was not identified on MRI for the recently treated IVa tumor; suggesting potentially different sensitivities of these modalities at different follow-up time points. Within chemical-shift MRI images, lipiodol accumulation delineated areas corresponding to necrotic tumor on the post-contrast MR scans. Perfusion and absence of lipiodol signal were clearly correlated. Enhancing regions lacking lipiodol signal were concerning for new cellular burden.

Conclusions: This early work demonstrates the feasibility of using chemical-shift MRI methods to quantitatively visualize lipiodol delivery to liver tumors following TACE. Multiple sequence weightings within a single exam should permit simultaneous quantitative assessments of lipiodol delivery and tumor perfusion with both serving as potential biomarkers for prediction of local response. Future work will be directed towards longitudinal imaging assessments of response and validation of lipiodol quantification biomarkers.

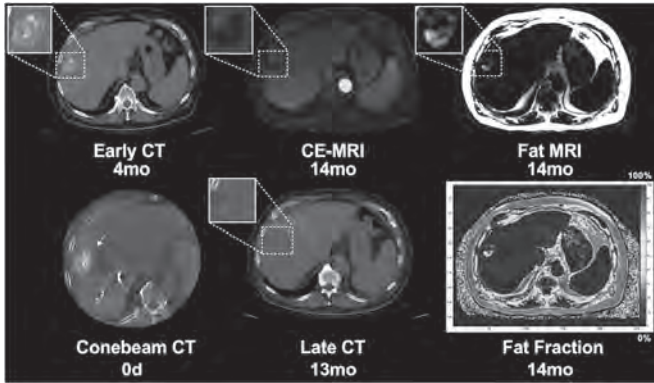


Figure 1. Images from a 73-year-old man with cirrhosis and HCC tumor in segment VIII (arrow) treated with TACE. Conebeam CT confirmed lipiodol delivery on day of treatment (lower left). CT identified lipiodol accumulation in the tumor and surrounding hepatic parenchyma 4mo after treatment. Late CT 13mo after treatment demonstrated markedly less attenuation in the treated segment VIII tumor. Follow-up MRI 1mo later showed persistent necrosis and anterior focal nodular enhancement on contrast-enhanced (CE) MRI that correlated with signal void in the fat image and the calculated fat fraction map.

Paper 20: 3D Quantitative Assessment of Lipiodol Retention on Cone-Beam CT: Can Intraprocedural Imaging Predict Enhancement Reduction on MRI After Chemoembolization in HCC Patients?

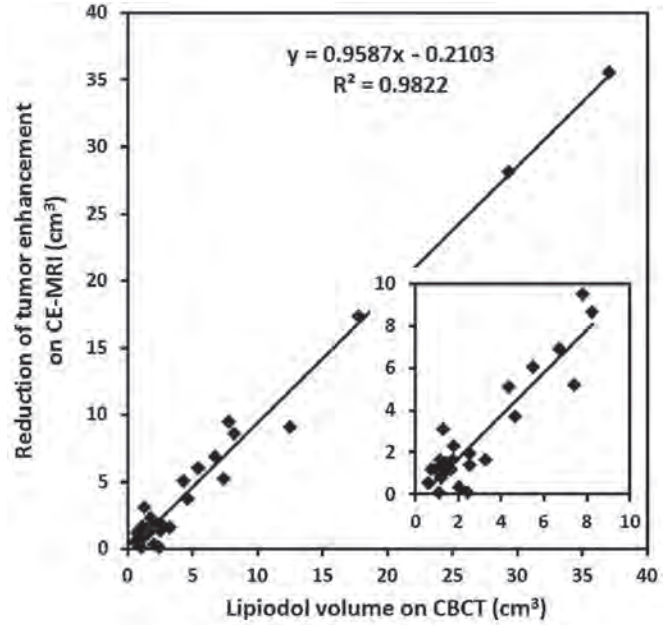
Z. Wang, R. Chen, G. Yenokyan, M. Lin, R. Scherthaner, R. Duran, J. Chapiro, J. Geschwind

Objectives: It is known that Lipiodol deposition after conventional TACE (cTACE) as seen in fluoroscopy or MDCT predicts subsequent short-term (1-month) enhancement decrease on contrast enhanced MRI (CE-MRI). However, until today this has been evaluated using 2-dimensional, post-procedural imaging. Our work evaluates whether 3D quantitative assessment on intraprocedural cone-beam CT (CBCT) of lipiodol retention can predict short-term enhancement reduction on CE-MRI in hepatocellular carcinoma (HCC).

Methods: This retrospective study was approved by the Institutional Review Board. From June 2012 to August 2013, 18 patients with a total of 30 unresectable HCC lesions (15 men, 3 women mean age, 57.4 years±7.0; mean tumor diameter 1.88±0.86 cm) were treated with conventional TACE (cTACE). All 30 target lesions met the inclusion criteria: treated for the first time; visualized well on both CBCT and contrast enhanced MRI (CE-MRI) 1 month after TACE. The tumor volumes were measured on CBCT and CE-MRI using a 3D semi-automatic segmentation software (1). From the 3D tumor segmentation, volumetric assessment of intratumoral lipiodol deposition on CBCT and the regions of decreased enhancement in the same tumor on CE-MRI after 1 month TACE were measured using a 3D enhancement analysis software. This software quantifies the volume of Lipiodol on CBCT as well as regions of decreased enhancement within the tumor volume on CE-MRI (2). The Lipiodol volume in CBCT was compared with the volume of decreased enhancement regions in CE-MRI using linear correlation regression. The statistical test was also applied to compare the percentage of intratumoral Lipiodol deposition in relation to the overall tumor volume on CBCT with the percentage of decreased enhancement in the overall tumor volume on CE-MRI.

Results: The volume of Lipiodol deposition within the tumor on intraprocedural CBCT was strongly correlated with the volume of decreased tumor enhancement on CE-MRI at 1-month after TACE (Linear correlation coefficient: R2=0.982, Figure 1). The percentage of Lipiodol deposition in the tumor on CBCT imaging strongly correlated with the decreased enhancement in the tumor in CE-MRI at 1-month after TACE (Linear correlation coefficient: R2=0.865).

Conclusions: 3D quantitative assessment of Lipiodol retention on CBCT immediately after cTACE can predict short-term (1-month post-TACE) enhancement reduction on CE-MRI in HCC. This may have potential clinical implication to offer immediate feedback during the TACE procedure. References: 1. Lin M, Pellerin O, Bhagat N, et al. Quantitative and volumetric European association for the study of the liver and response evaluation criteria in solid tumors measurements: feasibility of a semiautomated software method to assess tumor response after transcatheter arterial chemoembolization. *J Vasc Interv Radiol.* 2012; 23(12):1629-1637. 2. Wang ZJ, Lin M, Lesage D, et al. 3D volumetric evaluation of Lipiodol retention in HCC after chemoembolization: A quantitative comparison between CBCT and MDCT. *Academic Radiology*, Accepted 2013.



Paper 21: Accuracy of Immediate Post-Procedural PET-CT to Assess the Ablative Margins after PET-Guided Ablations

E. Violari, F. Cornelis, C.T. Sofocleous, J.P. Erinjeri, R.H. Siegelbaum, K.T. Brown, A.M. Covey, L. Brody, A. Aguado, S.B. Solomon

Objectives: To determine the accuracy of immediate post-procedural PET-CT, to predict recurrence after liver ablation.

Methods: This retrospective study was HIPAA compliant. From 2011 to 2013, data of 68 consecutive percutaneous PET-guided ablations (28 radiofrequency, 24 microwave, and 14 irreversible electroporation) of the liver performed on 68 lesions (49 patients), were reviewed. The split-dose technique was used for all patients. Ablations were performed in suite to treat liver metastases of colorectal carcinoma (N=62), pancreas (N=2), breast (N=2), sarcoma (N=1), and melanoma (N=1). Two readers independently assessed the presence of uptake before, at the end of ablation, at 3, 6 and 12 months follow-up. A 3 scale classification was used (none, equivocal, obvious). Descriptive statistics and ROC were used to compare each-time point.

Results: When comparing the immediate post-procedural PET with the 6 months follow-up PET, the area under the curve (AUC) was 0.9142. When comparing the 3 month PET with the 6 month PET the AUC was 0.9730. Compared to 12 months follow-up, AUCs were 0.9167, 0.9333 and 0.9667 for immediate, 3 months and 6 months follow-up. Compared to the 6 and 12 months follow-up, immediate assessment results showed sensitivity, specificity, PPV, NPV and accuracy of 0.96, 0.88, 0.97, 0.91 and 0.94, 0.88, 0.85, 0.96, 0.91 respectively.

Conclusions: Immediate post-procedural PET-CT showed comparative results to subsequent follow-up imaging at 6 and 12 month PET-CT studies.

Paper 22: Dynamic CT and FDG PET/CT findings after Y90 Selective Internal Radiation Therapy (SIRT) of Colon Cancer liver metastases

W. Shady, M. Gonen, N. Pandit-Taskar, R. Do, E.N. Petre, A. Garcia, E. Violari, A.P. Longing, L. Brody, W. Alago, R.H. Siegelbaum, J.P. Erinjeri, S.B. Solomon, A.M. Covey, R. Thornton, M. Maybody, N. Kemeny, J. Carrasquillo, C.T. Sofocleous

Objectives: To evaluate the relationship between change in tumor attenuation using Hounsfield units (HU) on portal venous (PV) phase CT and FDG PET/CT SUVmax after Y90 SIRT using SIR-spheres of unresectable colorectal liver metastases (CLM).

Methods: This is a retrospective review of a prospectively created and maintained HIPAA compliant Y90 SIRT clinical database. This study included patients undergoing SIRT treatment for unresectable CLM; treatment activity was based on the body surface area method. PV phase CT and FDG PET/CT scans were obtained at 1 month prior to treatment (baseline), and at 2-4 months post treatment to evaluate response. We excluded patients if baseline CT and FDG PET/CT scans were within more than 3 weeks of each other. Tumor response on a lesion by lesion basis was defined as: a greater than > 25% decrease in SUVmax (adopted from EORTC criteria), a greater than 15% decrease in tumor attenuation using HU (adopted from Choi's criteria), and a greater than 30% decrease in maximum diameter (adopted from RECIST criteria). The lesion HU was measured using a manual ROI positioned to encompass the lesion. Statistical analysis was performed using generalized estimating equations to adjust for clustering. Using 15% decrease in HU as a cut-off point, the sensitivity and specificity

for predicting response by FDG PET/CT SUVmax was evaluated. Both the percentage change in tumor attenuation and lesion size were correlated with percentage change in SUVmax using Spearman rank correlation.

Results: The study enrolled 24 patients: 16 males (67%) and 8 females (33%), with a median age of 57 years and 50 lesions that were treated between December 2009 and March 2013. Six patients had bilobar disease and underwent SIRT on 2 sessions separated by 4-8 weeks. The baseline mean tumor SUVmax was 9.9 +/- 5.7 and post treatment mean SUVmax 8.5 +/- 6.9 (P=0.001). Using 25% decrease in SUVmax as a threshold for response, 24 lesions (48%) were found as responders; there was no difference in baseline SUVmax between responders and non responders (P=0.1). The baseline mean tumor attenuation was 71 HU +/- 15 HU, and post treatment mean tumor attenuation 63 HU +/- 18 HU (P<0.001). Using a >15% decrease in HU as a threshold for response, 21 lesions (41%) were found as responders; there was no difference in baseline tumor HU between responders and non responders (P=0.9). The sensitivity and specificity of a 15% decrease in HU for predicting response by FDG PET/CT SUVmax was 75% (18/24) and 88% (23/26), respectively. The baseline mean lesion size was 4.0 cm +/- 2.7 cm and post treatment mean lesion size 4.4 cm +/- 3.2 cm (p<0.001). Using > 30% decrease in lesion size as a threshold for response, only 4 lesions (8%) were responders. The percentage change in tumor attenuation correlated significantly with percentage change in SUVmax (P<0.001; r=0.63), while percentage change in lesion size did not (P=0.3; r=0.12).

Conclusions: Percentage change in tumor attenuation using Hounsfield units on PV phase CT correlates with percentage change in FDG PET/CT SUVmax, and can predict response by SUVmax with a sensitivity of 75% and a specificity of 88% after Y90 SIRT of CLM.

Paper 23: Radiofrequency Ablation of Very Early-Stage hepatocellular Carcinoma (2 cm) Inconspicuous on Fusion Imaging with B-mode US: Value of Fusion Imaging with Contrast-enhanced US

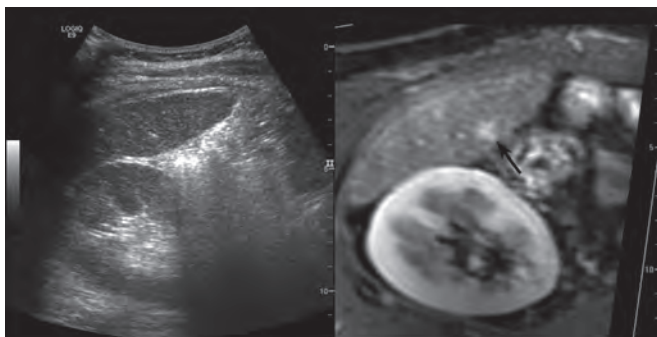
M. Lee, J. Min, H. Rhim, H. Lim

Objectives: To evaluate the value of fusion imaging with contrast-enhanced ultrasonography (CEUS) and CT/MR images for percutaneous radiofrequency ablation (RFA) of very early-stage hepatocellular carcinomas (HCCs) inconspicuous on fusion imaging with B-mode US and CT/MR images.

Methods: This retrospective study was approved by our institutional review board and informed consent was waived. For HCCs (< 2 cm) inconspicuous on fusion imaging with B-mode US, fusion imaging with CEUS using Sonazoid and CT/MR image was performed. We evaluated the number of cases that became conspicuous on fusion imaging with CEUS. Percutaneous RFA was performed under the guidance of fusion imaging with CEUS. Technical success and major complication rates were assessed.

Results: A total of 30 patients with 30 HCCs (mean, 1.2 cm; range, 0.6-1.7 cm) were included. Among 30 HCCs, 24 (80.0%) HCCs became conspicuous on fusion imaging with CEUS. Among them, 22 (73.3%) HCCs were could be treated with RFA. Blind RFA was performed for one HCC inconspicuous on fusion imaging with CEUS. The technical success and major complication rates were 91.3% (21/23) and 4.3% (1/23), respectively.

Conclusions: Fusion imaging with CEUS and CT/MR images is very effective for percutaneous RFA of very early-stage HCCs inconspicuous on fusion imaging with B-mode US and CT/MR images.



After applying the fusion imaging technique, a index tumor is definitely unidentifiable at the corresponding site (black arrow) on the fused MR image. The surrounding liver has heterogeneous echotexture and thus it is unclear whether the lesion is a true index tumor. Therefore, conspicuity score is graded as 4.



On fusion imaging with CEUS using Sonazoid, hypervascular mass (black arrow) is clearly identified on the arterial phase image at the corresponding site (black arrow) of the fused MR image.

Paper 24: Preoperative Evaluation of Gd-EOB-DTPA-Enhanced MR Imaging in Patients Undergoing Percutaneous Transhepatic Portal Embolization

Y. Sato, S. Matsushima, Y. Inaba, H. Yamaura, M. Kato, T. Sano

Objectives: This study aimed to evaluate changes in the hepatobiliary phase of gadoteric acid disodium (GD-EOB-DTPA)-enhanced magnetic resonance (MR) imaging as a preoperative estimation in patients undergoing percutaneous transhepatic portal embolization (PTPE).

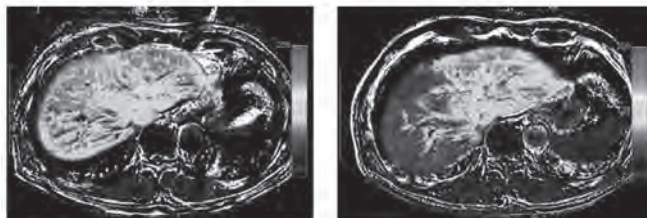
Methods: Between July 2010 and July 2013, twenty-six patients underwent PTPE prior to extended hepatectomy and Gd-EOB-DTPA-enhanced MR imaging before and after PTPE. The patients' characteristics (n = 26) were as follows: mean age (range), 61.6 years (33 - 77 years); sex (male/female), 16/10; liver tumor (metastatic liver tumor/biliary tract tumor/ primary liver tumor), 13/8/5. PTPE was performed under ultrasound guidance via the ipsilateral approach. A mixture of ethanol and iodized oil at a ratio of 5:1 or 10:1 was injected as embolic material with a 5.5-F or 5.2-F balloon catheter. In this study, the relative enhancement of liver parenchyma (RE) as a feature value was calculated (Figure 1a, 1b). Also, according to the previous report (Yamada A, et al. Radiology 2011), the hepatocellular uptake index (HUI) was analyzed. The RE was acquired using two kinds of liver images: pre-contrast enhancement images and hepatobiliary phase images, as follows: RE (%) = [(SIH - SIP) / SIP] x 100. SIH and SIP are the signal intensity in the hepatobiliary phase images of the liver and in the pre-contrast enhanced images of the liver, respectively. The HUI was defined by the following formula: HUI = (SIH - SIS) / SIS. SIS is the signal intensity in the hepatobiliary phase images of the spleen. In the future remnant liver (FRL), the RE, the HUI, the liver volume (VL), and the RE Index (RE x VL) were analyzed before and after PTPE. Also the spleen volume (VS) was evaluated. The indocyanine green clearance (ICG-K) is important index for estimating postoperative liver failure before hepatectomy. The ICG-K of the FRL (ICG-Krem) was calculated as the ratio of the future remnant liver (FRL) volume to the total liver volume. Correlations between ICG-Krem and acquired values on MRI were analyzed as preoperative estimations for hepatectomy.

Results: The RE Index, the HUI, VL, and VS were significantly changed from before PTPE to after PTPE (P < 0.01). However, no statistically significant change was observed in the RE (P = 0.304) (Table 1). The RE Index (r = 0.549, P = 0.004) and VL (r = 0.534, P = 0.005) significantly correlated with ICG-Krem after PTPE. Finally, 19 patients underwent the radical surgery. There was no postoperative mortality.

Conclusions: Heterogeneous uptake liver function in patients who have undergone PTPE could be evaluated by RE imaging on Gd-EOB-DTPA-enhanced MRI as a preoperative estimation.

Figure 1a: RE image before PTPE

Figure 1b: RE image after PTPE



Changes in calculated mean values before and after PTPE

	Before	After	Rate of change (%)	P value
RE	112.5	116.7	3.7	NS
HUI	0.451	0.702	55.7	P < 0.001
VL (L)	0.431	0.583	35.3	P < 0.001
RE Index	49.3	67.5	36.9	P < 0.001
VS (L)	0.126	0.148	17.5	P = 0.001

RE: relative enhancement of future remnant liver, HUI: hepatocellular uptake index of future remnant liver, VL: future remnant liver parenchymal volume, RE Index: RE × VL, VS: spleen volume

Paper 25: MR Apparent Diffusion Coefficient (ADC) at 3 months after Percutaneous Cryoablation for High-Risk Renal Cell Carcinomas (RCC) Predicts Tumor Viability: A Proof of a Concept Study

J.C. Camacho, N. Kokabi, M. Xing, V. Master, J. Pattaras, P.K. Mittal, H.S. Kim

Objectives: To evaluate changes in mean ADC as an imaging biomarker of tumor viability in high-risk RCC treated with percutaneous cryoablation

Methods: IRB approved prospective pilot study of 17 patients with high-risk RCC (Nephrometry score > 8) who underwent percutaneous cryoablation followed by MR imaging at 1-month and in every 3-months intervals after therapy to assess target loco-regional response over a 12-month period. Objective response was defined as no contrast-enhancement within the ablation site. DWI respiration triggered fat-suppressed single-shot echo-planar sequence with tri-directional diffusion gradients was used (b=50, 500 and 1000 s/mm²). Pixel-based ADC maps were generated and mean values were calculated after drawing a ROI at the ablation site. Paired t-test was used to compare different tumor ADC values before and after therapy. Significance levels were set at .05 and data was analyzed using SAS statistical package v9.2

Results: Of the 22 treated high risk RCCs, 7 (31.8%) had viable tumor at 3 months following cryoablation. Mean tumor size was 2.05 cm (0.7-3.9 cm, SD 0.73 cm). Pre-therapy mean overall ADC value was 0.942×10^{-3} mm²/sec while post-therapy (3-month) was 1.386×10^{-3} mm²/sec (p<0.001). With objective responses, mean baseline ADC of lesions was 0.835×10^{-3} mm²/sec; and in those with no objective response, baseline ADC value was 0.946×10^{-3} mm²/sec (p=0.497). When compared to baseline, mean ADC value in lesions evaluated < 45 days was 0.880×10^{-3} mm²/sec (p=0.331). At 3 months, mean post-ablation ADC of lesions with objective response was 1.508×10^{-3} mm²/sec; and in those with no objective response, ADC value was 1.112×10^{-3} mm²/sec (p<0.001). In the objective response group, a mean 89 % change in ADC values (approximately 0.600×10^{-3} mm²/sec) was seen following treatment when compared to a mean 15% change in the non-responder group (approximately 0.150×10^{-3} mm²/sec) (p<0.001)

Conclusions: Changes in ADC value at 3 month following cryotherapy is an objective imaging biomarker to assess tumor viability in high-risk RCC patients.

Paper 26: Intra-Procedure Statistical Analysis and Ablation Zone Segmentation in Low Dose Contrast-Enhanced CT

P. Wu, C.L. Brace

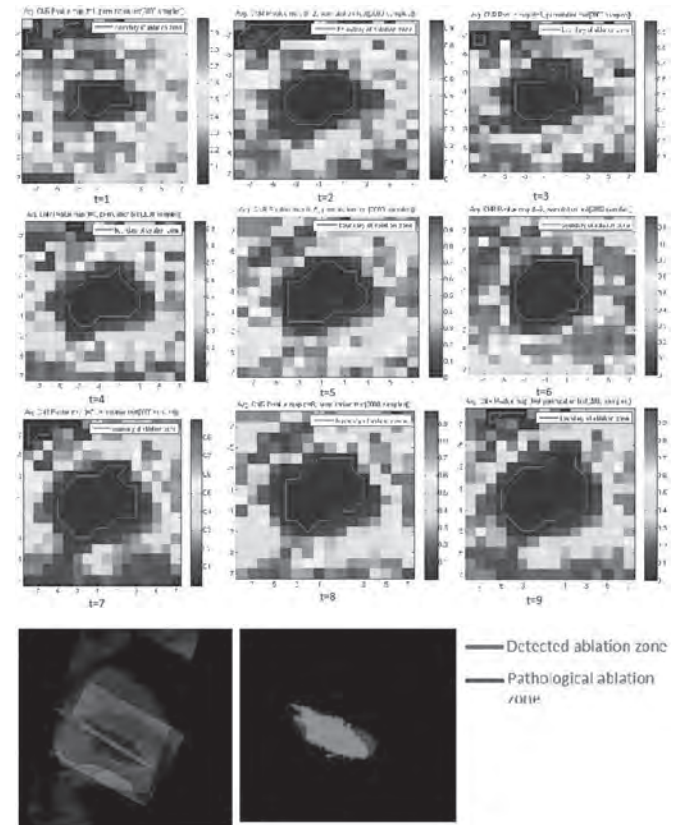
Objectives: Thermal ablation is widely used to treat tumors throughout the body. However, a lack of effective real time monitoring is a hurdle to adoption for new users and may increase the risk for procedural complications. Therefore, several groups are working to improve intraprocedural monitoring techniques during thermal ablation procedures. The objective of this study was to evaluate a statistical permutation test to autosegment the growing ablation zone during microwave ablation.

Methods: A total of 9 microwave ablations were created in the livers of four swine by applying 100W for 10 minutes. Iodinated contrast was delivered continually during ablation (125ml 300mg/ml iohexol, 0.3ml/s). Contrast enhanced CT volumes were acquired serially at one-minute intervals using a low-dose protocol (1.25mm slice thickness, 80kVp, 100mA) throughout each ablation. Serial CT volumes were co-registered to eliminate motion artifacts. Post-processing (HYPR-LR) was applied to each slice to reduce overall image noise. Processed volumes were then analyzed by projecting six slices through the center of the ablation zone, and then downsampling the projected image by a factor of four. The slice was cropped to an ROI centered around and including the ablation zone plus a margin of normal liver. In each sample, CNR was computed between each pixel in the ablation zone and an ROI in the normal enhancing liver. A one-tailed permutation test compared with CNR=0 (no ablation) was performed on corresponding pixels for all the CNR maps to generate a P-value map. P-value pixels below 0.05 were considered ablated. Correlation between autosegmented CT images based on CNR thresholds and manually segmented ablation zones at gross pathology were computed using the jaccard index, a measure of similarity

Results: CNR maps indicated the visibility of the ablation zone and were used to determine the extent of ablation manually, while P-value maps indicated pixels that were statistically different from zero to autosegment the ablation zone. The mean P-value map over all samples is shown in Fig1. P-value maps indicated ablation zone diameters of 10mm at 2 minutes, 15mm at 4 minutes and 24mm at 9 minutes. The final

autosegmented CT image demonstrated overall good correspondence with gross pathology, with a mean Jaccard Index of 0.71. An example result is shown in fig2.

Conclusions: Combining a novel noise reduction algorithm for temporally changing data (HYPR) with autosegmentation by a statistical permutation test allowed visualization of the growing zone even with low-dose CT scanning. Additional refinements in the algorithm may provide a more robust, quasi-realtime CT protocol for ablation monitoring.



Paper 27: Biofunctionalized Hybrid Magnetic/Gold Nanostructures as Catalysts for Photothermal Ablation of Colorectal Liver Metastases: An In Vitro Feasibility Study

S.B. White, Y. Guo, D. Kim, J. Chen, J. Nicolai, A.C. Larson

Objectives: Ablation has become a widely used treatment modality in treating colorectal liver metastases (CRLM). Ablation however is limited by size and location of tumors. Photothermal ablation can circumvent this problem by utilizing photothermal sensitizers to increase ablation zones. The purpose of our study is to demonstrate the feasibility of developing a new MRI-guided photothermal ablation therapy using anti-MG1 conjugated hybrid magnetic/gold nanostructures (HNS).

Methods: Multi-functional HNS coated with anti-MG1 mAb were synthesized and the coupling capacity was determined. In a 24 well plate, 2.5 x 10⁵ CC-531 cells (colorectal liver metastasis cell line) were incubated with the HNS for 24 hrs to allow for selective binding. The cells were then fixed and immunofluorescence was performed. Images were acquired with a laser scanning confocal microscope to validate selective binding. Voxel-wise R2 and R2* measurements were performed on a 7.0 T MRI using phantoms made of HNS at varying concentrations. ICP confirmed iron concentrations and correlations were made with Spearman's correlation. Then, 3 x 10⁴ cells were cultured in a 96 well plate and incubated with HNS. The cells were divided into 3 groups: (1) photothermal ablation (NIR Laser: 808nm, 1 Watt x 3 min), (2) HNS alone (3) those not treated. Intra-procedural temperature measurements were taken using a fiber optic probe. After ablation, the number of viable cells was counted using trypan blue staining and percent viability was determined.

Results: Immunofluorescence demonstrated selective binding of the HNS to CC-531 cellular membranes. MRI studies demonstrated that R2 and R2* measurements were well correlated to HNS concentrations (R2=0.99 for R2 and R2=0.99 for R2*). Temperature curves demonstrated increasing temperatures corresponding to increasing HNS concentration. Photothermal ablation of CC-531 cells demonstrated a change in the viability from 87% to 10%. with increasing HNS concentrations.

Conclusions: Multifunctional HNS have the ability to selectively bind to CRLM cells, be visualized and quantified with MRI and enhance ablation zones.

Paper 28: Pharmacokinetics and Antitumor Efficacy of Chemoembolization Using Novel 40- μ m Irinotecan-Loaded Microspheres (Embozene® TANDEM™) in a Rabbit Liver Tumor Model

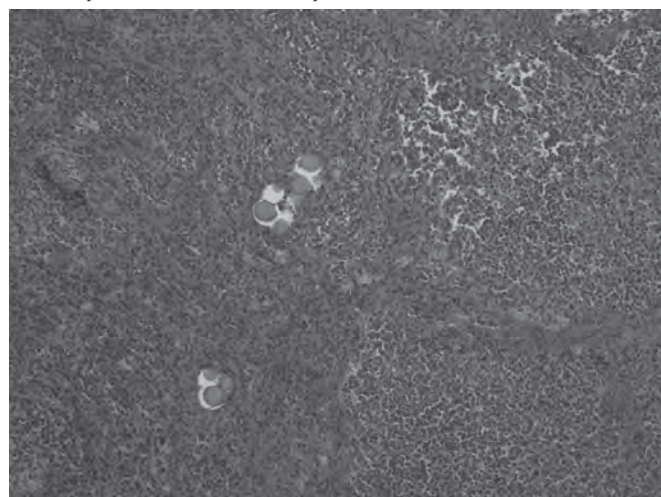
T. Tanaka, H. Nishiofuku, Y. Hukuoka, T. Sato, T. Masada, M. Takano, J. Ren, C.W. Gilbert, J. Bluemmel, S. Reinhardt, L. Sun, M. Schafer, C. Obayashi, K. Kichikawa

Objectives: To evaluate the pharmacological and histological advantages of newly developed 40- μ m irinotecan-loaded drug-eluting microspheres, Embozene® TANDEM™ (TANDEM-IRI).

Methods: 24 rabbits with VX2 liver tumor were divided into 3 groups: Group 1, full-dose (50 mg irinotecan/1 mL TANDEM) loaded / high-dose (1 mg irinotecan/kg) injection; Group 2, full-dose (50 mg/mL) loaded / low-dose (0.5 mg/kg) injection and Group 3, half-dose (25 mg/mL) loaded / low-dose (0.5 mg/kg) injection. TACE was conducted in each group under fluoroscopic guidance. Irinotecan and SN-38 in plasma and tumor were measured within 72 hours via LC-MS/MS. Histological examinations were conducted on days 1, 3 and 7.

Results: The mean administrated doses of irinotecan (mg) and volume of TANDEM (mL) were 3.42 and 0.068 in Group 1, 1.67 and 0.033 in Group 2, and 1.63 and 0.065 in Group 3. The serum irinotecan levels remained near the C MAX from 30 to 180 minutes after TACE; in Group 1, 351.4, 329.0 and 333.5 ng/mL at 30, 60 and 180 minutes, respectively. The AUC 0-24 hours of Group 1 were approximately 2 times higher than those of Group 2 and Group 3. High irinotecan and SN-38 concentrations in tumors (ng/gm tissue) were measured at both 24 hours and 72 hours (Table 1). After TACE, liver enzymes of AST and ALP levels in Group 1 elevated significantly higher than those in Group 2 and Group 3. Histological findings showed 40- μ m microspheres were deeply penetrated into tumors (Figure 1). Significantly higher tumor necrosis ratios in Group 1 (86.6-90.0%) and Group 3 (90.0-100%) were observed when compared with those of Group 2 (63.3-70%) ($P = 0.031$ and 0.016 , respectively).

Conclusions: 40- μ m TANDEM-IRI has the advantages of slow drug release and can achieve high tumor drug concentrations with a high antitumor response. The dose of irinotecan loaded on 40- μ m TANDEM could be reduced while maintaining efficacy, when complete arterial embolization is performed.



Microscopic examination of VX2 liver tumor in group 1, 7 days after chemoembolization (HES, original magnification X100); Coagulative tumor necrosis is predominant in the tissue section. 40- μ m TANDEM Microspheres are present in the small arteries inside of the tumor

Irinotecan and SN-38 concentrations in VX-2 tumor tissue at 24 and 72 hours

	24 hrs	72 hrs
Irinotecan (ng/gm tissue)		
Group 1	2841 \pm 1511	65 \pm 94
Group 2	857 \pm 353	25 \pm 14
Group 3	1049 \pm 835	11 \pm 12
SN-38 (ng/gm tissue)		
Group 1	2758 \pm 1376	266 \pm 230
Group 2	893 \pm 206	117 \pm 60
Group 3	1501 \pm 620	75 \pm 9

Paper 29: Experimental Determination of the Visible ("Ice-Ball") and Lethal Margins During Porcine Kidney Cryoablation

C. Georgiades, M. Lessne, R. Rodriguez

Objectives: Guidelines regarding the coverage of the "ice-ball" beyond the renal tumor for effective cryoablation vary and are unsubstantiated. Our objective was to

determine the distance between the visible "ice-ball" and the lethal temperature isotherm for normal renal tissue during cryoablation.

Methods: The Animal Care/Use Committee approved the study. Nine adult swine were anesthetized and under fluoroscopic guidance (MRI-angio hybrid machine) a catheter was placed in the renal artery. The animals were then transferred in the MRI portion and multiple locations in the kidneys were cryoablated under MR guidance. At the end of cryoablation, with the "ice-ball" at maximum size, frozen and not perfused, we infused the renal artery with intra-arterial stain. This infusion only stained the perfused tissue surrounding the "ice-ball". The probes were thawed and removed, the animals were sacrificed and the kidneys explanted. Under histological examination we determined the distance from the "ice-ball" (stain boundary) to the periphery of the ablated zone (necrotic margin). From each slide, we measured the max, min and an-in-between, distance from the stained to the lethal-tissue boundaries.

Results: 126 measurements of the margin (visible "ice-ball" – lethal margin) from 29 slides were taken. Mean width of the margin was 0.75 ± 0.44 mm. It was found to increase adjacent to large blood vessels (mean maximum 1.15 ± 0.51 mm). No "heat pump" effect was noted within the lethal zone.

Conclusions: Contrary to previously unsubstantiated published reports, which claim 5-10 mm "ice-ball" margin beyond the tumor, a margin of 2 mm seems adequate for effective cryoablation. This, provided that both the tumor and the "ice-ball" are well visualized, otherwise a wider margin may be necessary.

Paper 30: The Role of Heat Transfer in Thrombus Formation in Portal and Hepatic Vein during Thermal Ablations

J. Chiang, B.J. Willey, C.L. Brace

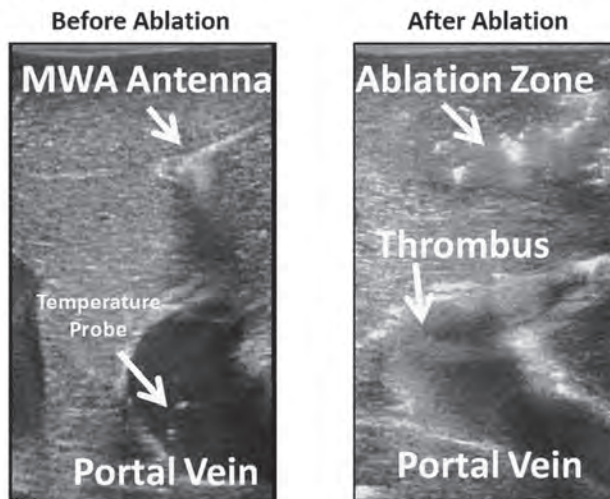
Objectives: Microwave tumor ablation is often cited as being capable of overcoming the heat-sink effect of larger vessels, creating more homogenous ablation zones and decreasing the risk for tumor recurrence when compared to radiofrequency ablation. Previous work has also shown that microwave ablations are capable of thrombosing hepatic vessels, with a particularly high rate in portal veins compared to hepatic veins. In this study, we aimed to investigate the basic mechanisms of heat transfer within blood vessels during microwave ablation in an in-vivo porcine model.

Methods: Microwave antennas were positioned near larger vessels within in-vivo porcine liver lobes ($n=6$). Vessel size, flow velocity and antenna spacing from nearby vessels were measured under ultrasound and Doppler imaging. Fiber-optic temperature probes were inserted into nearby portal and hepatic veins. Microwave ablations were then created (100 W for 5 min) and acute thrombus formation was detected afterwards. Rates of thrombus formation were monitored and compared against the intravascular temperature data.

Results: Thrombus formation was detected in 54.5% (6/11) of portal veins and 0.0% (0/12) of hepatic veins on ultrasound and Doppler imaging. Average vessel size, blood flow velocity and vessel-antenna spacing were equivalent between the targeted portal and hepatic veins. No significant difference in temperature elevation was observed between blood in the lumen of the portal vein and hepatic vein during the ablation period (0.24 ± 0.38 °C versus 0.63 ± 0.91 °C, $p=0.46$), even in the presence of thrombus. Conversely, a temperature measurement of the vessel wall showed temperatures exceeding 100 °C during the ablation period.

Conclusions: This study ruled out the possibility of differences in heat transfer between portal and hepatic veins as a contributory cause toward their different thrombus formation rates. The higher rate of thrombus formation in portal veins was consistent with previous studies and was observed even with near-equivalent energy deposition into both portal and hepatic veins. Further studies in determining the role of thermal damage in thrombus formation are warranted.

Fig 1



Ultrasound imaging revealing placement of MWA antenna next to the portal vein, along with the location of the temperature probe, before an ablation zone is created. The second image shows the presence of a thrombus in the portal vein after the ablation zone is created.

Paper 31: Feasibility of a Potential Strategy for Percutaneous Electrochemotherapy in the Liver: Transarterial Chemoembolisation (TACE) Combined with Irreversible Electroporation (IRE) in an Acute Pig Model

C.M. Sommer, S. Fritz, D. Vollherbst, S. Zelzer, F.M. Wachter, T. Gockner, T. Mokry, A. Schmitz, N. Bellemann, S. Aulmann, U. Stampfl, P.L. Pereira, H.U. Kauczor, J. Werner, B.A. Radeleff

Objectives: To study feasibility of a potential strategy for percutaneous electrochemotherapy in the liver by combining transarterial chemoembolisation (TACE) with irreversible electroporation (IRE) in an acute pig model.

Methods: Eighteen IREs were performed in the livers of six pigs. Five study groups were defined, each consisting of two pigs: Group 1 TACE before IRE, Group 2 TACE only, Group 3 IRE before TACE, Group 4 IRE only and Group 5 as control without any treatment. TACE was performed using a 2.8F microcatheter positioned in the main liver artery. The embolic agents consisted of calibrated microspheres (diameter of $100\pm 25\mu\text{m}$; injected until significant flow reduction) and an iodized oil/doxorubicin emulsion (37.5mg doxorubicin in 4ml iodized oil). All IREs were performed with identical system settings (2 applicators; electric field of 1750V/cm; 90 pulses each with a duration of 90 μs). Contrast-enhanced CT was used to determine size and shape of the electroporation zones applying a specific 3D software prototype (MITK; dkfz Heidelberg, Germany). Sacrifice followed 1 hour after the final intervention. Doxorubicin tissue concentrations were measured applying high performance liquid chromatography for Groups 1, 3 and 4 at the outer rim of the macroscopically visible electroporation zones as well as for Groups 2 and 5 outside of the macroscopically visible electroporation zones. Histopathological analyses were performed (e.g. TUNEL as marker for apoptosis).

Results: Median resulting voltage and amperage during IRE were 2553V/25.2A for Group 1, 2564V/22.4A for Group 3 and 2546V/25.6A for Group 4, respectively. Size and shape of the electroporation zones were not significantly different (e.g. median short axis/sphericity of 18.0mm/1.6 for Group 1, 20.4mm/1.5 for Group 3 and 15.7mm/1.7 for Group 4, respectively). Median doxorubicin tissue concentrations were 196.8ng/g for Group 1, 85.0ng/g for Group 2 and 124.8ng/g for Group 3 without significant differences. For Groups 4 and 5, median doxorubicin tissue concentrations were below the limit of detection. The marker for apoptosis was positive for Groups 1, 3 and 4 for the macroscopically visible electroporation zones as well as for Groups 2 and 5 and for Groups 1, 3 and 4 for the outer rim of the macroscopically visible electroporation zones.

Conclusions: In this acute pig liver study, feasibility of a potential strategy for percutaneous electrochemotherapy by combining TACE with IRE is demonstrated.

Paper 32: Microwave Ablation (MWA) with and without Previous Transarterial Embolization (TAE): Technical Parameters, Extent of Coagulation Including Chebyshev Center Analyses as well as Histopathology

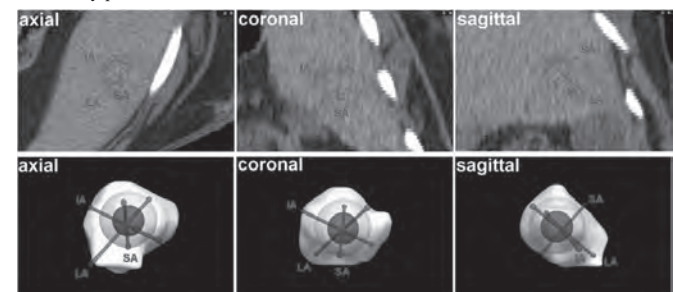
T.L. Gockner, S. Zelzer, T. Mokry, N. Bellemann, C. Mogler, E. Köllensperger, G. Germann, B.A. Radeleff, U. Stampfl, H. Kauczor, P.L. Pereira, C.M. Sommer

Objectives: To evaluate technical parameters, extent of coagulation including chebyshev center analyses as well as histopathology of microwave ablation (MWA) with and without previous transarterial embolization (TAE) in an acute sheep liver model.

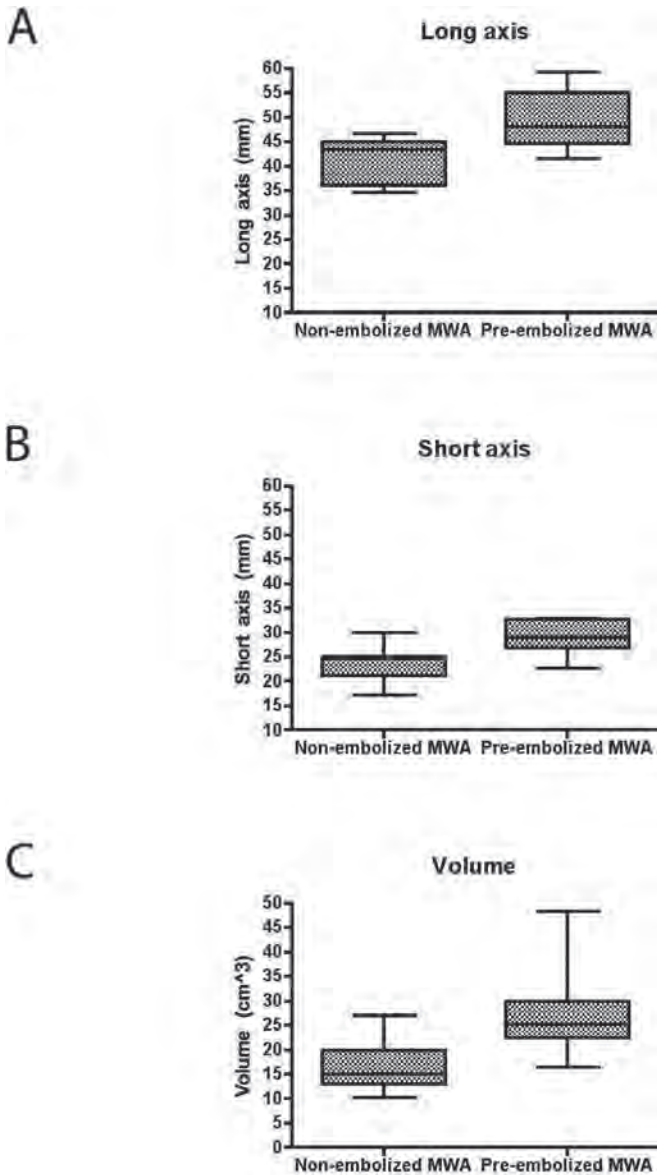
Methods: A total of six merino sheep were divided into two groups. In both groups, three MWA per liver were performed with identical microwave system settings (ablation time preset on 120s and power output preset on 80W). In group I (n=3 sheep), MWA was performed alone. In group II (n=3 sheep), MWA was performed after TAE. Using calibrated 40 μm microspheres, TAE was carried out from a central liver artery position. After contrast-enhanced CT, sheep were killed, and livers harvested. Technical parameters (resulting power output and ablation time) were analyzed. Extent of coagulation (coagulation short axis, volume and circularity as well as largest possible coagulation sphere diameter and barycenter offset) was determined applying a prototype 3D-segmentation software (MITK; German Cancer Research Center (DKFZ), Heidelberg, Germany). This software aligns automatically the largest possible coagulation sphere within the extent of coagulation applying the "Chebyshev center" concept. Barycenter offset is defined as the distance between the center of the largest possible coagulation sphere and the geometrical barycenter of the extent of coagulation. Tissue samples were analyzed regarding irreversible cell death using hematoxylin-eosin and Masson Goldner trichrome stainings.

Results: Resulting power output and ablation time were $78.7\pm 1.0\text{W}$ and $120\pm 0.0\text{s}$ for I as well as $78.4\pm 1.0\text{W}$ and $120\pm 0.0\text{s}$ for II (n.s., respectively). Coagulation short axis was $23.7\pm 3.7\text{mm}$ for I and $29.1\pm 3.4\text{mm}$ for II with significant differences ($p<0.01$). Coagulation volume was $16.5\pm 5.1\text{cm}^3$ for I and $27.1\pm 9.1\text{cm}^3$ for II with significant differences ($p<0.01$). Coagulation circularity was 0.6 ± 0.1 for I and 0.6 ± 0.1 for II (n.s.). Largest possible coagulation sphere diameter was $23.3\pm 2.7\text{mm}$ for I and $27.9\pm 3.1\text{mm}$ for II with significant differences ($p<0.01$). Barycenter offset was $5.0\pm 2.6\text{mm}$ for I and $4.9\pm 2.5\text{mm}$ for II (n.s.). The early signs of irreversible cell death could be demonstrated in both study groups without qualitative differences.

Conclusions: In this acute sheep liver model, MWA with previous TAE results in a larger extent of coagulation compared with MWA alone. Shape of coagulation, technical parameters as well as histopathological signs of cell death are not significantly affected by previous TAE.



CT 3D rendering using MITK (German Cancer Research Center (dkfz), Heidelberg, Germany)



under MRI near the liver tumors. Prussian blue staining confirmed primary microsphere deposition near tumors and no microspheres were seen in the lungs.

Conclusions: Our microspheres enable local delivery of sorafenib to liver tumors in a rabbit VX2 model and with MRI visualization. The developed microspheres can potentially improve sorafenib therapy and be combined with cTACE to improve survival.

Figure 1

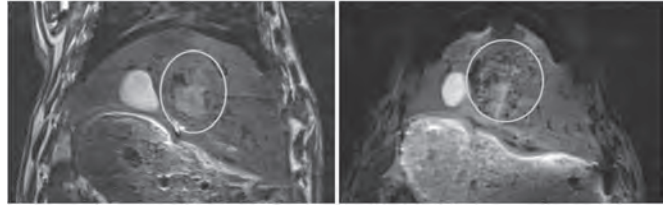


Figure 1: Pre (left)- and post (right)-procedural T2-weighted imaging shows areas of signal loss at the tumor due to the proper delivery of our microspheres.

Paper 34: Transcatheter Intraarterial Delivery of Iron Oxide-Labeled Anaerobes During Bacteriolytic Therapy for Liver Tumors

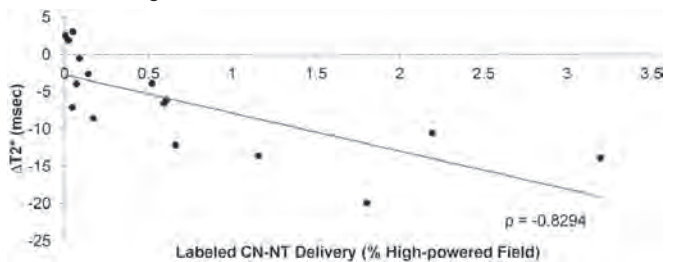
A.Y. Sheu, J. Nicolai, D. Kim, Z. Zhang, K. Khazaie, R.J. Lewandowski, A.C. Larson

Objectives: Bacteriolytic therapy offers potential benefits for the treatment of hypoxic tumors refractory to chemo/radiotherapies; anaerobic bacteria proliferate in hypoxic tissues and destroy tumor cells with degradative enzymes. Intraarterial (IA) infusion may increase selective delivery to hepatic tumors while limiting the potential toxicities associated with intravenous (IV) administration. Imaging anaerobe delivery to hepatic tumors may be critical for patient-specific optimization of procedures. The purpose of this study was to test the hypothesis that superparamagnetic iron oxide (SPIO) nanoparticle labeling permits magnetic resonance imaging (MRI)-based visualization of anaerobe delivery to hepatic tumors following transcatheter IA infusion.

Methods: Clostridium novyi NT (CNNT, nontoxic) anaerobes were incubated with ferumoxytol SPIO nanoparticles. MRI T2* measurements were performed in phantoms containing a range of SPIO-labeled CNNT concentrations uniformly suspended in growth medium. 4 Sprague Dawley rats were each implanted with McA-RH7777 hepatoma x 2. MRI confirmed tumor growth, and T2* measurements were compared pre and 1 day post infusion of 4x10⁶ CNNT via catheter placed in proper hepatic artery. Livers were harvested for histology to confirm labeled CNNT delivery; percentages of high-powered (20x) fields staining for Prussian blue were compared between tumor and normal tissues, and Gram-staining was performed. Correlation coefficient and t-test were used for statistical analyses.

Results: CNNT concentrations were inversely correlated with phantom T2* measurements (r=-0.99). 8/8 tumors grew successfully; tumor diameters were 0.72±0.09cmx0.51±0.10cm (mean±SD). IA CNNT infusions reduced tumor T2* (mean±SD, pre 26.7±3.7ms, post 15.9±5.1ms, p<0.01) between pre and post procedural MRI scans. ΔT2* and Prussian blue staining were greater in tumor than in normal liver (p<0.01). Post procedural ΔT2* measurements were inversely correlated with labeled CNNT delivery (ρ=-0.83, Fig 1). Gram-staining (Fig 2a) confirmed presence of CNNT in regions of Prussian blue staining (Fig 2b).

Conclusions: Transcatheter IA infusion permitted selective delivery of CNNT to hepatic tumors. The intrahepatic distribution of iron oxide labeled CNNT was quantitatively visualized with MRI. Future longitudinal studies will compare therapeutic outcomes following IV and IA administration routes.



Scatterplot depicts relationship between the decrease in T2* measurements and histological measurements of SPIO-labeled CNNT delivery; MR measurements were well-correlated with histological measurements of CNNT distribution in the tissue sections.

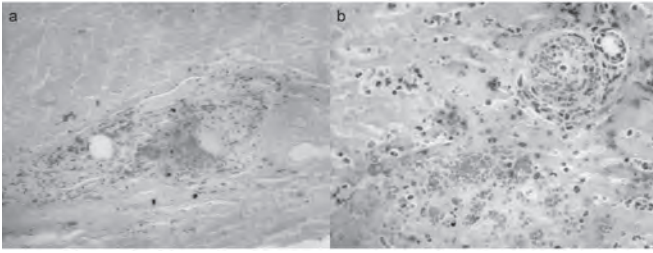
Paper 33: Poly(Lactide-co-Glycolide) Microspheres for Sorafenib Transarterial Chemoembolization: Validation in a Rabbit VX2 Model

J. Chen, S.B. White, K.R. Harris, J.W. Yap, L.D. Shea, A.C. Larson

Objectives: Transarterial chemoembolization (cTACE) is an established treatment for hepatocellular carcinoma (HCC). However, it can lead to an increase in VEGF levels, which is linked to poor patient outcomes. Sorafenib targets VEGF receptors and could modulate the observed increase in VEGF. Additionally, local delivery of sorafenib could increase tumor doses and decrease systemic side effects. Therefore, the purpose of this study is to develop polymer microspheres for sorafenib intra-arterial delivery, while incorporating iron oxide to allow MRI visualization. We also study the microspheres in a rabbit VX2 model.

Methods: Microspheres were fabricated via a double emulsion/solvent evaporation method in which polymer poly(lactide-co-glycolide) encloses sorafenib and iron oxide. Microspheres were characterized for size, loading, release, and MRI properties. Four rabbits were implanted with VX2 tumor fragments under US guidance (Mindray M7). They were catheterized and infused with 50 mgs of microspheres under xray DSA (GE OEC 9800) when the tumors reached ~1 cm in diameter. Pre and post-infusion 7T MRI (Bruker Clinscan) allowed evaluation of microsphere distribution. The rabbits were then sacrificed and the liver, lung, stomach and gallbladder were harvested. Prussian blue staining was performed for biodistribution analyses.

Results: Microspheres had diameters ranging from 2.5 - 63 μm with an average of 17 μm. Loading and release studies indicated that the weight percentage of sorafenib and iron oxide in the microspheres were 8.8% and 0.89%, respectively, and that 21% and 28% of the loaded sorafenib and iron oxide released in 72 hours, respectively. Phantom studies showed decreasing T2 from 111.1 to 33.3 ms with increasing microsphere concentrations from 0 to 5 mg/mL. After infusion, microspheres were depicted



Microscopy. 20× original magnification light microscopy. Gram stain (a) and Prussian blue iron stain (b) demonstrate labeled CNNT in the tumor. Different stains are of corresponding sections.

Paper 35: Dual Energy CT Improves Delineation of Hepatic Microwave Ablation Zones in a Swine Model

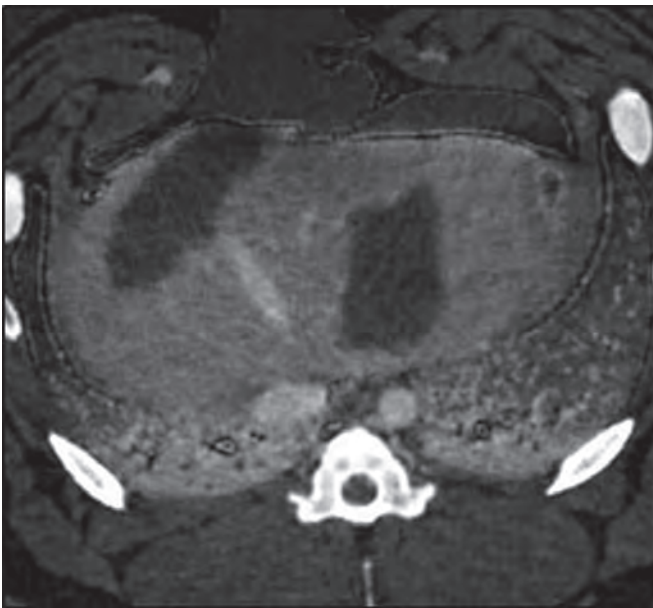
M.G. Lubner, T. Ziemlewicz, L. Hinshaw, F.T. Lee, L. Sampson, C.L. Brace

Objectives: To compare dual energy CT (DECT) to conventional contrast enhanced CT for the depiction/delineation of hepatic microwave ablation zones in a swine model.

Methods: Hepatic microwave ablations (n=21) were performed in 4 swine. Ablation zones were imaged with routine contrast-enhanced CT in the portal venous phase with additional 5 and 10 minute post contrast delayed imaging. DECT acquisition was performed immediately following the routine imaging at approximately 2, 5 and 10 minutes post contrast. Pixel intensity, image noise and contrast to noise ratios (CNR) between ablation zones and background liver were obtained on routine, iodine material and monospectral images at 51, 65, 105 keV and compared between groups using Anova and post-hoc t-tests. Metal artifact reduction (due to metal from ablation applicators) was evaluated comparing signal to noise ratios across groups.

Results: DECT iodine material and 51 keV monospectral images better delineated microwave ablation zones than routine CT with higher CNRs at time points out to 10 minutes post contrast. CNRs measured 5.6, 4.9, 1.1 and 1.3 on iodine material density images and 6.2, 4.9, 3.8, 1.4 on 51 KeV monoenergetic images at 2, 3, 5, and 10 minutes post contrast respectively compared to 2.8, 1.1, and 0.8 on routine contrast enhanced CT at 70 seconds, 5 minutes, and 10 minutes post contrast respectively (p<0.001 for paired comparisons). Metal artifact reduction was optimized between 65-105keV, but at the expense of ablation zone discernibility when compared to conventional CT.

Conclusions: DECT better delineates microwave ablation zones even in low contrast settings at more delayed time points. It can also help reduce ablation applicator-related metal artifact, making it a potentially valuable intra and post procedure monitoring tool.



Two ablation zones seen at the hepatic dome that are well delineated on dual energy iodine material density image.

Paper 36: Y90 Radioembolization Planning with MAA Shunt Study: Shunt Fraction as a Predictor of Overall Survival

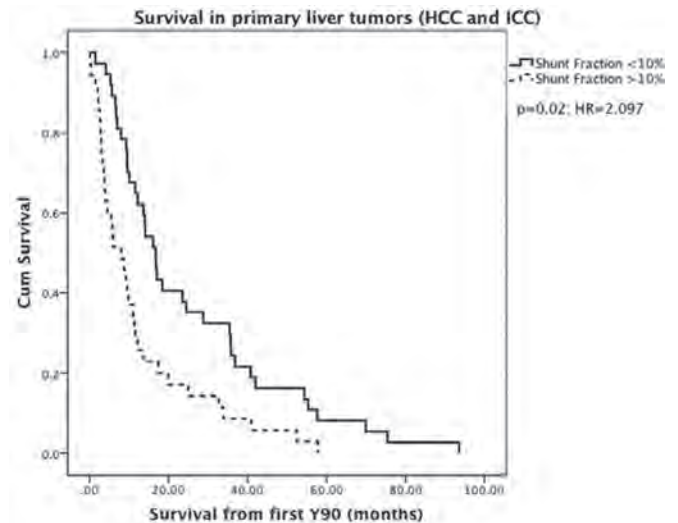
M. Xing, N. Kokabi, J.C. Camacho, D.M. Schuster, J. Galt, R. Williams, H.S. Kim

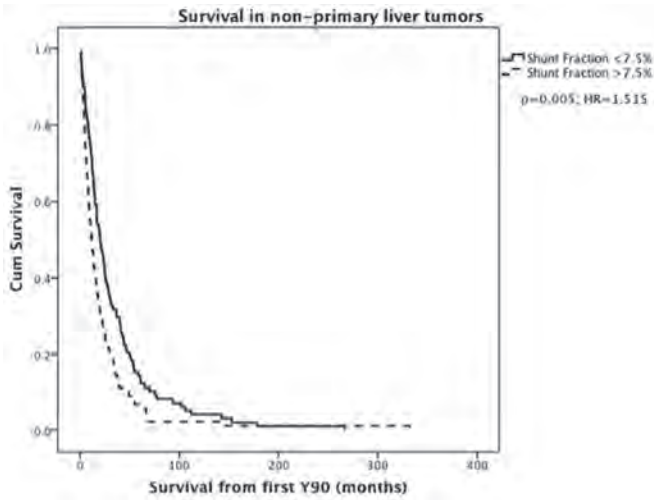
Objectives: To investigate pre-Yttrium-90 (Y90) shunt fraction as a prognostic factor for overall survival (OS) in Y90 (resin/glass) planning 99m-Tc-MAA hepatopulmonary shunt studies for primary (hepatocellular carcinoma, HCC; intrahepatic cholangiocarcinoma, ICC) and metastatic liver tumors.

Methods: A total of 366 consecutive patients with primary and metastatic liver tumors underwent pre-Y90 shunt study. Of these, 223 patients (mean age 59.2 yrs, 65% male) underwent Y90 therapy. MAA (mean activity=3.65 mCi) was administered via the proper hepatic artery. Shunted lung activity was obtained by planar scintigraphy. Mean shunt fraction (SF) values for primary tumors and metastases were compared with overall survival from first Y90 therapy via Kaplan-Meier estimation and log-rank test. Correlation between SF and tumor involvement on baseline cross-sectional imaging were analyzed using Pearson's coefficient (r). Patients with SF>20% were deemed unsuitable for Y90.

Results: The study included 48 (21.5%) colorectal cancer (CRC), 46 (20%) neuroendocrine tumor (NET), 43 (19.2%) HCC, 26 (11.7%) ICC, 23 melanoma (11.2%), 12 (5.4%) breast cancer, and 25 (11.2%) others including lung and pancreatic cancers. Of the 223 patients who received Y90 therapy, SF of <10% and 10-20% were observed in 143 (64.1%) and 80 (35.9%) patients, respectively. Mean SF were: CRC (8.73%), NET (8.58%), HCC (15.36%), cholangiocarcinoma (7.38%), melanoma (7.34%), breast cancer (8.58%) and others (10.25%). HCC mean SF was significantly higher than non-HCC tumors, 15.4 vs. 8.6 (p<0.01). SF≥10% in HCC correlated with poorer survival compared with SF<10% (7.7±3.1 vs. 18.5±3.1 months, p=0.006). Primary tumor (HCC and ICC) mean SF was similar to non-primary tumors, 9.55 vs. 9.0 (p=0.35). SF≥10% in primary liver tumors correlated with poorer survival compared with SF<10% (12.5±2.5 vs. 25.5±3.7 months, p=0.02). Similarly, in metastatic liver tumors, SF≥7.5% correlated with poorer survival compared with SF<7.5% (22.2±4.2 vs. 33.6±4.1 months, p=0.005). No correlation between tumor burden on cross-sectional imaging and SF was observed (r=0.35).

Conclusions: In patients who are candidates for Y90 therapy, higher shunt fraction is a poor prognostic factor for overall survival in primary and metastatic liver tumors.





Paper 37: PRRT-Induced Hepatotoxicity Following Liver-Directed Therapies in NET Patients

M.C. Soulen, B.P. Riff, Y. Yang, D.A. Pryma, B. Bennett, D. Wild, N. Guillaume, U. Teitelbaum, D.C. Metz

Objectives: Treatment of metastatic NETs with peptide receptor radionuclide therapy (PRRT) is effective in retarding tumor growth and abating hormone-related symptoms. Renal dysfunction, anemia and thrombocytopenia are well-described treatment-related toxicities. However, hepatotoxicity secondary to PRRT is not well recognized. We aimed to quantify the risk of hepatotoxicity following PRRT in metastatic NET patients with prior liver-directed therapies.

Methods: With IRB approval, we performed a retrospective cohort study of patients in our NET clinic with metastatic disease to the liver (N = 92). 17/92 (18%) received PRRT in Basel, Switzerland, after radiographic confirmation of disease progression following liver-directed therapies: resection 11/17 (65%), chemoembolization 6/17 (35%), radioembolization 8/17 (47%), and/or ablation 4/17 (24%). Hepatotoxicity was defined according to CTCAE Version 3.0 (total bilirubin > 1.5 ULN, transaminase > 2.5 ULN, or ascites requiring intervention).

Results: On average, each PRRT patient had received 2.5 liver-directed therapies prior to PRRT. PRRT patients were similar to the non-exposed patient population in gender, age and duration of disease. Baseline liver enzymes were similar for ALT (p = 0.32); AST (p = 0.29) and the non-exposed group had a higher bilirubin at baseline (0.93 v. 0.62, p < .001). In the non-exposed group, 23 of 75 patients (31%) had an episode of hepatotoxicity. 16/23 episodes of hepatotoxicity (70%) were acutely related to therapy; 13/16 resolved with 1 liver related mortality post TACE. The remaining 7/23 cases of liver dysfunction were due to progressive disease. In the PRRT group, 10 of 17 patients (59%) had an episode of hepatotoxicity. 8 of these (80%) were temporally related to the PRRT with an average time to event of 3 +/- 1.3 months; 1 patient developed malignant biliary obstruction and 1 developed progressive hepatic tumor burden. Ascites developed in 59% of the PRRT group v. 6.6% in the unexposed group (p < .001). 3 of 17 PRRT patients died of liver failure. The relative risk of hepatotoxicity related to PRRT exposure was 1.94 (95% Confidence Interval [CI]: 1.15-3.28).

Conclusions: Hepatotoxicity following PRRT for is more common and clinically significant than previously reported. This is the first study performed on an American population referred for PRRT therapy. It is possible that our patient population is different (i.e., higher disease burden, increased number of prior liver-directed therapies) from the European patient population because of difficulty in access to and financing of PRRT, exposing them to increased cumulative risk.

Paper 38: Standardized Added Metabolic Activity (SAM) as a Volume Independent Marker of Total Lesion Glycolysis Predicts Treatment Response in Patients with Unresectable Intrahepatic Cholangiocarcinoma (ICC) following Intra-Arterial Yttrium-90 (Y-90) Resin-Based Radioembolization: A Proof of a concept Study

J.C. Camacho, N. Kokabi, M. Xing, A.K. Karagulle-Kendi, J. Galt, D.M. Schuster, H.S. Kim

Objectives: To investigate metabolic measurements of tumor activity by (18) F-FDG PET-CT (total glycolytic activity (TGA), metabolic tumor volume (MTV) and standardized metabolic activity (SAM)) as imaging biomarkers in unresectable Intrahepatic Cholangiocarcinoma (ICC) after resin-based radioembolization therapy (Y-90) refractory to standard chemotherapy.

Methods: IRB approved prospective correlative imaging study in patients with ICC refractory to standard chemotherapy who underwent (18) F-FDG PET-CT before and

after resin-based Y-90 radioembolization. TGA, MVT and normalized SAM (nSAM) were calculated. Restaging imaging was obtained in 3-month intervals until deceased. Target treatment response was assessed through RECIST and mRECIST considering objective response the standard definitions of PR and CR. Relative change (RC) in TGA, MTV and nSAM of all lesions were measured on follow-ups. Correlation between TGA, MTV, SAM and nSAM RC in tumors and anatomical response were evaluated with paired t-test and receiver operator characteristic (ROC) curve ($\alpha=0.05$). (SPSS software v20.0, IBM, Armonk, NY).

Results: 9 consecutive patients were enrolled (56% men, mean age 58). Median overall survival (OS) from Y90 therapy was 14.1 months (95% CI 8.8-31.9 months). Target objective response rate was 6.2% for RECIST and 56.2% for mRECIST. Pre-therapy median TGA was 441.81 SUV/cm³ (range 77.67-1437.23), median MTV was 56.71 cm³ (range 15.1-373.38), and median nSAM was 161.5 (range 22.11-496.17). At 3 months, median TGA was 117.61 SUV/cm³ (range 0-1581.53), median MTV was 24.7 cm³ (range 15.1-373.38) and median nSAM was 24.5 (range 2.27-753.8). No statistically significant difference was found between pre and post therapy TGA or MTV in the responder group (p=0.114 and p=0.291, respectively). However, in lesions with objective response, there was a statistically significant difference between mean pre and post nSAM (179.3 vs. 5.4, p=0.018). According to the ROC curve analysis at 3 months, for an area under the curve of 0.87, a reduction of 60% or more in nSAM predicts anatomical response with 100% sensitivity and specificity.

Conclusions: Relative change in nSAM of >60% at 3-months following radioembolization therapy accurately predicts response in unresectable intrahepatic ICC refractory to standard chemotherapy. Changes in MTV or TGA do not correlate with therapy response.

Paper 39: Experience Palliative Treatment of Painful Bone Metastases with Magnetic Resonance Guided Focused Ultrasound

V. Turkevich, S. Kanaev, A. Mishchenko, D. Chervonenko, V. Savelyeva

Objectives: Bone pain is the primary factor negatively influencing quality of life for any patients with disseminated cancer. Magnetic Resonance guided Focused Ultrasound Surgery (MRgFUS) is an innovative technology combining noninvasive deposition of high intensity focused ultrasound energy into a specified target inside the body, with high resolution Magnetic Resonance Imaging (MRI) guidance and real-time thermal feedback. The ExAblate system is a noninvasive thermal ablation device that has been used for the ablation of tissue. This system combines a focused ultrasound surgery delivery system and a conventional diagnostic 1.5 T MRI scanner (MRgFUS/MR guided focused ultrasound surgery).

Methods: Treatment 35 patients with painful bone metastases was performed using the ExAblate™ MRgFUS system (InSightec, Tirat Carmel, Israel) at N.N.Petrov Research Institute of Oncology, St. Petersburg, Russian Federation. Immediately after procedure patients were examined for any adverse events and after a brief recovery discharged. Patients were followed up on 1 and 3 days, 1 and 2 weeks, 1, 2 and 3 months post treatment. During each visit, treatment safety was evaluated by recording and assessment of device or procedure related adverse events. Effectiveness of palliation was evaluated using the standard pain scale (0-no pain/10-worst pain imaginable) and by monitoring changes in the intake of pain-relieving medications. A reduction of 2 points or more on pain scale was considered a significant response to treatment. Male were 7 patients and 28 female. Mean age was 57 years old (19-79). The primary cancers were: 24 breast, 2 rectums, 2 bronchus, 2 bladders, 5 other. Targeted lesions were 8 osteolytic 27 mixed. 21 were pelvis metastases, 4 were located in the femoral bone, 3 were located in the upper extremity bones and 7 were located in the ribs.

Results: No significant device or procedure related adverse events were recorded. 3 patients died during the follow-up period due to disease progression, thus 3 months follow-up data includes only results of 32 patients. All 32 patients were reported significant improvement in pain with no change in their medication intake. Mean worst pain score at baseline, 1 day, 3 days, 1 week, 2 weeks, 1, 2 and 3 months post-treatment was 6.8, 6.2, 5.2, 3.6, 2.7, 1.9, 1.3 and 1.1 accordingly.

Conclusions: Palliative treatment patients with painful bone metastases performed using the noninvasive ExAblate™ MRgFUS system can provide effective and safe result. The ability to achieve rapid pain relief after only one treatment session, combined with the high safety profile of the procedure implies that MRgFUS has a significant potential for patients suffering from painful bone metastases.

Paper 40: Functional Outcomes After Percutaneous Stabilization of Metastatic Disease of the Acetabulum Using the Musculoskeletal Tumor Society Scoring System

M.P. Hartung, J. Neilson, S.B. White, D. King, S.M. Tutton

Objectives: Patients with painful periacetabular metastases and impending or pathologic fractures have limited palliative treatment options. Medical therapy does not prevent fracture and provides little improvement in mobility. Surgical reconstruction has high rates of complications and delays chemotherapy and radiation for 6 weeks. In a recently published series by Jaiswal et al. of 98 patients treated with surgery, nearly 60% had complications, including 30% infection and 32% re-operation. Through the

collaboration of orthopedic oncology and interventional radiology, we have developed a minimally invasive protocol to prevent or treat pathologic fractures while avoiding complications of major surgery. This approach improves pain and mobility, and allows for immediate postoperative chemotherapy and radiation. We present the results and evaluate functional outcomes using the Musculoskeletal Tumor Society (MSTS) scoring system.

Methods: 12 patients who underwent percutaneous screw fixation and polymethyl methacrylate augmentation for impending or non-displaced fractures of the acetabulum due to metastatic disease were retrospectively reviewed. Procedures were performed between 2011-2013. Adjuvant ablation was performed if indicated. Functional status was evaluated before and after surgery using the MSTS scoring system. The maximum MSTS score of 30 (or 100%) indicates normal function.

Results: 12 patients with a median age of 57 (range 18-75) and 9 primary cancers comprised our cohort. 8 patients presented with pathologic fractures of the acetabulum. Initial technical success rate was 100%, and postoperative infection rate was 0%. 7 patients had conscious sedation, and 5 had general anesthesia. All patients had minimal blood loss. 11 patients were eligible to immediately receive chemotherapy and radiation, and 1 patient was ineligible for 7 days due to delirium. 5 patients were discharged within 24 hours of surgery, with a mean hospital stay of 4 days (range 0 - 13 days). The mean preoperative MSTS functional score was 5.9/30 (20%, range 1-15), which improved to 13.3/30 (44%, range 6-25) after surgery, indicating that patients had achieved 44% of pre-morbid function. The mean MSTS pain scores improved from 0.2/5 (4%, range 0-1) to 1.5/5 (30%, range 1-3) after surgery. All patients were satisfied with the outcomes of surgery and reported improved pain and mobility. Of the six patients who were unable to walk preoperatively, 5 were able to walk with support and 1 without support following surgery. One patient developed a pathologic fracture of the superior pubic ramus after treatment, but remained ambulatory with a walker. No other major complications were reported.

Conclusions: Percutaneous acetabular stabilization improves pain and mobility in patients with painful metastatic disease and limited life expectancy. Our pain and functional outcomes are comparable to or better than those for surgery, with zero documented infections, short hospitalizations, and low complication rates. Postoperatively, patients can immediately receive chemotherapy and radiation. All patients reported improved pain and mobility, achieving 44% of pre-morbid function by the MSTS scoring system. Therefore, patients with painful periacetabular metastases and impending or pathologic fractures should be considered for stabilization through our multidisciplinary approach. The MSTS scoring system is a validated and objective approach to evaluate functional outcomes after surgery, and can be readily applied to patients undergoing minimally invasive pelvic stabilization.

Paper 41: Percutaneous CT-Guided Cryoablation of the Celiac Plexus in the Palliative Treatment of Pancreatic Cancer

K. Mortell, H. Yarmohammadi, M. Brocone, J. Haaga, D. Nakamoto

Objectives: The aim of our prospective study is to evaluate the safety and efficacy of percutaneous CT-guided cryoablation of the celiac plexus in the treatment of abdominal pain caused by pancreatic adenocarcinoma.

Methods: Nine consecutive patients with inoperable metastatic pancreatic adenocarcinoma and epigastric pain were screened and enrolled. All patients reported their daily "worst pain" as at least a "4" on a severity scale of 0 (no pain) to 10 (maximum pain) despite medical therapy. Additional inclusion criteria were that the patients had a baseline ECOG level of 0-3, INR of less than 1.5, an ANC level of at least 1000, and a platelet level of at least 50,000. Exclusion criteria included current use of any other investigational product or therapy, change in chemotherapy or radiation therapy within 14 days of screening, prior surgery within 4 weeks of screening, and prior alcohol neurolysis of the celiac plexus within 4 weeks of screening. Of the 9 patients enrolled, two had failed alcohol neurolysis performed 4-6 weeks prior to cryoablation. Each procedure was performed under CT guidance, without general anesthesia. Using a unilateral right or left paraspinous approach, a 20 gauge Chiba needle was used to instill local anesthesia with 1% Lidocaine directed towards the celiac plexus followed by a 17 gauge Ice Sphere (Galil Medical, Inc.) cryoablation probe under CT guidance. Each patient underwent two 10 minute freeze cycles followed by active thaw sequences. CT images confirmed ice ball formation at the site of the celiac plexus. Evaluation of pain was performed using the Brief Pain Inventory form produced by the Pain Research Group. Patients completed this form 24 hours prior to the cryoablation procedure and again at 24 hour, 1 week, 4 week, 8 week, and 12 week intervals following the procedure.

Results: One patient experienced diarrhea which developed immediately after the cryoablation and resolved spontaneously 3 hours later. No other complications were observed. One patient completed the study follow-up at 12 weeks, 2 patients died after the 4 week follow-up, 5 patients died after the 1 week follow-up, and one patient remains in the study at this time after completing the 1 week follow-up. All deaths were caused by pancreatic cancer. Five of the 9 patients had permanent decrease in or resolution of pain, including one patient who had failed alcohol neurolysis prior to undergoing cryoablation. Two patients had immediate post-procedure pain relief which lasted up to 8 weeks. Two patients did not experience pain relief following cryoablation.

Conclusions: Our study suggests that CT-guided cryoablation of the celiac plexus is a safe and feasible method of treating epigastric pain in pancreatic cancer patients. The localized tissue-destruction by cryoablation may make this modality more effective than alcohol neurolysis in the treatment of pain mediated by the celiac plexus, particularly in cases of extensive local tumor infiltration. In such patients, the infiltrated tissues may not permit alcohol to diffuse around the celiac plexus, thus limiting its effect. Future studies comparing cryoablation and alcohol neurolysis of the celiac plexus are needed.

Poster 1: Selective Internal Radiation Therapy: Quantifying Distal Penetration and Distribution of Resin and Glass Microspheres in a Surrogate Arterial Model

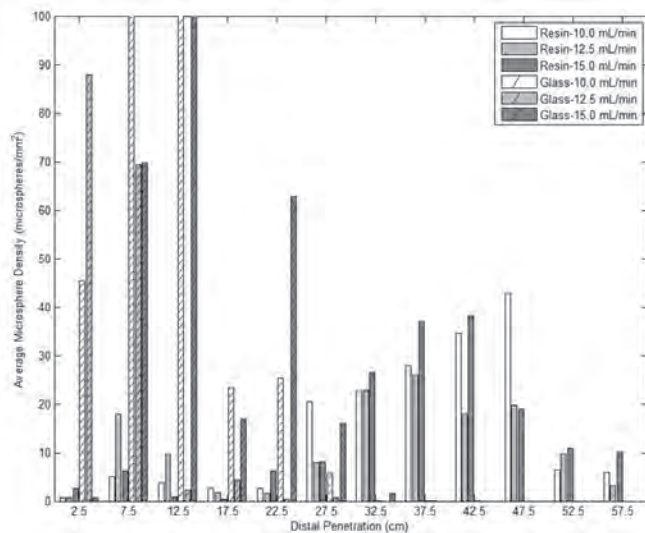
S.R. Jernigan, G. Buckner

Objectives: Selective Internal Radiation Therapy (SIRT) of unresectable liver tumors is performed via intra-arterial injection of Yttrium-90 infused microspheres. SIRT has proven effective in controlling liver tumors and improving patient outcomes as a stand-alone therapy and when used in combination with systemic chemotherapy across several disease states. Both resin and glass microspheres are commercially available, with notable differences in density. This research investigates the effect of microsphere density on distal penetration into a surrogate hepatic arterial system model.

Methods: A surrogate model of human hepatic anatomy was constructed based on 3D CT imaging. This planar model included left and right hepatic, gastroduodenal, and splenic arteries with flow terminating in 16 distal vessels. One distal vessel supplied flow to a planar silicone tumor model sandwiched between two glass plates. The tumor inlet fanned out to 64 tapered channels, each with outlet dimensions of 23.6-28.2 mm x 32.0 μm to approximate human distal vasculature. To simulate hepatic flow, the model was dynamically perfused (134.4 mmHg systolic, 58.0 mmHg diastolic, 60 cycles/min for the nominal case) with water at flow rates of 160, 200, and 240 mL/min (rates within the published range for these vessels). Pressure waveforms and flow rates were regulated using computer-controlled pumps and pinch valves on the distal vessels, providing tumor model flow rates of 10.0, 12.5 and 15.0 mL/min. Bland resin and glass microspheres with physical characteristics approximating those of commercially available products were injected according to manufacturer recommendations using a computer-controlled syringe pump and a delivery catheter positioned distal to the right hepatic artery. Perfusion of the model was maintained for 60 minutes following injection, a digital microscope mounted on a computer-controlled XY stage was used to document microsphere distributions within the tumor model. A total of 254 images were acquired for each of six test cases. Custom image analysis software was used to count microspheres in each image. Microsphere distributions were plotted vs. distance from the tumor model inlet. Averages of these distributions were computed to quantify distal penetration for each case. Paired t-tests were used to compare distal penetration for resin and glass microspheres.

Results: Average penetration depth and distribution of resin microspheres were significantly higher than those of glass microspheres across all test conditions (40.64 ± 9.13 cm vs. 13.19 ± 5.75 cm, p<0.001).

Conclusions: Tests conducted in a surrogate model of human hepatic anatomy demonstrated that the penetration depth and distribution of resin microspheres were significantly higher than those of glass microspheres.



"Microsphere Type"	"Tumor Flow Rate (mL/min)"	"Average Penetration (cm)"	"Standard Deviation (cm)"
Resin	10.0	40.91	8.60
Resin	12.5	39.54	10.43
Resin	15.0	41.48	8.37
Glass	10.0	12.71	5.24
Glass	12.5	8.91	5.71
Glass	15.0	17.94	6.29

Poster 2: Evaluation of Heat Stress Induced Cell Death Mechanisms in Hepatocytes and Hepatocellular Carcinoma

S.M. Thompson, K.A. Butters, M.R. Callstrom, D.A. Woodrum

Objectives: Thermal ablative therapies induce heat stress within hepatocytes and hepatocellular carcinoma (HCC) cells resulting in reversible cell injury and survival or irreversible cell injury and cell death. However, the thermal dose-dependent mechanisms of heat stress-induced cell death are not well understood, particularly at the ablation margin where lower temperatures are achieved or across different biological subtypes of HCC. The objectives of the present study were to investigate the thermal-dose dependent effect of heat stress on hepatocyte and HCC cell death mechanisms *in vitro* and to investigate apoptotic cell death induced by thermal ablation *in vivo*.

Methods: All studies were approved by the Institutional Animal Care and Use Committee. The rat hepatocyte (Clone9), poor prognostic HCC (N1S1) and better prognostic HCC (AS30D) cell lines were heat stressed at temperatures from 37°C to 60°C for 2 or 10 minutes and assessed for viability, cytotoxicity and caspase-3/7 activity at 6 and/or 24 hours post-heat stress (N=3). Similar experiments were repeated with pre-treatment of HCC cells with the RIPK1 inhibitor Necrostatin-1 to block programmed necrosis or necroptosis (N=3). Rats with orthotopic N1S1 HCC tumors stably expressing firefly luciferase underwent pre-ablation MRI, 2D bioluminescence imaging (BLI) and 3D diffuse luminescence tomography (DLIT) to assess tumor size, location and function (N=12). Rats were randomized to US-guided laser ablation (45 seconds at 3 watts for an intentional partial ablation; N=6) or sham (N=6) followed by post-ablation 2D BLI and/or 3D DLIT real-time caspase-3/7 bioluminescence imaging at 6 and 24 hours post-ablation to assess laser-ablation induced apoptosis. Apoptosis-induced luminescence (photons/sec/cm²) was compared between ablation and sham groups. Immunohistochemical staining for cleaved caspase-3 was performed to assess for induction of apoptosis throughout the ablation zone.

Results: Heat stress induced differential effects on both hepatocyte and HCC cell death with induction of apoptosis at lower temperatures (2.0-3.5 fold; greater at 6 than 24 hours) and necrosis at higher temperatures for a given exposure time *in vitro*. Inhibition of RIPK1-mediated necroptotic cell death induced a significant, differential increase in HCC cell viability under physiologic and hyperthermic heat stress (p<0.001). Intentional partial laser ablation induced a significant increase in caspase-3/7 activity in the laser versus sham ablation groups that was elevated at both 6 hours (10.1-fold, p<0.01) and 24 hours (16.7 fold, p<0.02). Immunohistochemical analysis demonstrated increased cleaved caspase-3 staining at the tumor ablation margin in the laser ablation group 24 hours post-ablation but minimal cleaved caspase-3 staining within the untreated tumor.

Conclusions: These data suggest that both regulated and non-regulated cell death mechanism mediate heat stress-induced HCC cell killing and that the regulation of heat stress-induced cell death may vary between hepatocytes and different HCC subtypes. Importantly, apoptosis may be a significant mechanism of regulated cell death at the tumor ablation margin *in vivo*. Further studies examining the molecular basis of heat stress-induced HCC cell death in different HCC subtypes may aid in the development of individualized adjuvant therapeutic strategies to enhance thermal ablation-induced HCC cell killing at lower temperatures, particularly at the ablation margin.

Poster 3: Heat Sink Effect in Microwave Ablation - an Experimental Pig Liver Model

H.J. Raatschen, C. Lutat, F. Wacker, K.I. Ringe

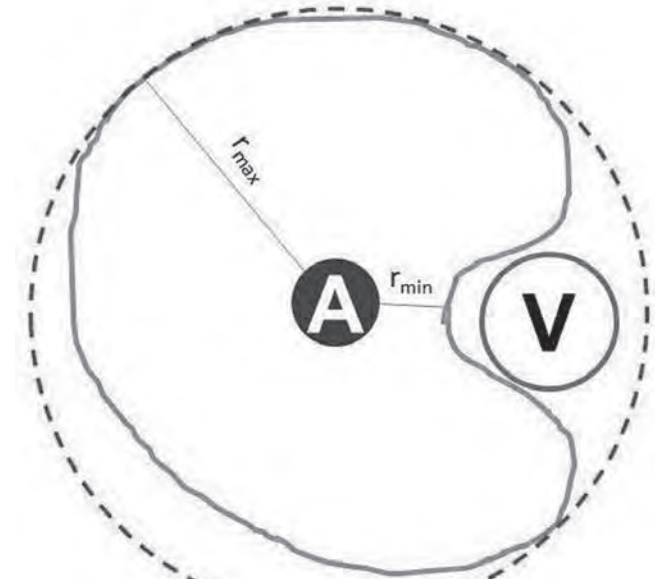
Objectives: To quantify the cooling effects of perfused vessels on lesion size in microwave ablation (MWA) of liver tissue.

Methods: Ex vivo MWA was performed in freshly slaughtered pig livers. Antennas (active tip 37 mm) were inserted parallel to non-perfused and perfused (700 and 1400 ml/min) glass tubes (diameter 10 mm) at different distances (10, 15 and 20 mm). Using dedicated software, different characteristics of the ablation zones (radius, lesion area and idealized lesion area) were analyzed and compared (Kruskal-Wallis Test). In addition, temperature close to the glass tubes was measured continuously throughout the ablation cycle (10 minutes).

Results: Maximum temperature during ablation decreased significantly with increasing flow and distance (p<0.05). Glass tubes without flow had no influence on the geometry of ablation zones, whereas perfused tubes within 15 mm significantly deformed the zone of ablation (p<0.05). Using a flow of 700 ml/min, minimal radius was reduced to 37.2% and 80.1% at 10 and 15mm tube distance, respectively; analogue, lesion area was reduced to 50.5% and 89.7%, respectively. Using a flow of 1400

ml/min, minimal radius was reduced to 33.7% and 58.7% at 10 and 15 mm tube distance, respectively; and lesion area was reduced to 53.8% and 66.8%, respectively.

Conclusions: A heat sink effect enhancing with increasing flow is present in MWA within 15mm distance to simulated hepatic vessels. This results in significant changes in geometry of the ablation zone and has to be taken into account when ablating lesions close to vessels.



Ablation zone characteristics analyzed in ex vivo micro wave ablation of pig

liver: The green area denotes the measured ablation zone, the red dashed line indicates the idealized, circular ablation zone based on the maximum radius (r_{max}) of the measured ablation zone. "A" denotes the position of the microwave antenna; "V" indicates the artificial vessel, perfused at 0 - 1400 ml/minute; r_{min} is the shortest radius from the antenna position to the lesion rim.

Poster 4: Efficacy & Safety of Percutaneous Cryoablation for Stage 1A and 1B Renal Cell Carcinoma: 5-year Follow Up

C. Georgiades, M. Lessne, R. Rodriguez

Objectives: Percutaneous cryoablation is rapidly becoming a curative option for stage 1 renal cell carcinoma (RCC), however 5-year, prospective data are lacking. We present the 5-year oncologic outcomes of such a prospective trial.

Methods: From 2006-2012 we treated a total of 265 patients with CT-guided, percutaneous cryoablation for solid renal masses up to 7 cm. Of these, 134 patients had biopsy proven RCC and were included in the study. Technical objective was for the "ice-ball" to cover the lesion plus a 5 mm margin. Efficacy was defined as the lack of enhancement and/or enlargement of a previously enhancing lesion, on follow up imaging. Safety was assessed using the CTCAE v.4.0 criteria. Patients were followed up at 3-, 6-, 9-, 12-months and then annually, with contrast enhanced CT or MRI.

Results: The 1-, 2-, 3-, 4- and 5-year efficacy of percutaneous cryoablation for RCC was 99.2%, 99.2%, 98.9%, 98.5% and 97.0%, respectively. Though none from RCC, all cause mortality during the study period was 3. Overall 5-year survival of 97.8% and cancer-specific 5-year survival was 100%. Median tumor size was 2.8 cm. There was one 30-day mortality unrelated to the procedure. No patient developed metastatic disease during the follow up period. The overall significant CTCAE v 4.0 complication rate (>2) was 6% with the most frequent being hemorrhage (1.6%).

Conclusions: Our study shows that the efficacy of CT-guided, percutaneous cryoablation for Stage 1 A&B renal cancer can approach that of the gold standard, with a lower complication rate.

Poster 5: Percutaneous Cryoablation Of Adrenal Gland: Catecholamine Related Complications and Prevention

C. Georgiades, M. Lessne, R. Rodriguez

Objectives: Our objective was to document and classify the types of catecholamine related complications from adrenal injury due to cryoablation based on our experience and perform a literature review.

Methods: Data were prospectively collected from an IRB approved study. During a period of 6 years we treated 261 renal tumors with percutaneous cryoablation. In twenty-six of these procedure the adrenal was within the "ice-ball" or was the actual target due to local spread of renal cell carcinoma (RCC). The first two patients were not premedicated. The remaining 24 patients were premedicated with both alpha- and

beta-blockers for > 5 days prior to procedure. All procedures were performed under conscious sedation with continuous pressure, EKG and O2 monitoring.

Results: The two non-premedicated patients experienced life-threatening arrhythmias. One had ventricular tachycardia and hypotension and the second had asystole. Both were resuscitated and suffered no long-term injury. None of the premedicated patients had a hypertensive crisis or arrhythmia. In addition, none of the patients whose adrenal gland was not injured had any such complications. Both complications occurred during the first active thaw cycle. Literature review suggests a higher rate of adrenal crises for cryoablation versus RFA, and that complications likely arise during the thaw cycles.

Conclusions: Non-premedicated patients are at high risk for catecholamine-related complications during adrenal cryoablation, and premedication with alpha- and beta-blockers is an effective mitigating strategy. Operators should expect this type of complication during the thaw cycle of the cryoablation as presumably the catecholamines are released into the bloodstream.

Poster 6: Percutaneous Microwave Ablation of Renal Cell Carcinoma: Multicenter Evaluation of Feasibility, Safety, and Early Clinical Efficacy

A.J. Moreland, S.A. Wells, A. Fischman, T.J. Ziemlewicz, S.L. Best, N.S. Shenkman, M.C. Lippert, J.L. Hinshaw, M.G. Lubner, C.L. Brace, E.J. Abel, F.T. Lee

Objectives: To evaluate the feasibility, safety, and preliminary effectiveness of a high-powered, gas-cooled microwave ablation system for percutaneous treatment of biopsy-proven renal cell carcinoma in a retrospective, multicenter case series.

Methods: Between 1/2011 and 11/2013, 89 biopsy-proven renal cell carcinomas were treated in 87 patients using ultrasound and CT-guided microwave ablation with a high-powered, gas-cooled microwave ablation system (NeuWave Medical, Madison, WI) at three academic medical centers. Histologic subtypes included clear cell (n=57), papillary (n=24), chromophobe (n=1) and unspecified (n=7). Gradable tumors included Fuhrman grades 1 (n=18), 2 (n=35), and 3 (n=1). Mean patient age was 66 years, and each patient underwent a single primary treatment session. Post-procedure imaging was performed by CT or MRI to evaluate for recurrence.

Results: Mean tumor diameter was 2.8 cm (range: 1.0-7.1). Tumor volume decreased by a mean of 51% (IQR: 37-68%) as assessed on immediate post-ablation CT. A mean of 1.9 antennas were used per tumor, and the mean duration of power application was 6.6 minutes at a mean generator power of 69 W. Technical success (no residual tumor on immediate post-ablation CT) was achieved for all tumors. Two grade 1 complications (urinary retention, cystitis) and two grade 2 complications (pyelonephritis, retroperitoneal hematoma) were reported by Clavien-Dindo classification. There was no significant change to eGFR pre- to post-ablation (mean: -1.6 mL/min/1.73 m²; p=0.18). Median length of hospitalization was 1 day. All patients are currently alive and without evidence of metastatic disease with the exception of one unrelated death, amounting to a renal cell carcinoma-specific survival of 100%. Mean and median length of follow-up were 10.6 and 7.5 months, respectively (IQR: 3.0-14.0 months). 39 patients have had follow-up imaging at a mean of 7.1 months post ablation (range: 1-19 months) with local progression noted in one case. This tumor was subsequently retreated with a technically successful repeat ablation, conferring an overall primary treatment effectiveness of 97.4% and secondary treatment effectiveness of 100%.

Conclusions: This multi-institutional study is the largest series to date using percutaneous microwave ablation for the treatment of renal cell carcinoma, and demonstrates that the procedure is technically feasible, safe, and efficacious at early follow-up. Further studies are warranted to demonstrate long-term oncologic outcomes in comparison to predecessor ablation modalities.

Poster 7: Quantitative and Qualitative Efficacy of Multiphasic MDCT in Characterizing Renal Lesion Histology on Percutaneous Biopsy

N. Alle, E. Felker, S. Lee-Felker, N. Tan, J. Huang, D. Lu, S. Raman

Objectives: To determine the qualitative and quantitative efficacy of MDCT imaging in characterizing biopsy proven renal masses

Methods: Institutional review board approval was obtained, and informed consent was waived for this HIPAA-compliant retrospective study. From January 2008 through May 2013, our renal biopsy database was queried to select all patients who had pre-biopsy multiphasic MDCT (unenhanced, corticomedullary, nephrographic, and excretory phases). The study cohort was comprised of 35 consecutive histologically biopsy proven renal masses with multiphasic MDCT. These studies were reviewed by two experienced abdominal imagers who qualitatively evaluated a variety of imaging features (lesion attenuation, contour, and presence of calcifications and neovascularity) and rendered diagnosis. Quantitatively, the peak attenuation was measured with region of interest (ROI) for each lesion on all phases and compared.

Results: Quantitatively, clear cell RCC (ccRCC) enhanced more avidly than other lesions; 17/18 (94.4%) of ccRCCs show an avid peak enhancement >120 HU (mean 185 HU) in the corticomedullary phase and a rapid corresponding de-enhancement <120 HU in 13/18 lesions (72.2%, mean 108 HU) in the nephrographic phase. Papillary RCC (pRCC) had a relatively high attenuation on unenhanced scans (mean 25.3 HU). pRCC enhanced much less avidly than ccRCC in all phases with a peak enhance-

ment <90 HU in the nephrographic phase (mean 76.9 HU) (83.3% (5/6) of lesions) and mean corticomedullary phase attenuation of 57.9 HU. Oncocytomas also peak enhanced in the corticomedullary phase with 80% (4/5) lesions enhancing >120 HU (mean 186.9 HU) with a less marked de-enhancement in the nephrographic phase (mean 120.6 HU) in comparison to ccRCC (80% (4/5)) oncocytomas still enhancing to >120 HU). On unenhanced scans, lipid poor angiomyolipomas (LP-AML) had the highest attenuation of all lesions averaging to 49.3 HU. They avidly enhanced with peak enhancement >120 HU (mean 148 HU) in 75% (3/4) of lesions in the corticomedullary phase, though to a lesser degree than ccRCC and oncocytomas. Like ccRCC and oncocytomas, there was rapid de-enhancement in the nephrographic phase (mean 93.4 HU). Using qualitative features, the majority of ccRCC (83% reader 1 and 72.2% reader 2), pRCC (0% reader 1 and 83% reader 2), and oncocytomas (100% for readers 1 and 2) enhanced heterogeneously. Calcifications were not more common in one subtype over another. Neovascularity was present more commonly in ccRCC (27.8% for reader 1 and 38.9% for reader 2) more commonly than in other lesions. In characterizing individual lesions, reader 1 correctly characterized 94.4% (17/18) of ccRCC, 100% (6/6) of pRCC, 0% (0/2) of oncocytic papillary RCC, 40% (2/5) of oncocytomas and 100% (4/4) of LP-AML. Reader 2 correctly characterized 100% (18/18) of ccRCC, 50% (3/6) of pRCC, 0% (0/2) of oncocytic papillary RCC, 0% (0/5) of oncocytomas, and 0% (0/4) of LP-AML.

Conclusions: Multiphasic MDCT enables characterization of the majority of common renal masses prior to biopsy using qualitative analysis of lesion morphology and enhancement and quantitative analysis of enhancement profiles.

Poster 8: Interventional Management of Gynecologic Cancers

Q. Al-Tariq, J. Park, J. Anaokar, D. Lu

Objectives: While interventional oncology is limited in the primary management of gynecologic malignancies, there is a definite role in the management of secondary manifestations, which include local/distant metastases/carcinomatosis, malignant ascites, and pelvic hemorrhage. The purpose of this poster presentation is to familiarize the reader with various interventional strategies, which will include roles of image guided biopsy, trans-arterial catheter directed embolization, and placement of indwelling drainage catheters, as they relate to the above. The use of thermoablative techniques for both palliation and treatment of non malignant gynecologic conditions will also be addressed.

Methods: This will be an image rich poster presentation which will highlight the management strategies listed above using clinical cases seen at our institution. There will also be treatment algorithms, which will aid the viewer in deciding upon the most appropriate imaging guided intervention.

Results: Image guided biopsy has a role in distinguishing between advanced ovarian cancer and peritoneal and adnexal metastases from other primary tumors, thereby allowing for the most appropriate therapy and potentially avoiding unnecessary surgery. Advanced gynecologic malignancies may lead to pelvic hemorrhage, which may be successfully managed using trans-arterial embolization, using a variety of embolic agents. Indwelling and semi-permanent intraperitoneal drains are a reasonable alternative to serial paracentesis. Thermal ablation techniques may be used for both palliation of painful metastases as well as for the treatment of abdominal wall endometriosis. HIFU may be safely used in patients with cervical ectopy, as an alternative surgical treatments, which are often associated with significant morbidity.

Conclusions: Image guided interventions play a large role in the diagnosis, treatment, and palliation of patients with genitourinary malignancies.

Poster 9: Hemorrhagic Complications of Percutaneous Cryoablation for Renal cancer: Results of a Prospective 5-year Study

C. Georgiades, M. Lessne, R. Rodriguez

Objectives: Much has been said about the vulnerability of cryoablation to hemorrhagic complications. Our objective was to establish the hemorrhage-related complications of percutaneous cryoablation for renal cell carcinoma and tabulate the types, locations and severity in a prospective, rigorous manner.

Methods: Over a 6-year period, we treated 246 patients with 261 renal masses with CT-guided, percutaneous cryoablation. We documented all hemorrhagic complications whether they were symptomatic or not, as they appeared on the procedural and post-procedural CT, and categorized them according to location, tumor size, patient age, probe number and intervention required. Safety was assessed using the CTCAE v.4.0 criteria.

Results: The significant CTCAE v 4.0 hemorrhage-related complication rate was 3.4%. Four patients required transfusion, 3 emergent angiograms and 2 bladder irrigation due to bladder outlet obstruction from clot (total of 9 significant complications). Hemorrhages were localized in three distinct locations: the peri-renal, the para-renal space and the collecting system. The former appeared more susceptible to clinically significant hemorrhage (CTCAE >2). Although not statistically significant, in the significant hemorrhage risk group, there was a tendency for older age, larger tumor, malignant histology and more probes. Procedure-related mortality was 0%.

Conclusions: Percutaneous cryoablation carries a small risk of clinically significant hemorrhagic complications and similar to that reported for radiofrequency ablation and open or laparoscopic cryoablation. Older patients with larger, malignant tumors and peri-renal space hemorrhage should be monitored more closely than others in the post-operative period. In this group, pre-ablation embolization may be beneficial.

Poster 10: Percutaneous Microwave Ablation for the Treatment of Renal Angiomyolipoma: Initial Experience

M. Cristescu, T.J. Ziemlewicz, E.J. Abel, D. Kitchin, M.G. Lubner, J.L. Hinshaw, C.L. Brace, F.T. Lee

Objectives: Microwave (MW) ablation is known to be effective in penetrating biologic tissues which act as electrical insulators (i.e. fat) and thrombosing tumor vasculature. These properties give MW ablation the potential to be an excellent treatment modality for fat-containing tumors such as renal angiomyolipoma (AML), and possibly also increase its effectiveness compared to other ablation modalities and embolization. We hypothesize that percutaneous microwave ablation is efficacious in devascularizing and arresting the growth of renal AMLs and describe our early experience with its use in treating these tumors.

Methods: This study was IRB approved and HIPAA compliant. Between January 2011 and November 2013, 6 patients (5 female, mean age 51 years) with renal AML (5 sporadic-type, 1 tuberous sclerosis-associated) were treated with MW ablation. Two patients had previously undergone embolization which did not completely devascularize their tumor. Indications for treatment included growing tumors approaching 4 cm (n=4), and continued growth despite prior treatment (n=2). All patients were treated using either two or three gas-cooled 17-gauge antennas (Neuwave Medical, Madison, WI). All patients received hydrodissection to protect non-target structures (5% dextrose in water or normal saline). Immediate post-ablation dual phase CT of the abdomen was performed in all patients, and three of six patients have undergone delayed follow-up imaging using CECT or MRI to date. Tumor volume was measured pre-procedure, immediate post-procedure, and on delayed scans using a GE Advantage Windows Workstation (GE Healthcare, Waukesha, WI).

Results: All ablations were technically successful and no major complications were encountered. Mean tumor diameter prior to ablation was 3.6 cm. Mean ablation time was 5.3 minutes (range 4-8 minutes) and mean ablation power was 65 W (range 50-70 W). An average of 322 mL of hydrodissection fluid was used per patient. Immediately post-ablation, mean tumor volume decreased 6.0% (33.2 to 31.0 cm³). Delayed imaging (performed up to a mean of 21 months post-procedure to date) demonstrated that mean diameter had decreased 19% (3.6 to 3.1 cm) and mean volume had decreased 47% (33.2 to 18.7 cm³) overall. No tumoral enhancement was noted on immediate post-procedure or delayed imaging, indicating tumor devascularization. No patients required additional intervention and no patients experienced spontaneous bleeding post-ablation.

Conclusions: Our early experience with high-powered, gas-cooled percutaneous microwave ablation demonstrates it to be a safe and effective modality to devascularize and decrease the size of renal angiomyolipomas. Continued study is warranted to evaluate the long-term efficacy of microwave ablation in arresting the growth of renal AMLs and preventing episodes of spontaneous bleeding.

Poster 11: MRI/Ultrasound Fusion Guided HIFU Ablation of Prostate Cancer: Phantoms Studies

S. Xu, H. Amalou, H. Agarwal, A. Negussie, B. Turkbey, P. Pinto, P. Choyke, B. Wood

Objectives: Prostate cancer is often over treated with side-effects such as Incontinence and impotence. High intensity focused ultrasound (HIFU) offers a minimally invasive treatment option for localized prostate cancer. However, ultrasound has poor visibility of prostate cancer. Multi-parametric MRI has demonstrated promising resolution in differentiating prostate cancer. Since it is expensive and requires MRI compatibility to perform interventional procedures in an MRI suite, image fusion of preoperative MRI with real-time ultrasound is desirable for guiding HIFU treatment of prostate cancer. The purpose of this study is to show the feasibility of fusion guidance for transrectal HIFU ablation.

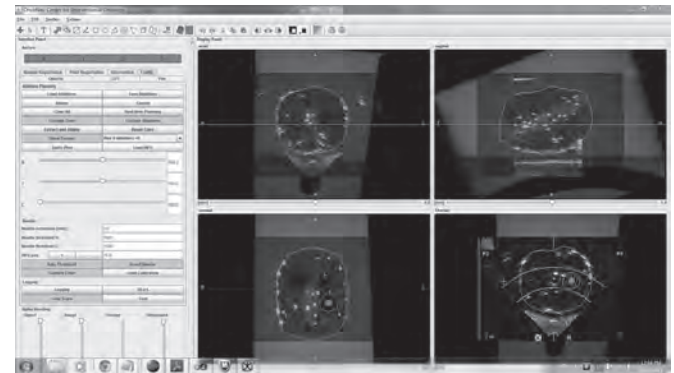
Methods: A custom software platform was developed for segmentation, registration, and treatment planning for MRI/ultrasound fusion guided HIFU. A commercial ultrasound guided HIFU system (Sonablate, SonaCare Medical LLC.) was integrated with the fusion platform to allow guidance with real time ultrasound as well as pre-procedural MRI. The boundaries of prostate tumors were identified in multi-parametric MRI (e.g. T2, DWI, DCE etc...) and segmented in T2-weighted MRI. A 3D ultrasound volume was acquired using the transducer of the HIFU system right before the treatment. Registration between HIFU and MRI was accomplished by semi-automatic alignment of the boundaries of the prostate in MRI and ultrasound without optical or electromagnetic tracking. HIFU ablation zones were then planned in the 3D ultrasound volume with fusion of the MRI images. MRI targets were overlaid on the axial slices of the 3D ultrasound volume to determine the treatment boundary on each slice. HIFU treatment was carried out according to the plan.

Results: The system was evaluated in two custom-built prostate tissue mimicking prostate phantoms. The first prostate phantom generates different gray scales in T2-weighted MRI at temperatures below and above sixty degrees. The second prostate phantom changes colors at different temperatures. Segmentation, registration and planning were carried out in both phantom studies before HIFU treatment. The experiments demonstrated clinically acceptable workflow. Tissues at the planned locations were ablated. The sizes of the ablation zones were in-line with the planned treatment volumes.

Conclusions: Pre-procedural multi-parametric MRI can be used to guide HIFU with image fusion for focal prostate cancer treatment. The navigation system does not require optical or electromagnetic tracking hardware to register MRI to ultrasound. The treatment procedure can be conducted outside the MRI suite, which may potentially lower the cost, shorten the procedure time, and enable HIFU treatment of MRI targets without requiring MRI compatibility.



System and color changing phantom



Treatment planning using MRI/ultrasound fusion. The bottom-right window shows the HIFU treatment area in relation to an MRI target

Poster 12: CT-Guided Biopsy Radiation Dose Estimate Can Be Reduced Using the Prospective Native Fiducial (PNF) Method

A. Sag, S. Tewari, D. Li, S.B. Solomon, K.T. Brown, C.T. Sofocleous, A.M. Covey, W. Alago, L. Brody, R.H. Siegelbaum, J.C. Durack, A. Aguado, J.P. Erinjeri, G.I. Getrajdman, M. Maybody, H. Yarmohammadi, L. Dauer, R. Thornton

Objectives: Localization scanning accounts for a substantial portion of dose from CT-guided biopsy. The authors describe a method to reduce this dose by using pre-procedural imaging to limit localization.

Methods: With IRB approval, 65 consecutive CT-guided biopsies from January to May 2012 were reviewed; Retroperitoneal lymph node (RP) (n=25), liver (n=20) and renal (n=20). Patients were supine for liver biopsy and prone for RP and renal biopsy; Preceding diagnostic imaging was always supine. In our current practice, position and length of localization scans obtained at 60mA are selected ad lib ("ad lib" method) referencing pre-biopsy imaging. For reviewed biopsies, scan length and dose-length product (DLP) for localization and for total procedure were separately recorded. For imaging review, biopsy targets were first identified on in-biopsy CT. Next, pre-biopsy CT was reviewed and the vertebral endplate nearest the target was assigned the "prospective native fiducial" (PNF). Finally, CT scout and axial images of lesion local-

ization during biopsy were co-registered; Craniocaudal distance between the PNF and target was measured and termed “fiducial offset” (FO). After analyzing the FO distribution for each anatomic biopsy group, the optimal PNF-centric localization scan length capturing non-outlier FOs was determined. Dose reduction to the patient was estimated comparing the PNF method. Descriptive statistics were calculated.

Results: Ad lib method revealed significant procedural dose from localization scans (Table 1). PNF method revealed substantial reduction of dose estimates (Table 2).

Conclusions: When ad-lib localization was performed, more than 1/3 of radiation dose estimate for CT-guided biopsy came from localization scanning. Approximately 50% reduction in radiation dose estimate can be achieved using the PNF method to image 70-75% of targets depending on anatomic location.

Ad Lib Localization Scanning

Biopsy	N	Localizer length Average (Range) cm	Mean localizer DLP Gyem2	Mean total procedural DLP Gyem2	Localization is what % of total procedural dose
RP	25	12.9 (7-20)	164.8	490	34%
Liver	20	11.2 (4.6 - 22.2)	313	726	43%
Kidney	20	12.9 (7.2-21.5)	260	681	38%

Table 1. Ad lib localization results.

Targeted Localization Scanning Using Prospective Native Fiducial (“PNF” method)

Biopsy	N	FO Mean (range) mm Positive values mean target was cranial to the PNF; Negative are caudal	Outliers mm Positive values mean target was cranial to the PNF; Negative are caudal	Localizer length to capture all non-outliers (number of targets captured, %)	Dose reduction for localization mean %
RP	25	+11 (+42, -13)	+36, +42	6 cm (23/25 targets, 75%)	54%
Liver	20	+13 (+57, -14)	+33, +40, +47, +57	6 cm (14/20 targets, 70%)	46%
Kidney	20	+15 (+70, -44)	+40, +40, +66, +70, -44	6 cm (15/20 targets, 75%)	54%

Table 2. Dose estimate reductions when utilizing the PNF method instead of ad lib method.

Poster 13: Ultrasound Predicts Pathologic Zone of Necrosis Better Than Non-Contrast CT During RF and Microwave Ablation

T. Ziemlewicz, C.L. Brace, B.J. Willey, M.G. Lubner, L. Hinshaw, L. Sampson, F.T. Lee

Objectives: Understanding the relationship between intra-procedure imaging findings and the true zone of coagulation is of critical importance to ensure tumor death and protect critical structures. The goal of this study was to correlate intra-procedural ablation zone appearance on CT and ultrasound with pathologic findings.

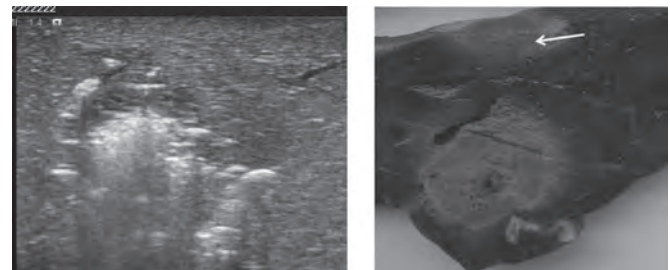
Methods: Twenty-one 5 minute ablations were performed in vivo in swine liver with 1) microwave (MW) at 140W, 2) MW at 70W, or 3) radiofrequency (RF) at 200W (n=7 each). An ultrasound probe was fixed at the liver surface perpendicular to the applicator. Non-contrast CT and US images were obtained simultaneously at 1, 3, and 5 minutes during ablation and 2, 5, and 10 minutes post-ablation. Each ablation was then sectioned in the plane of the ultrasound image and underwent vital staining to reveal the zone of cellular necrosis. CT data were reformatted to the same slice plane. Images were analyzed by two readers, each measuring the transverse diameters of gas and hypoechoic/hypodense zones at each time point. CT, ultrasound and gross pathologic diameter measurements were compared using Student’s t-tests.

Results: Both RF and MW ablations exhibited gas on US and CT images taken intraprocedurally. The size of the gas zone was greater for MW ablations, and increased with applied power. However, the pathologic zone of necrosis was larger than the zone of visible gas on US (mean 2.7 mm for MW, 6.3 mm for RF) and CT (7.6 mm MW, 13.9 mm RF) images (P<0.05). The hypoechoic zone on US was 0.4 mm larger with MW and 3.0 mm smaller with RF than the pathologic zone of necrosis (p=0.38). The hypodense zone on CT was 5.5 mm larger with MW (p<0.05) and 2.2 mm smaller with RF (p=0.31) than the pathologic zone of necrosis. Therefore, visible gas and the peripheral hypoechoic zone on US images were more predictive of the pathologic ablation zone than CT findings (P<0.05) overall.

Conclusions: US may be preferred to non-contrast CT for intra-procedure ablation monitoring, particularly when precise definition of margins is needed.



Experimental set-up.



US and corresponding vital stained pathology slice from a MW ablation at 140W. Yellow arrow points to surface mark created at site of ultrasound transducer.

Poster 14: Comparison of Performance as a Cohort of Experienced IR Physicians versus Novice CT-Guided Robotic Positioning System Operators for Needle Placements to Small In-Vivo Targets

G. Srimathveeravalli, H. Takaki, F. Cornelis, M. Lakshmanan, M. Maybody, G.I. Getrajdman, C.T. Sofocleous, J.C. Durack, J.P. Erinjeri, S.B. Solomon

Objectives: As a cohort, experienced IR physicians can be characterized by their ability to perform needle placement with similar outcomes in terms of accuracy of placement, time taken to complete the task and the number of needle manipulations required to reach a target. We wish to assess whether untrained operators of a CT-guided robotic positioning system will demonstrate similar behavior if evaluated as a cohort.

Methods: Seven experienced IR physicians were recruited to participate in this study. Four 5mm 18G metallic fiducial markers were placed in different lobes of the swine liver at depths varying from 50-120mm (7 animals, 28 targets). Physicians employed standard clinical practices using either sequential CT (1) or CT-fluoroscopy (6) guidance to target the markers with 18G, 100 or 150mm length coaxial needles. Manual needle insertion was followed by robot-assisted needle insertion using the Maxio platform (Perfint Healthcare Inc.). The physicians were provided orientation for the use of the Maxio platform but were not given specific training or practice sessions in using the system. Accuracy of targeting was measured as the shortest distance between the needle tip and the closest point on the targeted seed. The number of confirmation scans and needle course manipulations were recorded. The overall procedure time, starting with the planning scan and ending with final positioning scan was recorded. Needle

placement results from each physician was compared to outcomes from others participants in the same cohort (manual or robot-assisted). Variation in performance within a cohort was statistically assessed using one-way ANOVA.

Results: When evaluated for performance as a cohort, results indicate that experienced IR physicians performing manual needle placements behaved with limited variability when considering accuracy (mean= 4.308mm; F=1.2; p=0.3383), the number of check scans used to place the needle (mean= 5.7; F=1.63; p=0.1737), and for the number of needle manipulations required to reach the target (mean= 4; F=2.0; p=0.067). Similarly, results indicate that as a cohort, novice operators of CT-guided robotic needle placements exhibited insignificant variation in their performance despite limited training on the system. (Accuracy of placement: mean= 4.423mm; F=0.7; p=0.649), (Check scans: mean= 1.35; F=1.57; p=0.206), (Needle manipulations: mean= 0.32; F=1.36; p=0.276). However, both experienced IR physicians (mean= 5.67 minutes; F=4.03; p=0.00407) and novice robot operators (Procedure time: mean= 9.24 minutes; F=2.35; p=0.068) demonstrated moderately significant variation in the time taken to complete their procedures.

Conclusions: Despite minimal training, when evaluated as a cohort, novice CT guided robotic system operators were able to place needles to targets with minimal inter-personal variation in their performance. This limited inter-personal variation in the cohort was similar to the performance of a group of experienced IR physicians performing manual needle placements. Procedure time was the only variable factor with significant inter-individual differences in both groups.

Poster 15: Utility of C-arm Cone Beam Computed Tomography and Ablation Software for Planning and Monitoring of Percutaneous Kidney Tumor Thermal Ablations

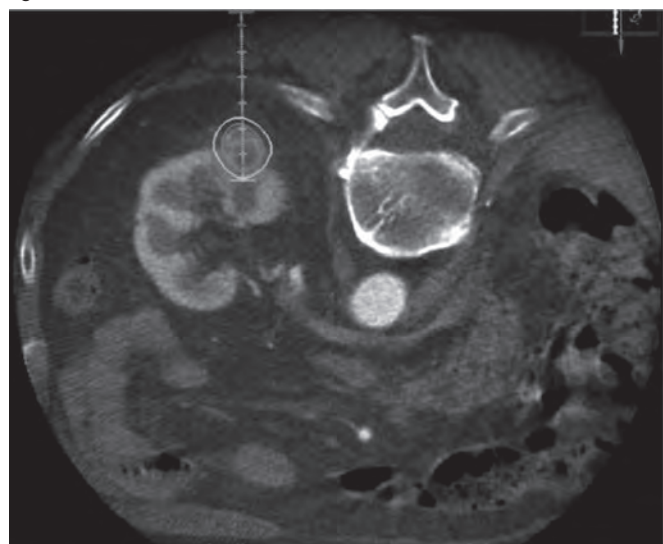
C. Floridi, A. Ierardi, F. Fontana, Y. Yangué, G. Carrafiello

Objectives: To prospectively evaluate the utility of C-arm Cone Beam Computer Tomography (CBCT) and ablation software for planning and monitoring of percutaneous kidney tumor microwave ablations (MWA) and rapport on feasibility.

Methods: Between November 2012 and December 2013 ten patients (7 men, 3 women; mean age, 77.7 years) underwent MWA of renal lesions (9 Renal Cell Carcinoma; 1 oncocytoma; mean size 21mm) using a C-arm CBCT. Intra-procedural dual-phase CBCT (arterial and venous) after intravenous contrast administration was performed to determine optimal approach to the lesion using dedicated ablation planning software. MW antennas were positioned under fluoroscopy with Xperguide system (5 cases) or under ultrasound guidance (5 cases) and non-enhanced CBCT was performed after deployment. CBCT acquired before and after antenna deployment was registered to evaluate tumour targeting. Diagnostic contrast-enhanced CT was used in case CBCT did not accurately depict lesions. CBCT lesion detection accuracy and number of needle re-positioning on the basis of CBCT and software information were recorded. Clinical success was measured on follow-up contrast-enhanced CT

Results: All procedures were completed without complications. C-arm CBCT detected all lesions (100%) and we used registration with diagnostic CT only in 1. MW antennas were repositioned on the basis of CBCT and software in 5 lesions (50%). Clinical success was achieved in 9 ablations (90%) while 1 (10 %) presented with residual lesion on CT follow-up

Conclusions: Planning and Monitoring of percutaneous MWA of kidney tumors using C-arm CBCT and ablation software is feasible and leads to safe needle positioning within the lesion to treat.



contrast enhancement Intraprocedural CBCT with ablation planning

Poster 16: Utility of C-arm Cone Beam Computed Tomography and Ablation Software for Planning and Predicting Thermal Ablation of Lung Malignancies

C. Floridi, M. Petrillo, A. Ierardi, F. Fontana, G. Carrafiello

Objectives: To retrospectively evaluate the utility of C-arm Cone Beam Computer Tomography (CBCT) and ablation software for planning the thermal ablation of lung malignancies and obtaining safe margins of ablation area.

Methods: Between 2012 and December 2013, 23 Patients (13 men, 10 women with a mean age of 73.5 years) underwent thermal ablations of lung malignancies (18 non small cell lung cancers; 5 metastasis); twelve procedures (4 Radio frequency ablations; 8 Microwave ablations) were completed under C arm CBCT with a new ablation dedicated software and constitute the study cohort. Pre-procedural CBCT was performed and the ablation was planned determining optimal approach to the lesion, using the dedicated software. Under fluoroscopy, with navigation system, ablation devices were positioned into the lung lesion and intra-procedural CBCT was performed to check device position within the lesion. CBCT lesion detection accuracy and ablation device positioning accuracy on the basis of CBCT and software information were recorded. Moreover, one month follow-up Computed Tomography and intra-procedural CBCT were retrospectively registered to evaluate the accuracy of CBCT ablation software to predict the safe margins of ablation area.

Results: All procedures were completed without major complications. C-arm CBCT detected all lesions (100%). In five cases, the ablation devices were repositioned on the basis of CBCT (41,6%). At the 1st month follow-up CECT, we obtained complete ablation in 8 cases. In the other cases the residual disease was seen at lesion periphery, where the CBCT software showed lack of safe margins of planned ablation area.

Conclusions: Planning and Monitoring of percutaneous lung malignancies thermal ablation using C-arm CBCT and ablation software is feasible and leads to safe needle positioning within the lesion to treat.

Poster 17: A Prospective Randomized Clinical Trial on 90Yttrium Transarterial Radioembolization (Therasphere®) vs Standard of Care (Sorafenib) for the Treatment of Advanced Hepatocellular Carcinoma with Portal Vein Thrombosis

P. Sinclair

Objectives: Primary liver cancer is a global health problem; the fifth most commonly diagnosed cancer in men and eighth most common in women. Currently, sorafenib (Raf kinase and VEGF receptor kinase inhibitor) is suggested as the standard-of-care (SOC) treatment for patients with advanced hepatocellular carcinoma (HCC), however, it is associated with only a modest improvement in median survival compared to best supportive care. Furthermore, sorafenib treatment is associated with significant toxicity. TheraSphere® (yttrium-90 glass microspheres) is approved as a humanitarian use device in the United States for use in radiation treatment or as a neoadjuvant to surgery or transplantation in patients with unresectable HCC who can have placement of appropriately positioned hepatic arterial catheters. It is also indicated for HCC patients with partial or branch portal vein thrombosis (PVT)/occlusion when clinical evaluation warrants the treatment. The effectiveness of this device for this use has not been demonstrated. Clinical studies have evaluated the safety and efficacy of TheraSphere® in patients with unresectable HCC. Recent clinical data in patients with HCC and PVT indicate that this group of patients may have improved outcomes following TheraSphere® treatment as compared with sorafenib. The purpose of this study is to determine whether TheraSphere® provides a meaningful benefit in survival in comparison with sorafenib in patients with HCC associated with PVT. The objective of this study is to assess the efficacy and safety of TheraSphere® in comparison with sorafenib in the treatment of patients with PVT associated with unresectable HCC.

Methods: This phase III, two-arm, open-label, prospective, multi-center, randomized, active-controlled study will evaluate treatment with TheraSphere® compared with sorafenib in 328 patients diagnosed with PVT associated with unresectable HCC who are not eligible for any curative procedure. Eligible patients will be randomized 1:1 to control and treatment groups. The control group will receive sorafenib in accordance with the product label and the treatment group will receive TheraSphere® in accordance with the product label. The primary endpoint is overall survival from the time of randomization until time of event (death). Secondary endpoints include time to progression/symptomatic progression, time to worsening of PVT, tumor response (RECIST 1.1 and EASL), patient-reported outcome assessments, and adverse events. Following randomization, patients will receive treatment within 2 to 4 weeks, with study visits every 4 weeks up to 24 weeks or until progression. After week 24, in the absence of progression, follow-up visits will occur every 8 weeks until progression. After progression visits will occur every 8 weeks until death.

Results: This study is ongoing.

Conclusions: This phase III, two-arm, multicenter, randomized study will evaluate the use of TheraSphere® in patients with PVT associated with unresectable HCC, given the potential of TheraSphere® to enhance survival with less toxicity than the current SOC sorafenib.

Poster 18: Histopathological Efficacy and Side Effects of TACE in Bridging of HCC Patients to Liver Transplantation

U. Stampfl, J. Bermejo, C. Sommer, K. Hoffmann, K. Weiss, P. Schirmacher, P. Schemmer, H. Kauczor, G. Richter, B.A. Radeleff, T. Longerich

Objectives: To histologically evaluate efficacy and non-target effects induced by transarterial chemoembolization (TACE) in bridging of HCC patients to liver transplantation (LT) and its relation to patients survival

Methods: Between 10/2003 and 01/2011, 51 HCC patients underwent LT after TACE using a sandwich technique with iodized oil, small spherical particles as embolic agent, and carboplatin. The efficacy and side effects of TACE were determined histologically in explanted livers and their impact on survival after LT was analyzed.

Results: 126 TACE procedures were performed in these 51 patients; the median number of procedures per patient was 3 (range 1 to 6). The extent of HCC necrosis was <50% in 20%, ≥50-90% in 44%, and ≥90-99% in 26% of treated HCCs, while 12% showed complete necrosis of the lesion. The most common side effects were focal necrosis of the non-neoplastic liver parenchyma adjacent to the embolized HCC nodule (28%), intralesional (micro-)abscess formation (26%), intralesional hemorrhage (22%), and peritumoral bile duct necrosis (12%). Based on detailed histopathological examination 35% of patients were outside the Milan criteria. However, none of these findings was significantly associated with patients survival after LT.

Conclusions: TACE induces histopathological confirmed HCC necrosis with high efficacy. Although histopathology revealed side effects in a subset of patients, these did not impair patients' survival. Neither histologically proven complete HCC necrosis nor Milan criteria as determined by histopathology were predictive of survival in this cohort of patients.

Poster 19: Short-Term Interval Combined Transcatheter Arterial Chemoembolization and Radiofrequency Ablation for Hepatocellular Carcinoma: Effect on Liver Function During 1 Year Follow Up

Y. Kim

Objectives: To investigate changes in liver function during 1 year follow up period after short term interval (0-2 days) combined radiofrequency (RF) ablation with transcatheter arterial chemoembolization (TACE) in patients with hepatocellular carcinoma (HCC).

Methods: A total of 118 cirrhotic patients with HCC <5.0cm underwent combined RF ablation with TACE at a time-interval of 0-2 days between July 2005 and September 2011. Of them, 24 patients received further hepatic directed treatment altering liver function after the combined treatment during 1 year follow up period due to local tumor progression (n=3) or intrahepatic remote recurrence or distant metastasis (n=21), thus were excluded from the analysis. The remaining 94 patients without recurrence at 1-year follow up were finally included in this retrospective study. The liver function parameters before and after combination therapy were analysed to clarify risk-factor for aggravation of Child-Pugh scores (CPs).

Results: In 94 patients surviving without HCC-recurrence at 1-year, 5 patients (5.3%) experienced the transient rise in CPs at 1-month after the procedure, and the CPs were returned to each baseline score at 3-months in all patients. Only CPs ≥8 prior-to the treatment was identified as the factor for worsening of CPs at 1 month after TACE+RFA (vs. ≤7, p=0.027).

Conclusions: Sequential application of TACE-RFA at interval of 0-2 days is safe with regard to the liver function for patients with HCC <5 cm. However, patients with CPs ≥8 cirrhosis are at increased risk for transient damage of liver functional reserves, so it is necessary to require attention for applying this treatment modality to them.

Poster 20: Idarubicin-Loaded TANDEM® for Chemoembolization of HCC: In Vitro Loading and Release, and In Vivo Pharmacokinetics

B. Guiu, A. Schmitt, S. Reinhardt, T. Pohl, M. Wendremaire, S. Hamza, A. Denys, J. Bluemmel, M. Boulin

Objectives: Idarubicin has been shown as the most effective drug for chemoembolization of HCC in vitro. TANDEM® are new drug-eluting microspheres which could act as a vector for idarubicin. We aimed to assess in vitro loading and release of idarubicin from TANDEM® microspheres, as well as in vivo pharmacokinetics of idarubicin-loaded TANDEM® in humans.

Methods: In vitro study: For all experiments, we used 6 samples of TANDEM® 100 µm loaded with 5 mg idarubicin-HCl (1 mg/ml, Zavedos®, Pfizer) per ml microspheres. Idarubicin loading was monitored every 10 minutes. Particle sizes were measured by optical microscopy. In vitro drug releases were performed with a SOTAX flow cell apparatus at 37°C and 5 ml/min saline and were evaluated using HPLC. In vivo study: Two BCLC B patients were treated by lobar TACE using 2 ml of 100 µm TANDEM® loaded with 10 mg idarubicin (i.e. 5 mg per ml microspheres). Peripheral blood samples were collected at baseline (i.e., just after the end of TACE) and at 5, 10, 15, 30 min, 2 and 24 hours after completion of TACE procedure. Idarubicin and its major metabolite idarubicinol were measured using a reversed-phase liquid chromatog-

raphy with tandem mass spectrometry. The lower limit of quantification for both, drug and metabolite, was 1 ng/ml.

Results: In vitro study: Idarubicin loading was completed (i.e. > 99%) within 10 minutes. Unloaded particle size was 99 (±12) µm. Calibration of idarubicin-loaded TANDEM® was excellent: idarubicin-loaded particle size was 105 (±12) µm, whereas the particle size was 96 (±10) µm after idarubicin release. TANDEM® exhibited a sustained release of idarubicin: the first two releases of idarubicin from microspheres lasted 7 hours each. During the first period, 58.0 (±0.8) % of the drug was released, whereas in total 87.4 (±1.4) % was released after the second period. Idarubicin could be completely released from microspheres with more release procedures. In vivo study: The two patients exhibited no ≥ grade 3 toxicities (NCI-CTCAE) and were discharged 2 days after the TACE procedure. Pharmacokinetic data demonstrated a very low and sustained systemic exposure: T_{max} of idarubicin were 10 and 5 min, for the 1st and 2nd patient respectively; C_{max} of idarubicin were 2.5 and 6.1 ng/ml respectively. Idarubicin concentrations were too low to be measured at 24 hours. Idarubicinol concentrations were undetectable in the 1st patient and too low to be measured before 2 hours after end of TACE procedure in the second patient. Highest concentration of idarubicinol was 1.5 ng/ml at 24 hours. The AUC₀₋₂₄ for idarubicin were 16 and 22 ng×h/ml respectively, which is approximately 20 times less than that reported for intravenous administration.

Conclusions: 100 µm TANDEM® microspheres allow a fast and complete loading of 5 mg idarubicin per ml microspheres as well as a slow and sustained release. In vivo, they exhibit a very favorable pharmacokinetic profile with a constant but very low systemic exposure to idarubicin and idarubicinol, meaning that most of the idarubicin stays in the liver. Clinical studies using idarubicin-loaded TANDEM® are needed.

Poster 21: Hepatocellular Carcinoma Survival Outcome: DEB-TACE and the Multimodal Treatment Approach

C. Hacking, P. Kumar, D. Flowers, J. Coyne, B. Stedman, T. Bryant, S. George, M. Wright, K. Nash, C. Hollywood, N. Pearce, M. Abu Hilal, J. Primrose, D. Breen

Objectives: We investigated the long-term survival outcome of HCC patients treated with DEB-TACE as part of a multimodal therapeutic strategy

Methods: Between August 2006 and February 2011, 81 patients with hepatocellular carcinoma were treated with DEB-TACE alone or combined with surgery and/ or percutaneous thermal ablation according to BCLC stage. Patient demographics, clinical data and outcome measures were studied. Median age was 68 years (range 33-87). Median follow-up was 19.7 months (range 19 days – 54.2 months). Mean tumour size was 6.0 cm. All patients were included in the final survival analysis. Survival was estimated by the Kaplan-Meier method.

Results: DEB-TACE was technically successful in all cases. There were no deaths at 30 days following a DEB-TACE treatment session. The 1-, 2- and 5-year survival of the multimodal treatment group was 89.5%, 83.5% and 30% respectively. Median survival with multimodal treatment was 43.4 months. Overall, Child-Pugh class and tumour burden were predictors of survival on multivariate analysis.

Conclusions: DEB-TACE is a safe and effective technique when applied to patients with early or intermediate stage HCC within a multimodality treatment protocol and results in favourable survival outcomes.

Poster 22: Immediate Post-Doxorubicin Drug-Eluting Beads Chemoembolization MR Apparent Diffusion Coefficient Quantification Predicts Response in Unresectable Hepatocellular Carcinoma

N. Kokabi, J.C. Camacho, M. Xing, F. Edalat, P.K. Mittal, H.S. Kim

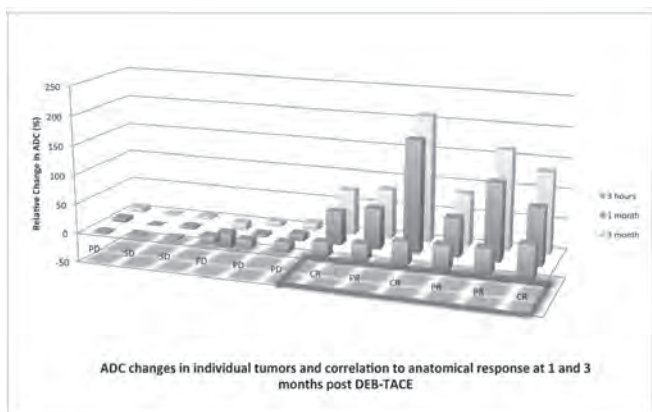
Objectives: To investigate magnetic resonance (MR) diffusion weighted imaging (DWI) of hepatocellular carcinoma (HCC) within 3 hrs post doxorubicin drug-eluting beads transcatheter arterial chemoembolization (DEB-TACE) therapy as an early imaging biomarker of response

Methods: In an IRB-approved, prospective pilot study, 12 consecutive patients (9 males) median age 64 yrs (range 50-82 yrs) underwent 18 DEB-TACE therapies for unresectable HCC. Anatomic and DWI (b=50,400,1000 s/mm²) MR was performed using a 1.5T unit at baseline, within 3 hrs, and at 1 and 3 mo post therapy. Treatment response was evaluated using target modified Response Evaluation Criteria in Solid Tumors (mRECIST) and European Association for the Study of the Liver (EASL) guidelines with complete/partial response considered objective. Relative change (RC) in apparent diffusion coefficient (ADC) of all targeted lesions were measured on follow-ups. Correlation between ADC RC in tumors and anatomical response were evaluated with paired t-test and receiver operator characteristic (ROC) curve (α=0.05).

Results: Mean ADC value of all targeted lesions pre and post DEB-TACE were 0.894 ± 0.28 mm²/s and 1.15 ± 0.26 mm²/s respectively. Compared to baseline, mean ADC increased significantly for responders within 3 hrs post DEB-TACE (0.73 ± 0.20 mm²/s at baseline vs. 0.99 ± 0.28 mm²/s ×10⁻³ at 3 hrs (p=0.001)). There was no statistically significant difference in ADC within 3 hrs for non-responders (1.07 ± 0.21 mm²/s vs. 1.12 ± 0.22 mm²/s ×10⁻³ (p=0.22)). The mean ADC for responders continued to significantly increase at 1 and 3 mo compared to baseline 1.39 ± 0.31 mm²/s

and $1.54 \pm 0.27 \text{ mm}^2/\text{s} \times 10^{-3}$ ($p < 0.05$) while ADC values for non-responders did not change significantly throughout ($1.04 \pm 0.27 \text{ mm}^2/\text{s}$ and $1.10 \pm 0.25 \text{ mm}^2/\text{s} \times 10^{-3}$ at 1 and 3 mo respectively ($p > 0.05$)). For an area under the curve of 0.89, ADC RC threshold of 20% within 3 hours post DEB-TACE has 100% sensitivity and specificity in predicting anatomical response according to mRECIST and EASL at 1 and 3 mo. Figure 1 illustrates ADC value changes for each tumor throughout the study.

Conclusions: ADC relative change of $>20\%$ within 3 hours post DEB-TACE can accurately predict anatomical response of unresectable HCC at 1 and 3 months.



Poster 23: Baseline MR Apparent Diffusion Coefficient Quantification as a Predictor of Response of Unresectable Hepatocellular Carcinoma to Doxorubicin Drug-Eluting Beads Chemoembolization

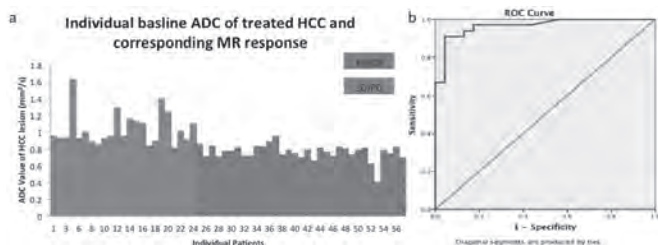
N. Kokabi, J.C. Camacho, F. Edalat, M. Xing, P.K. Mittal, H.S. Kim

Objectives: To investigate baseline magnetic resonance (MR) diffusion weighted imaging (DWI) as a predictor of therapy response in unresectable hepatocellular carcinoma (HCC) treated with doxorubicin drug-eluting beads transcatheter arterial chemoembolization (DEB-TACE)

Methods: In an IRB-approved prospective pilot study, 57 consecutive patients (37 males), median age 64 yrs (25-85 yrs), underwent a total of 72 separate DEB-TACE for unresectable HCC. MR anatomic and diffusion imaging ($b=50,400$, and 1000 s/mm^2) was performed using a 1.5T unit at baseline, and at 1 and 3 months after therapy. Treatment response was evaluated at 1 and 3 months post DEB-TACE therapy using target modified Response Evaluation Criteria in Solid Tumors (mRECIST) and European Association for the Study of the Liver (EASL) guidelines with complete and partial response considered objective. Correlation between baseline ADC of tumors and anatomical objective response were evaluated with paired t-test comparing mean ADC of responders vs. non-responders and receiver operator characteristic (ROC) curve ($\alpha=0.05$).

Results: ADC values for targeted HCC lesions at baseline varied greatly ranging from $0.41 \times 10^{-3} \text{ mm}^2/\text{s}$ to $1.632 \text{ mm}^2/\text{s}$ (mean \pm SD = $0.95 \pm 0.21 \times 10^{-3} \text{ mm}^2/\text{s}$). At 1 and 3-month post DEB-TACE, objective response was observed in 33(60%) patients (21 CR, 12 PR) according to mRECIST and EASL. At baseline, tumors with objective response at 1 and 3-month showed significantly more restricted diffusion compared to others ($0.731 \pm 0.201 \text{ mm}^2/\text{s}$ vs. $1.057 \pm 0.215 \text{ mm}^2/\text{s} \times 10^{-3}$ for responders and non-responders respectively ($p=0.031$)). Individual baseline ADC's are illustrated in figure 1a. For an area under the curve of 0.965, the sensitivity and specificity of predicting objective tumor response at 1 month using baseline HCC ADC value $0.83 \text{ mm}^2/\text{s}$ was 91% and 96% respectively (figure 1b).

Conclusions: In unresectable HCC, ADC value of $\leq 0.83 \text{ mm}^2/\text{s}$ at baseline predicts anatomical response at 1 and 3 months post DEB-TACE with high sensitivity and specificity.



Poster 24: In Vivo Eradication of HCC using Synchronous Thermal Ablation and HSP90 Chemotherapy with Protein Engineered, Tri-Block Biopolymer-Geldanamycin Conjugates

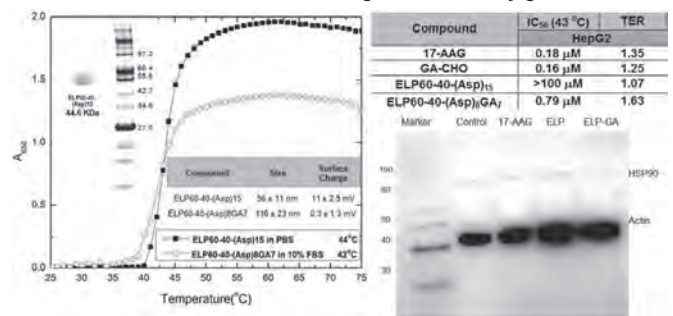
Y. Chen, P. Youn, D.Y. Furgeson

Objectives: Hepatocellular carcinoma (HCC) remains a lethal cancer with extremely low survival rates. Standard thermal, chemo-, and radio-therapies suffer high rates of tumor relapse. Incomplete ablation of tumor margins, poor drug formulation, and lack of drug targeting are suggested as major causes of poor clinical outcomes. Heat shock protein 90 (HSP90) is induced upon thermal stress and shows elevated, native expression in HCC. By chaperoning numerous pro-oncogenic proteins, HSP90 contributes significantly to tumor survival and recurrence. We propose thermoresponsive elastin-based biopolymers (ELPs) conjugated to HSP90 inhibitor, geldanamycin (GA) to specifically target hyperthermia-treated tumor margins. We hypothesize that the combination of thermal ablation to kill the tumor core and elastin-GA bioconjugates, as a chemotherapeutic depot, to eradicate HCC margins will establish a new paradigm for HCC treatment.

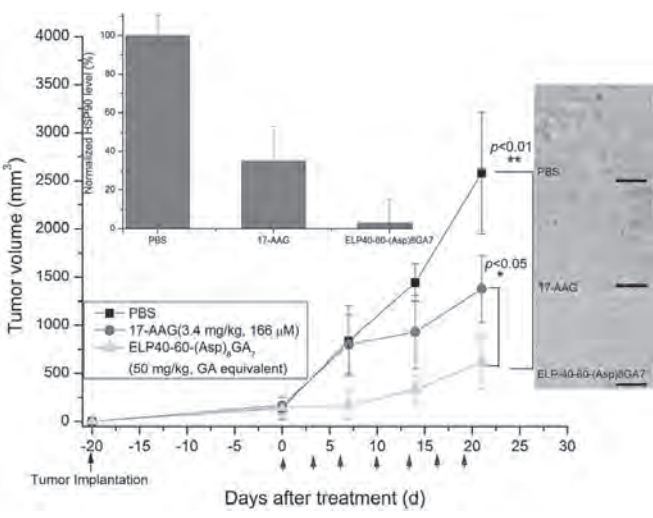
Methods: Recombinant-triblock ELP biopolymer, ELP60-40-(DADAV)_nD were expressed and purified from BLR cells by inverse transition cycling. Aspartic acid residues (D) on ELP were conjugated with GA aldehydes through pH-sensitive, hydrazone bonds to yield ELP-GA conjugates: ELP60-40-Asp(15-m)-GA_m (m: # of GA/polymer). *In vitro* cytotoxicity against HepG2 cells were evaluated by CCK-8 assay. Anti-cancer efficacy was tested in HepG2 tumor-bearing mice. HSP90 expression levels were evaluated by Western blot and immunohistochemistry.

Results: ~50% GA-conjugation was achieved while maintaining a sharp thermal transition near clinical hyperthermic temperatures. The ELP-GA conjugates retained cytotoxicity toward HCCs and were further enhanced with hyperthermia (Fig 1). In addition, the ELP-GA conjugates ($IC_{50} 790 \text{ nM}$) showed a 4.2-fold suppressed tumor growth in an HCC animal model by HSP90 inhibition in the tumor margins (Fig 2).

Conclusions: ELP-GA conjugates show effective suppression of cellular HSP90 expression under hyperthermia and inhibition of tumor growth in mice. Experiments are ongoing evaluating *in vivo* efficacy combining thermal ablation (electrocautery) and concomitant administration of thermo-targeted ELP-GA conjugates.



High purity ELP triblock copolymers were obtained as shown in the SDS-PAGE. ~50% of Asp sites were conjugated with GA [(Asp)₈GA₇]. The conjugates doubled to 116 nm in hydrodynamic size with a neutral surface charge. The conjugate displayed acute thermo-responsiveness in 50% serum with a $T_t \sim 42^\circ\text{C}$ and displayed 1.6-3.0 fold higher cytotoxicity under only 30 min of hyperthermia. Western blot showed effective inhibition of HSP90 by ELP-GA conjugates (1 μM GA equivalent).



17-AAG and ELP-GA conjugates exhibited 2.2- and 4.2- times tumor inhibition compared to PBS control. ELP-GA conjugates (2.7% relative expression) showed 12.1- times more HSP90 inhibition than 17-AAG alone (35%) in tumor margins (scale bar, 100 μm).

Poster 25: Superselective Trans-Arterial Embolization in a Translational Rat Model of Hepatocellular Carcinoma

N. Harrison, S. Hunt, G. Nadolski, C.N. Weber, M. Knaus, M.C. Soulen, C. Simon, T. Gade

Objectives: Recent advances in the molecular biology of hepatocellular carcinoma (HCC) have identified new therapeutic targets that may potentiate the effects of transarterial embolization (TAE). Development of these new therapies requires a pre-clinical model that recapitulates the human disease and allows minimally invasive TAE that mimics the protocol used in patients. We describe a minimally invasive, superselective TAE in a translational rat model of HCC.

Methods: Autochthonous HCCs were induced in Wistar rats (n=26) using an established protocol including ad libitum oral intake of 0.01% diethylnitrosamine (DEN) for 14 weeks. Rats with liver tumors >1 cm in diameter on MRI were selected to undergo the procedure. A single cohort was utilized for protocol development and validation (n=10). Two additional cohorts were selected to undergo selective (n=10) and superselective (n=6) TAE: After anesthetization with isoflurane, the left common carotid artery (LCCA) was exposed via a 3cm incision in the left neck. A 1.5Fr catheter was advanced through an arteriotomy in the LCCA until its tip terminated within the selected lobar artery. In animals selected for superselective embolization, a 1 Fr microcatheter was advanced coaxially through the 1.5 Fr catheter into a segmental artery. Embolization was performed using 40-120μm Embospheres. Upon completion, the arteriotomy was repaired with sutures and the incision was closed primarily.

Results: DEN induced HCCs in the setting of cirrhosis in 26 of 26 rats. Selective lobar artery catheterization with the 1.5 Fr catheter was successful in 16/16 rats, but the 1.5 F catheter could not be advanced more selectively in to segmental branches. Lobar embolization was successfully performed in 10 rats. The use of a 1 Fr catheter co-axially through the 1.5 Fr catheter enabled superselective embolization of segmental arteries in 5 of 6 treated rats.

Conclusions: Minimally invasive, superselective TAE was reproducibly achieved through a LCCA approach in a translational rat model of HCC. This approach allows the opportunity for longitudinal studies of TAE in a clinically relevant HCC model with the potential for repeat therapy on the same animal.

Poster 26: Minimizing Bile Duct Injury During Percutaneous Liver Radiofrequency Ablation: Cooling via Endoscopic Nasobiliary Drainage Tube

E. Felker, S. Lee-Felker, K. Ajwichai, N. Tan, N. Nayak, D. Lu, S. Raman

Objectives: While generally rare, biliary injury has been reported in up to 17% of patients who undergo radiofrequency ablation (RFA) of liver tumors. These complications are more common for tumors located close to the hepatic hilum. Consequently, RFA has generally been considered relatively contraindicated for central liver tumors. The purpose of this study is to investigate whether bile duct injury is reduced by intraductal cooling via an endoscopic nasobiliary drainage (ENBD) tube during radiofrequency ablation (RFA) of liver tumors close to the major bile ducts.

Methods: Of approximately 700 patients treated with RFA for liver lesions between August 2007 and March 2013, 11 consecutive patients underwent 16 RFAs with intraductal cooling via ENBD tube placement for liver tumors close to major bile ducts (< 2 cm from the common bile duct, common hepatic duct, right or left main hepatic duct)

in this IRB-approved, HIPAA-compliant, retrospective study. Chilled D5W (6-8 C) was infused at a rate of 1-2 cc/sec through an endoscopically placed 5 Fr nasobiliary tube to prevent thermal damage during RFA. As controls, 27 patients who underwent 34 RFAs for liver tumors close to major bile ducts without ENBD tube placement were evaluated. The primary study outcome was rate of biliary complications. Local tumor progression (LTP) was a secondary outcome. Fisher's exact tests and Mann-Whitney tests were used to compare the two groups. A P value of less than 0.05 was considered statistically significant.

Results: Of 38 patients, 18 (47%) were male. Mean patient age was 65 years (37-84 years). Mean follow-up was 14 months. Treated tumors included: 35 hepatocellular carcinomas, 4 cholangiocarcinomas, and 11 metastatic tumors. Mean tumor size was 3.2 cm. Mean tumor-to-bile-duct-distance was 6.4 mm. There were no differences between mean patient age, mean tumor-to-bile-duct-distance, and mean tumor size between the cooling and non-cooling groups (P = 0.22, P = 0.46, P = 0.21, respectively). Technical success was 100% (50/50). The rate of biliary complications was significantly lower in the cooling group compared to the non-cooling group (0% versus 29%, P = 0.02). There was no difference in the rates of LTP (27% versus 37%, P = 0.7).

Conclusions: Cooling of the bile ducts with an ENBD tube can prevent biliary complications induced by RFA for liver tumors close to the main bile ducts without increasing rates of LTP.

Poster 27: Ruptured Hepatocellular Carcinoma Following Chemoembolization: Predisposing Factors and Pictorial Review

R.J. Pierami Neto, D. Sella

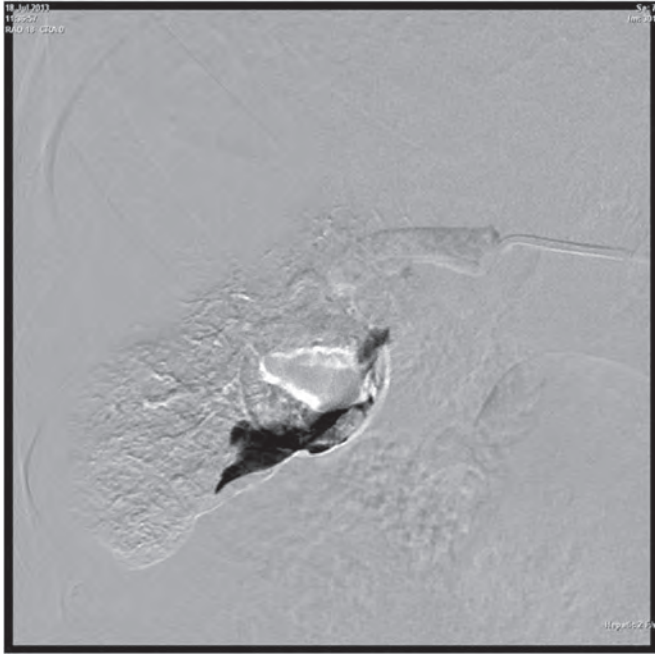
Objectives: In this pictorial review, we discuss the predisposing factors for HCC rupture following chemoembolization, as well as describe adverse events causing morbidity and mortality associated with transarterial chemoembolization.

Methods: Hepatocellular carcinoma incidence has increased worldwide, and HCC has been reported as the third most common cause of cancer related deaths. As a result of its therapeutic successes, survival advantage and minimally invasive technique, transarterial chemoembolization (TACE) has become a well accepted treatment for inoperable HCC. We present pictures of our recent ruptured HCC following chemoembolization case.

Results: Minor complications such as postembolization syndrome, impaired liver function, and leukocytopenia are described in many publications. Rupture following TACE is a rare and ominous complication. Other major complications include a irreversible liver failure, as well as liver abscess, upper gastrointestinal bleeding, bile duct complications, acalculous cholecystitis, pulmonary embolism, spasm or occlusion of hepatic artery and acute renal failure

Conclusions: Ruptured HCC following TACE is a rare but serious complication. Exophytic growth of the tumor, large tumor size and male sex may be predisposing factors for rupture.





Poster 28: Imaging Characteristics, Li-Rads Nomenclature and Treatment Algorithms in Patients with Hepatocellular Carcinoma: An Up-To-Date Primer for Medical Students, Residents and Fellows

H.S. Jagait, R.J. Brandt, M. Tsapakos

Objectives: 1. To demonstrate the imaging characteristics of hepatocellular carcinoma (HCC) and introduce the updated multidisciplinary liver imaging reporting and data system (LIRADS) nomenclature using CT and MR images 2. To comprehensively review treatment paradigms of HCC using LIRADS nomenclature including short-term imaging follow-up guidelines, interventional treatments, and surgical options
Methods: We searched the imaging database at our institution from 2010 to 2014 to obtain high quality CT and MR images of patients with diagnostic criteria or pathology proven HCC. We also demonstrate our institutional experience with multidisciplinary liver tumor conference and our approach to HCC treatment paradigms (short interval imaging follow-up, medical therapy, thermal ablation, loco-regional embolization, surgical transplant) using the LIRADS nomenclature.

Results: The following are presented in didactic format: 1. Pictorial review of the different characteristics of HCC using LI-RADS with multi-modality imaging correlates using CT and MR. 2. Review available treatment options, indications, and a treatment algorithm incorporating the LIRADS classification for patients with HCC.

Conclusions: The updated LIRADS classification tool is an important development in the growing multidisciplinary evaluation and treatment of comprehensive cancer care in patients with HCC. There are a multitude of treatment options spanning the medical, interventional and surgical realms of medicine. This coordinated care and effort requires the requisite understanding by imaging professionals to appropriately describe hepatic lesions utilizing the vernacular spoken by specialists involved in this type of care. This agreed upon lexicon must be familiar to burgeoning radiology professionals as well as understanding the treatment implications in an effort to improve communication, information delivery and ultimately affect patient outcomes.

Poster 29: Revised Recist 1.1 and Volumetric Evaluation for Tumor Response: A Pictorial Review and Comparison

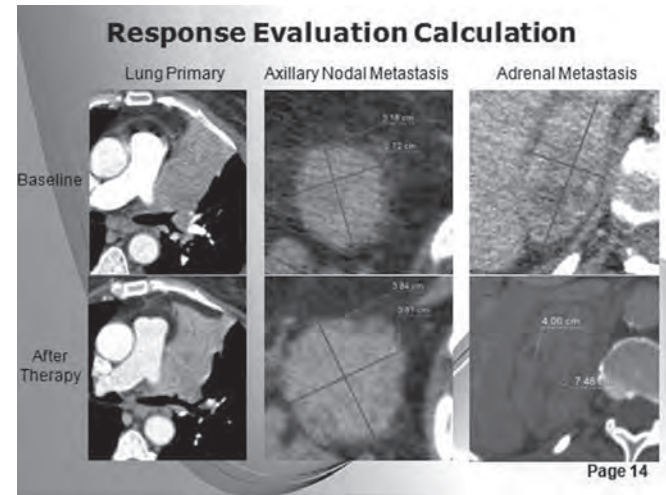
R.J. Pierami Neto, J. Mckinney

Objectives: In this pictorial review, we describe evolution of tumor response criteria and summarize changes between RECIST 1.0 and RECIST 1.1. We describe all response categories and discuss recent data comparing RECIST 1.1 and Volumetric Evaluation (VE) for tumor response.

Methods: Assessment of the change in tumor burden is an important feature of the clinical evaluation of cancer therapeutics: both tumor response and disease progression are useful information in clinical management. RECIST may not estimate disease burden accurately because the one dimensional (1D) measurement often may not produce the actual longest diameter. We reviewed data comparing one-dimensional measurement and VE for tumor response.

Results: Recent data showed excellent correlation between VE and RECIST 1.1. Volumetric Evaluation demonstrated slightly better agreement with RECIST for enlarging lesions than for shrinking lesions.

Conclusions: Volumetric Evaluation (VE) exhibited good concordance with RECIST. VE might be more useful than RECIST for evaluation of shrinking lesions and conglomerate metastases. Overall, one-dimensional (1D) measurements are comparable to volumetric methods, but simpler to implement for routine clinical use and for clinical trials.



Poster 30: Serial Imaging after Irreversible Electroporation

B.J. Bates, J. Ouellette, M. Hellan, R. Brittain, S. Kauffman

Objectives: Irreversible electroporation (IRE) is a new ablative technique in which short, high-voltage pulses are applied to tissues to permeabilize the cell membranes. As little to no thermal energy is created it can be used close to vital structures. Here we report our experience with multiple imaging techniques following IRE treatments, assess for radiologic trends, and begin to correlate these findings with patient outcomes.

Methods: We performed a retrospective data review of all IRE cases performed at our institution from September 2010 to September 2013. Both pre and post procedure imaging studies were collected and data was gathered from the radiology reports including size measurements, changes in enhancement, and descriptive changes. These patients were also evaluated for additional treatments and oncologic outcome. A total of 28 IRE procedures on 27 patients were studied.

Results: 28 IRE procedures were performed in the following anatomic locations: 9 liver, 7 pancreas, 5 lymph nodes (3 pelvic, 1 retroperitoneal, and 1 mesenteric lymph node), 4 pelvis, 1 retroperitoneal, 1 lung, and 1 chest wall. The lesion types consisted of 14 metastases, 8 primary tumors, 5 local recurrences, and 1 lesion not confirmed malignant. The different imaging modalities used included CT, MRI, and PET. 4 cases where imaging was obtained 1-3 days following the procedure showed an initial increase in lesion size with return to normal size or decreased size by follow-up imaging at greater than 1 month. Post ablation changes seen at 1-3 days included air bubbles, fluid collections, and inflammatory stranding and decreased enhancement. 14 cases showed decrease in the lesion size by the first follow-up imaging at greater than 1 month (median 1.75 months), 5 cases showed no change in size on first follow-up imaging at greater than 1 month (median 1.25 months), 2 lesions were immediately resected as the IRE was used for treatment of the tumor margin, and the last 7 were unable to obtain accurate serial measurements for trending purposes. Measurements of the liver lesion's borders post IRE were obscured in a few cases due to the ablation area being larger than the mass itself. Precise measurements of several pancreas lesions were also difficult to after IRE and only decreased enhancement was noted. 6 of the patients had radiologic evidence of disease recurrence at the IRE site at a median time interval of 5.6 months (3 suggested with PET, 2 with CT, and 1 with MRI). The overall median length of follow-up is 8 months (range 1 to 30 months).

Conclusions: Our comprehensive early imaging data review demonstrates the radiographic changes seen in the immediate and early post procedure course of lesions treated with IRE. Our data appears to suggest prognostic information is available from follow-up imaging studies. Longer term imaging and outcomes studies are warranted.

Poster 31: Radioembolisation using Sirtex microspheres; Correlation between pre-treatment Technetium (Tc) 99m - Macroaggregated albumin (MAA) scan and post-treatment Bremsstrahlung Imaging (BSI)

J. Coyne, D. Flowers, I.D. Wilson, B. Stedman

Objectives: The MAA study aims to evaluate presence and degree of pulmonary or splanchnic shunting. Results may also be factored into administered activity calculations. However, the utility of MAA scanning may be overemphasised. The risk of radiation pneumonitis is rare, historically estimated at <1 % and in doses exceeding 30 Gy. Additionally, patients at increased risk of lung shunting are generally predictable

by tumour type and burden. The presence of free ^{99m}Tc-pertechnetate can lead to equivocal or false positive extra-hepatic uptake. MAA closely mimics properties of SIR-spheres so dosimetry is based on the assumption that distribution is identical. But, it has a smaller particle size (10-30µm) than SIR-spheres (35µm +/-5) and is ten-fold less concentrated therefore may not have the same biodistribution. We aimed to evaluate the concordance between pretreatment MAA scan and post-treatment BSI and clinicoradiological follow-up.

Methods: The work-up for Sirtex is extensive involving angiography with coil embolisation of the gastroduodenal artery and right gastric artery to isolate the liver. Following this ^{99m}Tc-MAA is infused from the intended treatment point and distribution assessed on SPECT-CT. Retrospective review of 46 consecutive cases worked up for Sirtex was performed. Angiographic findings were documented and data collated on calculated lung shunt and any extra-hepatic uptake on SPECT-CT following MAA infusion. Tumour type, disease volume and previous therapies were recorded. Comparison was made with subsequent BSI and clinicoradiological follow-up.

Results: SPECT-CT following MAA administration showed non-hepatic uptake in 19/46 patients (41.3%); >10% lung shunting in 6/46 patients (13.0%), gallbladder uptake in 4/46 (8.7%) and other extrahepatic uptake in 15/46 patients (32.6%). Seven patients were excluded on the basis of work-up. Three (6.5%) were excluded on angiographic findings alone. All 7 patients had clear risk factors for shunting including previous hepatic surgery, portal vein embolisation and large volume lesions. The remaining 39 patients underwent Sirtex microsphere treatment followed by subsequent BSI. Dose reduction was applied as per guidelines in the 4 included patients with lung shunting >10%. Only 1 subsequently demonstrated lung activity on post-treatment scan. Extra-hepatic abdominal uptake (excluding gallbladder) was the least concordant, seen in only 1 patient (9.1%) versus the 11 depicted on the MAA work up. Four patients had gallbladder uptake on MAA imaging and 75% of these had corresponding uptake on BSI. In two other patients foci of non-hepatic supply were identified that had not been predicted on work-up SPECT-CT. No adverse clinical events, in particular no gastritis, ulceration, cholecystitis or radiation pneumonitis were observed on follow up.

Conclusions: In our experience, SPECT-CT overcalls extra-hepatic uptake following MAA administration. This may be due to several factors; free technetium may lead to false positive results, MAA may not exactly mirror distribution of SIR-spheres, or coil embolisation may not have produced complete occlusion at the time of the initial scan. This can lead to unnecessary exclusion of suitable patients if not suspected and judicious clinical judgement applied. The use of oral perchlorate should also be considered to avoid equivocal results from free technetium uptake in extra-hepatic tissues. A further aspect to consider is whether MAA scanning is required in all patients as all excluded patients in our experience had predictable clinical and / or angiographic risk factors for shunting .

Poster 32: PERCIST Criteria Predict Survival Following Intra-Arterial Resin-Based Yttrium-90 (Y90) Radioembolization Therapy for Unresectable Chemorefractory Liver Metastatic Disease

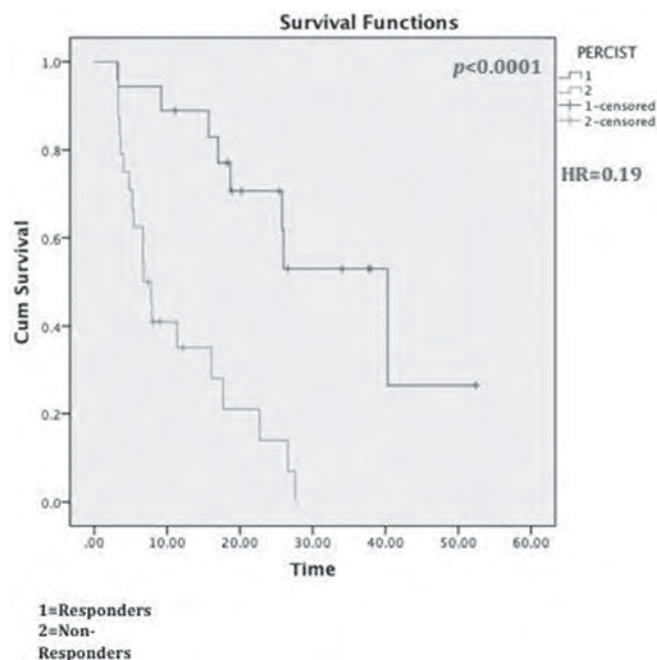
F. Edalat, J.C. Camacho, N. Kokabi, H.S. Kim

Objectives: PET Response Criteria for Solid Tumors (PERCIST) were assessed and correlated with survival analysis after resin-based yttrium-90 (Y90) radioembolization therapy for unresectable, chemorefractory metastatic disease to the liver.

Methods: IRB-approved prospective correlative study of patients with unresectable, metastatic disease to the liver refractory to standard chemotherapy who underwent 18F-FDG PET-CT before and after resin-based Y90 radioembolization. Target PERCIST treatment response was assessed. Significant measurable tumor was defined as lesions ≥1 cm in diameter and maxSUV ≥ 2.5 in targeted and non-targeted lesions. Percentage changes in SUVmax were calculated at baseline and 1-6-months post-Y90 therapy. Objective response included CR and PR. Survival analyses by Kaplan-Meier and Log-Rank proportional models were performed using SPSS software v22.0 (IBM, Armonk, NY) and significance was set at <0.05.

Results: 38 patients and 42 Y90 therapies (57% female, mean age of 63) were included. Cohort included patients with metastatic colorectal carcinoma (48%), melanoma (17%), breast cancer (17%), neuroendocrine tumor (12%), lung cancer (5%) and tonsillar squamous cell carcinoma (2%). After Y90 therapy, target PERCIST criteria showed an objective response rate of 43% (17% CR, 26% PR). Of the remaining patients, 43% demonstrated SD and 14% PD while in therapy. Median overall survival (OS) of the cohort after Y90 was 17.0 (CI 95% 13.0-21.0). Patients demonstrating objective response had a median OS of 40.3 (CI 95% 24.3-56.3) vs. 6.8 (CI 95% 4.5-9.1) in those with SD/PD (p<0.0001). Hazard ratio for the objective response group was 0.19 (p<0.0001) with SD/PD group as reference. Within the metastatic colorectal carcinoma subgroup (n=20, 65% male, mean age of 64), median OS after Y90 was 7.9 (CI 95% 5.0-10.8) and 17.0 (CI 95% 7.3-26.7) in those with objective response vs. 6.7 (CI 95% 4.0-9.4) in patients with SD/PD (p<0.05) with hazard ratio for objective response of 0.30 (p<0.05) with SD/PD group as reference.

Conclusions: In hepatic metastatic disease refractory to standard chemotherapy, PERCIST criteria predict OS for assessment of response following Y90 radioembolization therapy.



Poster 33: Safety of Hepatic Radioembolization Following Major Liver Resection

J. Kessler, R. Nelson, J. Kim, G. Singh, Y. Chen, J.J. Park

Objectives: The purpose of this study was to evaluate the safety of hepatic radioembolization following major liver resection.

Methods: A retrospective review was performed of consecutive patients who had previously undergone major liver resection and were subsequently treated with radioembolization at a single center from 2008-2013. Demographic data, prior surgical history, hepatic volumes, and treatment related toxicities were systematically reviewed. Data were summarized using medians and interquartile ranges (IQR) for continuous data and patient number and percentages for categorical data. Linear regression and the Fisher Z transformations were used to calculate the Pearson correlation coefficient and 95% confidence interval, respectively.

Results: The study population was comprised of 12 men (66.7%) and 6 women. Median age at treatment was 65 (IQR 60-68). Underlying malignancies were colorectal (n=8), hepatocellular (n=5), neuroendocrine (n= 4), and parathyroid (n=1). Prior surgical resection included wedge/segmental (n=9) and lobar hepatectomy or greater (n=9). Prior locoregional treatments included thermal ablation (n=8) and transarterial therapy (n=5). Median follow up was 241 days (IQR 174-373). 15 patients were treated with resin microspheres and 3 were treated with glass microspheres. In 9 patients, the entire remnant liver was treated in a single session, whereas the other 9 patients were treated in 2 sessions. Median dose for the first treatment was 1.2 Gbq (IQR 0.8-1.4) and 0.7 Gbq (IQR 0.6-1) for the second treatment. Toxicities within 90 days of radioembolization included 13 grade 1/2 in 10 patients and no grade 3/4. Minor toxicities included pain (n=4), nausea (n= 3), fatigue (n=2), bilirubin (n=2), ALT/AST (n= 1), albumin (n= 1). Median calculated liver volume based on body surface area (BSA) was 1455 ml (IQR 1321-1664). Median measured liver volume was 1298 ml (IQR 1100-1603). Liver volume calculated from body surface area prior to radioembolization was only weakly correlated with actual measured liver volumes (correlation coefficient 0.45, 95% CI: -0.02-0.76). No significant differences were noted at follow up between patients treated using a single whole liver session or split dose over two sessions.

Conclusions: Yttrium-90 hepatic radioembolization appears safe in patients who have undergone both minor and major hepatic resections. Treatment in a single session to the entire remnant liver demonstrated no increased toxicity. The correlation between BSA calculated and actual liver volumes in this population was weak. Further investigation is required to identify the ideal dosing for these patients.

Poster 34: Y-90 Radioembolization of Pancreatic Cancer Metastatic to the Liver

T. Techasith, Z. Devcic, A. Banerjee, G.A. Fisher, P.L. Kunz, J.D. Louie, D.Y. Sze

Objectives: Non-neuroendocrine pancreatic cancer carries an extremely poor prognosis, with median overall survival (OS) of 6 months for stage 4 disease. Eventual treatment failure while on systemic chemotherapy is inevitable, with local and hepatic metastases being the most frequent sources of morbidity and mortality. We present our

initial data on Y-90 radioembolization (RE) of pancreatic cancer metastatic to the liver after failure of systemic chemotherapies.

Methods: Between April 2008 and September 2013, 10 patients with pancreatic cancer and liver-dominant metastatic disease underwent RE treatment. All patients had progressive disease during or after pancreatic resection and/or systemic chemotherapy, with exposure to a median of 2 different regimens. All patients received whole liver RE treatment performed with resin microspheres. Eight of 10 patients had pathologic diagnosis of pancreatic adenocarcinoma; 1 had acinar cell carcinoma and 1 had solid pseudopapillary tumor. Clinical and biochemical toxicities graded by NCI-CTCAE v4.03, ECOG performance status, and serum tumor marker (CA 19-9) were recorded at baseline, 2 weeks, 4 weeks, and every 4 weeks thereafter. Radiographic response was recorded every 2-3 months and classified according to RECIST.

Results: Median time from diagnosis of pancreatic cancer to RE treatment was 447 days, and median time from diagnosis of hepatic metastases to treatment was 353 days. The median dose delivered was 1.78 GBq. Baseline performance status of all patients was either 0 or 1, which was maintained by 9 of 10 patients at 4-week follow-up. One patient had a significant decline (0 to 3) at 4 weeks and did not survive to the next follow-up, succumbing to progressive disease. The most common clinical toxicity encountered was grade 1-2 abdominal pain, either self-limited or responsive to analgesics and proton-pump inhibitors, occurring in 8 patients. Three of 8 patients reported similar pain at baseline before RE treatment. Other significant clinical toxicities included ascites, occurring in 4 patients, possibly related to portal hypertension and/or tumor progression. No significant biochemical toxicity was observed. Tumor marker responses varied. Six patients had an elevated CA 19-9 at baseline and adequate follow-up. Initial follow-up at 2 weeks demonstrated an increased tumor marker in 4 of 6 patients, presumably secondary to tumor lysis. At subsequent follow-up, all patients demonstrated either return to baseline or lower than baseline, with 2 of 6 showing an overall decrease of >50%. Follow-up imaging was available in 8 of 10 patients. Of these, 6 demonstrated stable disease (SD) and 2 demonstrated progressive disease (PD) at 3 months, for a disease control rate of 60%. Four patients resumed systemic treatment after RE. Median overall survival was 155 days after RE. When including only patients with pancreatic adenocarcinoma, the median overall survival was 139 days. Seven of 10 patients died during the follow up period, all of whom had pancreatic adenocarcinoma, with post-RE survival ranging from 44 to 360 days. One patient with pancreatic adenocarcinoma remains alive 100 days after RE and 2 patients with other tumor subtypes remain alive, including 1 patient with metastatic acinar cell carcinoma alive and without evidence of disease over 5 years after RE.

Conclusions: Salvage therapy Y-90 RE of hepatic metastases from pancreatic cancer demonstrated modest benefit with median overall survival of approximately 5 months and disease control rate of 60%, comparing favorably to other salvage therapies with reported survivals of 3-5 months and disease control rates of about 20%. Cell types other than adenocarcinoma may benefit even more.

Poster 35: Comparison of Resin versus Glass Microsphere Radioembolization for Neuroendocrine Hepatic Metastasis: Clinical and Imaging Response

C. Ahuja, M. Chadha, J.J. Critchfield, Y. Kharoti, J.A. Kaufman, K. Farsad, K.J. Kolbeck

Objectives: To compare clinical and imaging response of resin versus glass microsphere Y-90 radioembolization for treatment of unresectable hepatic neuroendocrine metastasis.

Methods: This is a two institution retrospective study of 26+24 (Group A and B) patients treated with Y-90 radioembolization. Clinical symptoms, biochemical markers and imaging at 1, 3, 6, 12, and 18 months were reviewed. Tumor response was evaluated using response evaluation criteria in solid tumors RESIST 1.1. Other medical and interventional therapies were also recorded.

Results: Patient subset: Group A, 26 patients with mean age 60 treated with resin microspheres (SirSpheres). Group B, 24 patients with mean age 59 treated with glass microspheres (TheraSpheres). Site of primary: pancreas 13 (6 from group A and 7 from group B), small bowel 20 (10 from group A and 10 from group B), colon 8 (4 each from group A and group B), other 7 (4 from group A and 3 from group B), unknown 2 from group A. All patients were on octreotide therapy. Other procedures: TACE 25 (21 from group A and 4 from group B), Bland embolization 1 from group B, RFA 8 (6 from group A and 2 from group B), Cryo 1 from group B. Y-90 Tt: Single 25 (20 from group A and 5 from group B), Multiple 25 (6 from group A and 19 from group B) Tumor response RESIST 1.1: Partial 40% (11 from group A and 9 from group B), Stable 52% (13 from group A and 13 from group B), Progressive 8% (2 each from group A and B) Symptomatic response: Improved 72% (18 each from group A and B), Stable 28% (8 from group A and 6 from group B) Biochemical response: Improved 42% (10 from group A and 11 from group B), Stable 56% (15 from group A and 13 from group B), Worsened 2% (1 from group A).

Conclusions: The glass microspheres group B patients received more bilobar treatments. The group A patients treated with resin microspheres received more unilobar treatments to the tumor dominant lobe with the other lobe treated with TACE as per institutional guidelines. There was no outcome difference between the tumor non dom-

inant lobe treated with radioembolization versus TACE. Y-90 microsphere radioembolization (resin or glass microspheres) is a safe and effective therapy for hepatic neuroendocrine metastasis. There was no statistically significant difference in outcomes between the two types of radioembolization.

Poster 36: Effect of Substituting 50% Isovue for Sterile Water as the Delivery Medium for SIR-Spheres: Improved Delivery and Decreased Administration Time

C. Chao, J.I. Mondschein, M. Dagli, D. Sudheendra, S. Stavropoulos, M.C. Soulen

Objectives: To evaluate the effect of substituting 50% Isovue for sterile water as the injection medium during SIR-Spheres radioembolization on percentage delivery of the radioembolic agent and on administration time.

Methods: We reviewed all radioembolization procedures at our facility using SIR-Spheres from January 1, 2011 to December 31, 2013. Beginning May 1, 2013, one experienced proctor used 50% Isovue in saline instead of sterile water in both the "B" and "D" lines of the infusion set. We compared the fraction of the prepared dose Y-90 SIR-Spheres delivered when using sterile water versus contrast as well as the administration times. We also recorded if the embolization was terminated because of stasis or decreased flow.

Results: 168 radioembolizations were performed using SIR-Spheres, 78% with sterile water as the delivery medium and 22% (37 cases) with 50% Isovue in saline as the delivery medium. The mean percentage of Y-90 dose administered was 98% with contrast versus 87% for sterile water ($p = 0.00000001$). >97% of the cases using contrast resulted in greater than or equal to 90% delivery of the Y-90 dose, versus 59% cases with sterile water ($p = 0.00000001$). For cases using water, 17% were terminated for stasis or decreased flow versus 3% (1 case) using contrast. The average administration time of the Y-90 dose was 7 minutes with contrast versus 23 minutes for sterile water ($p = 0.016$). Excluding cases requiring coil embolization, mean fluoroscopy time for contrast administration was 8.4 minutes versus 11.5 minutes with water ($p = 0.009$).

Conclusions: Near-complete delivery of the prepared SIR-Sphere dose was consistently achieved when using dilute contrast as the delivery medium, a significant technical improvement over water delivery. Termination for stasis occurred in only one case. The average administration time was 3 times shorter when using dilute contrast, with significant reduction in fluoroscopy time. Using contrast as the delivery medium allowed continuous real-time monitoring of the Y-90 microsphere administration, mitigating the chance of reflux and non-target embolization.

Poster 37: Impact of WHO 2010 Histologic Classification on Hepatic-PFS Following Radioembolization of NET Metastases

C. Chao, M. Dagli, J.I. Mondschein, S. Stavropoulos, M.C. Soulen

Objectives: In 2010 the World Health Organization (WHO) and European Neuroendocrine Tumor Society (ENETS) adopted a new grading scheme for neuroendocrine tumors based on the mitotic index and Ki-67 staining. Tumors with 0-1 mitoses per 10 high-power fields and Ki-67 staining of <2% are Grade 1, 2-20 mitoses/10 HPF or Ki-67 of 3%-20% are grade 2, and above this are grade 3. While there has been some debate about the exact cutoff between grade 1 and 2, this grading system has been validated for prevalence of metastases at diagnosis, recurrence following curative resection, and overall survival. The relevance of histologic grade to disease control following liver-directed therapy is not known. We did an exploratory retrospective analysis of a cohort of patients treated with radioembolization since the initiation of the new grading system.

Methods: From 2011-2013, 26 patients with NET liver metastases with known histologic grade were treated with radioembolization using resin microspheres dosed according to the BSA method. Triple-phase imaging was obtained at baseline, every three months for the first year, and every 4-6 months thereafter in the absence of progression. Hepatic progression was defined by RECIST criteria. Patients with hepatic progression were retreated if eligible, but only the first cycle of radioembolization was included in the analysis.

Results: WHO 2010 Grades were 1 in six patients, 2 in 14 patients, and 3 in six patients. Most grade 1 and 2 patients were on Sandostatin. All Grade 3 patients received systemic chemotherapy either before or concurrently with radioembolization. Two patients received PRRT in addition to radioembolization. At six months and one year, the disease control rate in the liver was 100% and 100% for Grade 1, 92% and 69% in grade 2, and 80% and 80% in Grade 3 ($p = 0.48$). Among the grade 1 patients, only a single case of hepatic progression was observed, at 23 months.

Conclusions: This exploratory analysis suggests that radioembolization provides durable control of hepatic metastases irrespective of grade.

Poster 38: Standardized Added Metabolic Activity (SAM) in Predicting Survival Following Intra-Arterial Resin-Based Yttrium-90 (Y90) Radioembolization Therapy for Unresectable Chemorefractory Metastatic Colorectal Cancer to Liver

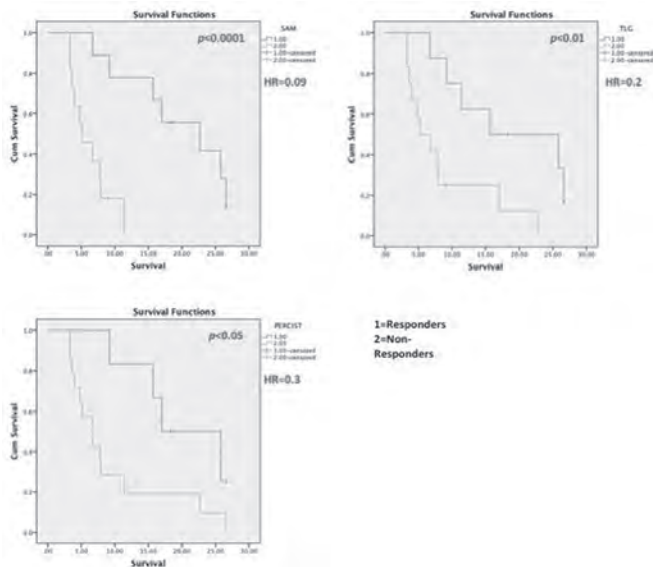
F. Edalat, J.C. Camacho, N. Kokabi, H.S. Kim

Objectives: Standardized added metabolic activity (SAM), total lesion glycolysis (TLG) and PET Response Criteria for Solid Tumors (PERCIST) were assessed and correlated with survival analysis after resin-based yttrium-90 (Y90) radioembolization therapy for unresectable, chemorefractory colorectal liver metastatic disease.

Methods: IRB-approved prospective correlative study of patients with unresectable, colorectal liver metastatic disease refractory to standard chemotherapy who underwent 18F-FDG PET-CT before and 1-6 months after resin-based Y90 radioembolization. Target ΔSAM, ΔTLG, and PERCIST treatment response was assessed. Significant measurable tumor was defined as lesions ≥1 cm in diameter and maxSUV ≥ 2.5 in targeted lesions. Percentage changes in maxSUV, TLG and SAM were calculated at baseline and 1-6-months post-Y90 therapy and objective response was defined as >30% change (responders). Survival analyses by Kaplan-Meier, Log-Rank and Cox proportional models were performed using SPSS software v22.0 (IBM, Armonk, NY) and significance was set at <0.05.

Results: 17 patients and 20 Y90 therapies (65% male, mean age of 64) were included. After Y90 therapy, target ΔSAM showed an objective response rate of 45% vs. 45 and 30% for assessment based on target ΔTLG and PERCIST criteria, respectively. Median overall survival (OS) of the cohort after Y90 was 7.9 (CI 95% 5.0-10.8). Patients demonstrating objective response based on ΔSAM had a median OS of 22.7 (CI 95% 8.8-36.6) vs. 5.2 (CI 95% 2.3-8.1) in non-responders (p<0.0001). Kaplan-Meier survival curves for OS based on ΔSAM, ΔTGL and PERCIST criteria are included in figure 1. Hazard ratio for the objective response group based on target ΔSAM was 0.092 (p=0.003) vs. 0.236 (p=0.016) and 0.297 (p=0.039) based on target ΔTLG and PERCIST criteria, respectively, with non-responder group as reference.

Conclusions: In colorectal liver metastatic disease refractory to standard chemotherapy, ΔSAM, ΔTLG and PERCIST criteria predict OS for assessment of response following Y90 radioembolization therapy.



Poster 39: Survival, Tolerability, and Objective Response Following Selective Internal Radiotherapy (SIRT) Using Yttrium-90 Labeled Sirsphere Microspheres for Hepatic Metastases in Chemotherapy Refractory Metastatic Breast Cancer

A. Moin, N. Sharma, F. Moeslein

Objectives: To assess survival, tolerability, and objective response following Selective Internal Radiotherapy (SIRT) using yttrium-90 labeled SirSphere microspheres for hepatic metastases in chemotherapy refractory metastatic breast cancer.

Methods: A single institution, retrospective review focused on overall survival, objective response and adverse events of 16 female patients with chemotherapy refractory metastatic breast cancer and liver dominant metastatic disease who underwent SIRT using yttrium labeled SirSphere microspheres between 2007 and 2012.

Results: The mean age of the 16 treated patients was 52.8 years. Thirteen patients (81%) were eligible for inclusion for Kaplan-Meier analysis as three patients were still living at the time of review. The range of overall survival after microsphere therapy was 45 days to 623 days with median survival of 235 days. At least eleven patients (69%) were undergoing some concurrent systemic chemotherapy at the time of initial therapy. Fourteen patients (88%) underwent at least two sessions of single lobe micros-

phere therapy; one patient had a single session of whole liver therapy and another patient received a single session of single lobe therapy. Using mRECIST criteria at 3 months post-treatment there were no Complete responses (CR), 5 (56%) Partial responses (PR), 3 (33%) Stable Disease (SD), and 1 (11%) Progressive Disease (PD) responses. (Note 3 patients had either no available pre-treatment or follow-up imaging and were not included in this analysis.) No Grade 4 or 5 Adverse Events were reported.

Conclusions: Metastatic breast cancer with hepatic spread portends a poor prognosis, with historical median survivals of 4-6 months. SIRT for management of hepatic metastases in patients with chemotherapy refractory metastatic breast cancer provides a survival advantage while simultaneously being well tolerated with few systemic and regional side effects. Further prospective studies to better determine when and how to incorporate SIRT into the routine management of metastatic breast cancer are needed.

Poster 40: Bevacizumab-Associated Angiographic Findings and Complications During Radioembolization Planning and Treatment in Metastatic Colorectal Patients

D. Goldin, D. Jack, E. Walsh, J. Handel, M. Savin

Objectives: To demonstrate and discuss angiographic findings and clinical implications of bevacizumab during arterial based liver-directed therapy.

Methods: A retrospective review of metastatic colorectal patients undergoing radioembolization between 2008-2013 was performed. Cases were selected to illustrate angiographic findings seen in patients pretreated with bevacizumab. Current literature regarding bevacizumab with attention to angiographic findings, treatment-related angiographic complications, and potential implications for arterial based treatments was reviewed.

Results: The majority (77%) of metastatic colorectal patients between 2008-2012 had received bevacizumab prior to radioembolization, with 44% of these patients having a short interval (<3 months) between radioembolization and their last dose of bevacizumab. Several examples demonstrate marked decrease in the hepatic arterial size and flow. We show a case of dissection of a replaced right hepatic artery during hepatic arteriography for radioembolization planning. The dissection, occurring with minimal arterial manipulation, led to termination of the procedure and the inability to treat as scheduled. The frequency of bevacizumab use and its long half-life (up to 20 days) highlights the potential importance of prior usage. When considering angiography and radioembolization, treatment-related complications may increase with prior/recent bevacizumab use, requiring a cautious approach to the procedure.

Conclusions: Potential bevacizumab effects, including slow flow and arterial dissection, necessitate caution during hepatic angiographic procedures to limit complications. Temporary cessation of bevacizumab should be considered prior to arteriography.

Poster 41: Combination Treatment with Comprehensive Cryoablation and Immunotherapy in Metastatic Hepatocellular Cancer

C. Jibing

Objectives: To retrospectively assess the effect of comprehensive cryosurgery (ablation of intra- and extrahepatic tumors) plus dendritic cell-cytokine-induced killer cell immunotherapy in metastatic hepatocellular cancer.

Methods: We divided 45 patients into cryo-immunotherapy (21 patients), cryotherapy (n = 12), immunotherapy (n = 5) and untreated (n = 7) groups. Overall survival (OS) after diagnosis of metastatic hepatocellular cancer was assessed after an 8-year follow-up.

Results: Median OS was higher following cryo-immunotherapy (32 mo) or cryotherapy (17.5 mo; P < 0.05) than in the untreated group (3 mo) and was higher in the cryo-immunotherapy group than in the cryotherapy group (P < 0.05). In the cryo-immunotherapy group, median OS was higher after multiple treatments (36.5 mo) than after a single treatment (21 mo; P < 0.05).

Conclusions: Cryotherapy and, especially, cryoimmunotherapy significantly increased OS in metastatic hepatocellular cancer patients. Multiple cryo-immunotherapy was associated with a better prognosis than single cryo-immunotherapy.

Poster 42: Percutaneous Ultrasonography and Computed Tomography Guided Pancreatic Cryoablation: Feasibility and Safety Assessment

N. Ilzhi

Objectives: To assess the safety and feasibility of percutaneous cryoablation on pancreatic cancer via ultrasonography (US) and computed tomography (CT) guidance.

Methods: This retrospective review was approved by the institutional review board and of informed consent. Thirty-two patients (18 men and 14 women; median age 62; age range, 30–77 years) with pancreatic cancer (stage II/III/IV, 3/11/18) treated with percutaneous US and CT guided cryoablations between February 2009 and February 2010 were eligible for this review. Thirteen tumors in pancreatic head and 19 in pancreatic body and/or tail measuring 2–11 cm (mean, 5.2 cm ± 8 [standard deviation]) were ablated with 49 procedures in total. Feasibility was analyzed by enhanced CT 1–3 months post procedure and safety was assessed by clinical signs, symptoms and laboratory results.

Results: Neither procedural death nor serious complications occurred. Fifteen tumors (46.9%) smaller than 5 cm were successfully ablated by one session of cryoablation. Twenty-seven patients experienced a P50% reduction in pain score, 22 experienced a 50% decrease in analgesic consumption and 16 experienced a P20 increase in Karnofsky Performance Status (KPS) Score. Partial response (PR) and stable disease (SD) turned up in 9 and 21 patients, respectively, lesions in whom were identified controlled by none enhancement on enhanced CT. Mean and median survival was 15.9 and 12.6 months, respectively. The 6-, 12- and 24-month survival rates were 82.8%, 54.7% and 27.3%, respectively.

Conclusions: US and CT guided percutaneous cryoablation is a safe and promising local treatment for pancreatic cancer.

Poster 43: Longitudinal Quality of Life Assessment in Patients with Hepatic Metastatic Neuroendocrine Tumors Treated with Yttrium-90 Transarterial Radioembolization

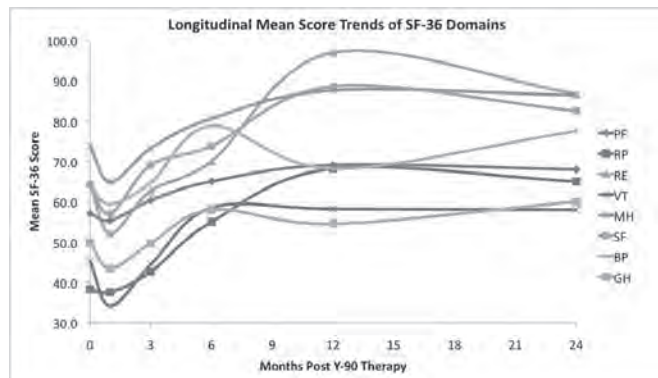
B. Cramer, M. Xing, G. Webber, H.S. Kim

Objectives: To determine the longitudinal effect of Yttrium-90 (Y-90) transarterial radioembolization therapy on health-related quality of life (HRQOL) in patients with neuroendocrine tumor (NET) hepatic metastases.

Methods: Single-center IRB-approved prospective health-related quality of life study using the Short-Form 36 (SF-36) assessment tool pre- and post-Y-90 radioembolization. Baseline HRQOL scores were evaluated for significant ($p < 0.05$) change within the total patient population at 1, 3, 6, 12, and 24 months following treatment using the paired t-test. Patient HRQOL norm-based summary scores before and after treatment with Y-90 radioembolization were compared to the U.S. healthy population and were correlated with mean survival time from Y-90 treatment.

Results: Thirty patients (13 males, 17 females) with NET hepatic metastases were enrolled. Patient age ranged from 25 to 76 years with a mean of 60 years. The median length of time from initial Y-90 treatment to the first follow-up survey was 63 days. There were no significant differences in General Health, Physical Functioning, Bodily Pain, Vitality, Role-Physical, or Role-Emotional domains when comparing pre-treatment scores to 1, 3, 6, 12, and 24-month follow-up scores. In the Mental Health (MH) domain, mean score at 6 month follow-up was significantly higher than pre-treatment mean score (80.60 vs. 73.83, $p = 0.007$). However, there were no significant differences when comparing pre-treatment (73.83) to follow-up MH mean scores at 1 month (64.81, $p = 0.282$), 3 months (73.24, $p = 0.615$), 12 months (87.64, $p = 0.541$), or 24 months (86.40, $p = 0.456$). In the Social Functioning (SF) domain, mean score at 12-month follow-up was significantly higher than pre-treatment mean score (88.64 vs. 64.17, $p = 0.019$). However, there were no significant differences when comparing pre-treatment (64.17) to follow-up SF mean scores at 1 month (57.03, $p = 0.406$), 3 months (69.12, $p = 0.366$), 6 months (73.75, $p = 0.496$), or 24 months (82.50, $p = 0.208$). Enrolled patients had decreased mean baseline HRQOL Mental Component Summary (MCS) and Physical Component Summary (PCS) norm-based scores compared to the U.S. healthy population (MCS 47.8 vs. 50.0; PCS 39.4 vs. 50.0). After treatment, mean MCS was higher compared to the U.S. healthy population at 6 months (51.0 vs. 50.0), 12 months (57.9 vs. 50.0), and 24 months (55.2 vs. 50.0). After treatment, mean PCS remained lower compared to the U.S. healthy population at 1, 3, 6, 12, and 24 months (39.4-44.4 vs. 50.0). At the conclusion of data collection, 19 of 30 enrolled patients were living. Of the deceased ($n = 11$), mean survival was 18.0 months after Y-90 radioembolization. Deceased patients with pre-treatment MCS over 50.0 ($n = 5$) had significantly longer survival than those with pre-treatment MCS under 50.0 ($n = 6$) (10.4 vs. 27.2 months, $p = 0.043$). Deceased patients with pre-treatment PCS over 50.0 ($n = 2$) had significantly longer survival than those with pre-treatment PCS under 50.0 ($n = 9$) (42.3 vs. 12.7 months, $p = 0.001$).

Conclusions: Patients with hepatic metastatic NET are not likely to perceive decreases in any of the HRQOL domains at 1, 3, 6, 12, or 24 months after Y-90 radioembolization. Patients may perceive temporary increases in MH and SF domains at medium-term (6 and 12-month) follow-up.



Poster 44: Percutaneous Augmented Peripheral Osteoplasty in Oncologic Patients: Clinical Experience and Results

A. Kelekis, D. Filippiadis, G. Velonakis, E. Alexopoulou, A. Malagari, E. Brountzos, N. Kelekis

Objectives: To evaluate clinical efficacy and safety of augmented peripheral osteoplasty in a series of consecutive oncologic patients. To evaluate long term follow-up in oncologic patients who underwent augmented peripheral osteoplasty in symptomatic lesions of long bones.

Methods: Percutaneous augmented peripheral osteoplasty was performed in 12 patients (10 male / 2 female) suffering from symptomatic lesions of long bones with pain resistant to medication. Malignant substrate of the lesions included multiple myeloma (3 patients), hepatocellular carcinoma metastasis (3 patients), bronchogenic carcinoma metastasis (3 patients), renal cell carcinoma metastasis (1 patient), prostate carcinoma metastasis (1 patient) and neuroesthesioblastoma metastasis (1 patient). Locations included femoral bone (9 patients) and humeral bone (3 patients). Under extensive local sterility measures (including prophylactic antibiotics), general anaesthesia and fluoroscopic guidance, a direct access to the lesion was obtained by 11G vertebroplasty needles. Multiple fluoroscopic projections and a contrast medium injection verified the proper needle placement inside the lesion. Then, coaxially, a metallic mesh consisting of 25 - 50 stainless steel micro-wires (22 G, 2 - 6 cm length) was inserted in the lesion of interest under fluoroscopic control followed by PMMA injection. CT assessed implant position 24 hours post treatment. Clinical evaluation included immediate and delayed follow-up studies of patient's general condition and neurological status. An NVS scale on a questionnaire helped assessing pain relief degree and overall mobility improvement.

Results: Mean follow-up was 16.17 ± 10.93 months (range 2-36 months). Comparing the patient's scores prior (8.33 ± 1.67 NVS units) and post (1.42 ± 1.62 NVS units) augmented peripheral osteoplasty, patients in our study presented a mean decrease of 6.92 ± 1.51 NVS units. Overall mobility improved in 12/12 patients. No complication was observed. There was no change or migration of the implant during the follow-up period.

Conclusions: Percutaneous augmented peripheral osteoplasty (metallic mesh of stainless steel micro-wires and PMMA injection) for symptomatic malignant lesions in long bones seems to be a possible new technique for bone stabilization. This combination seems to provide the necessary stability against the shearing forces applied in long bones during weight bearing. Which patients will benefit from this new technique still remains a question that requires further study.

Poster 45: CT-Guided Percutaneous Cryoablation of Bone and Soft Tissue Tumors

Y. Xiao

Objectives: To assess the safety and efficacy of the CT-guided percutaneous cryoablation of bone tumors.

Methods: From January 2007 to July 2013, 98 patients with bone and soft tissue tumors were treated with CT-guided percutaneous cryoablation. Their mean age was 56 years (ranging from 10-85 years). The approval from the local ethics committee and individual patient consent were acquired before each operation. The procedures were carried out under conscious sedation and local anesthesia. CT system (Philips Brilliance Big Bore 16, slice thickness: 2 mm, KV120, MAS: 250) was used for procedural planning, instrument guidance and procedural monitoring of the ice ball formation. An argon-based cryoablation system was used (CryoHit; Galil Medical, Yokneam, Israel). Each cryoablation included two freezing-thawing cycles. Follow-up was performed to assess technical and clinical outcome. The mean follow-up period was 28.7 months (ranging from 18-36 months).

Results: Cryoablation were successfully performed on all patients. No major immediate or postponed complications were observed. Clinical success rate was 100.0% in all. Significant pain relief was observed in all patients after operation. Specifically, the degree of pain relief evaluated in visual analogue scores (VAS) were and before and one month after each operation, respectively. Pain recurrence was observed 30 patients with metastasis of bone and soft tissues. Moderate fever (lower than 38°C) was observed in 20 patients one day after operation.

Conclusions: CT-guided percutaneous cryoablation is a safe and effective minimally invasive procedure for the treatment of bone and soft tissue tumors.

Poster 46: Imaging Findings and Clinical Outcomes in Percutaneous Cryoablation of Extra-Abdominal Desmoid Tumors

P.G. Wortley, D. Monson, G. Webber, T. Seale, R. Williams

Objectives: To investigate the imaging changes and associated clinical outcomes in patients with extra-abdominal desmoid tumors treated with percutaneous cryoablation.

Methods: This was a retrospective non-IRB approved study between April 2012 and December 2013, 8 patients (5 female and 3 male; age range from 25-71, mean age 38) underwent CT guided percutaneous cryoablation for palliation of extra-abdominal desmoid tumors. Patients were referred for either local tumor/pain control or improved

range of motion. 3 patients (38%) had undergone prior treatment consisting of either surgical resection (3/8) and/or radiation (2/8). Tumor size ranged from 4.7 cm to 22 cm in largest diameter and 22 cm³ to 8,220 cm³ in volume. Tumors were located in the trunk, paraspinous region, hip, and thigh. Patient imaging response, clinical success, and complications were evaluated. Imaging response was characterized by change in size along with change in signal characteristics and morphology on MRI and change in attenuation on CT. Technical success was defined as serial regional low density consistent with cryoablation confined to the lesion preserving native muscle or neurovascular structures. Clinical success was defined as improvement in clinical symptoms of pain, range of motion, and subjective tumor size following cryoablation.

Results: A total of 17 percutaneous cryoablation procedures were performed in 8 patients with biopsy proven extra-abdominal desmoid tumors. Multiple ablations were performed on 4 patients (50%). 3 tumors (38%) showed decrease in size, with mean decrease in volume of 70% on follow up imaging and no tumors increased in size. The two largest tumors treated (volumes of 8,220 cm³ and 1,927 cm³) showed no change in overall size. CT follow up was available for 4 patients (50%), with all demonstrating decreased attenuation in an area of >50% of the ablation zone. MRI follow up was available in 6 of 8 (75%) patients and all tumors demonstrated increased T2 signal in an area of >50% of the ablation zone size. 3 tumors (50%) showed increased T1 signal in the ablation zone in a similar distribution to the changes on T2 weighted images. These signal changes persisted on multiple follow up exams. Contrast enhanced imaging was only obtained in 2 patients and both demonstrated lack of contrast enhancement in the ablation zone, which corresponded to the area of T2 hyperintensity that occurred in all patients. Clinical follow up was available for 6 of 8 (75%) patients, with clinical success occurring in 5 out of 6 of these patients (83%). No minor complications occurred. Major complications occurred in 2 patients (25%, SIR category C and E, respectively), both related to nerve injuries. Both of these patients had tumors intimately associated with major neurovascular structures.

Conclusions: Percutaneous cryoablation is a suitable alternative treatment in the management of extra-abdominal desmoid tumors, for which the standard treatment of surgical excision carries a high rate of morbidity in many patients. Care must be taken with tumors in close proximity to major neurovascular structures.

Poster 47: Palliation of Malignant Biliary Obstruction with Percutaneous Biliary Drains

J.G. Mammarrappallil, S. Bao, J. Requarth

Objectives: Percutaneous transhepatic biliary drain (PTBD) placement is a commonly used interventional radiology technique for the palliation of patients with malignant biliary obstruction. The obstruction of PTBDs is easily diagnosed and treated, but PTBDs are thought to be unacceptably painful and body dysmorphic. This study aims to examine the outcomes of patients who have had PTBD placement for palliative care in preparation for a comparative effectiveness analysis of different palliative care drainage techniques.

Methods: This retrospective study analyzed patients who underwent PTBD placement for malignant biliary obstruction at an academic interventional radiology practice between 2007 to 2010. The demographics, level of obstruction (hilar or common bile duct), number of drains, and dates of drain placement and exchanges were ascertained from the electronic medical record. Patients who subsequently had their drains removed for self-expanding covered stents or surgery were excluded. Values are given as mean +/- standard deviation. The time between the first drain placement and the last drain exchange is used as a rough gauge for survival. Statistical analysis was conducted using Fisher's exact test with a 2-tailed P-value; a P-value of less than 0.05 was considered significant.

Results: A total of 94 patients were included in this study: 61 men and 33 women. Women (72.6 +/- 11.8 years) were significantly older than men (64.6 +/- 11.9 years) at the time of initial PTBD placement (P=0.002). Hilar obstruction was seen in 51.1%, and the common bile duct was obstructed in 48.9%. Patients with CBD obstruction only received 1 drain; whereas, those with hilar obstruction were apt to receive 2 drains (50%). Although there was no difference between the percentage of men and women with hilar obstruction, women were statistically more likely to receive 2 drains for hilar obstruction (p=0.01). Patients with hilar and CBD obstruction were not different in terms of age, length of survival, number of changes, and days between changes. Patients had an average of 7 drain changes; the average time between PTBD change was 20 days. Women had an average of 9.3 changes, whereas men had average of 5.8 changes, (p=0.053). Woman went 25.7 days between changes and men went 17 days between changes (p=0.03). In the group of patients who returned, women were significantly older than the men, (72.5 vs 62.6 years; p=0.02), and the average length of survival is estimated at 154 days, with the longest being 766 days. Women had an average survival estimate of 256 days and men 112 days (p=0.01). An important finding of this study was that 51% of the patients did not return for subsequent PTBD change after the first hospitalization for drain placement. The non-return rate could not be differentiated by sex, tumor location or age.

Conclusions: At our institution, 51% of patients who undergo PTBD placement for palliation of malignant bile duct obstruction do not return for follow up drain change. We found no differentiating variables to predict non-return. But, this rate seems exces-

sive in light of the average survival of the returning patients (158 days). Reasons for non-return needs to be better understood; it is possible that improved palliative care consultation and post-procedural care might decrease the rate of non-return and increase the overall post-procedural survival.

Poster 48: Is Percutaneous Biliary Drainage Effective in Lowering Serum Bilirubin for Chemotherapy?

J. Levy, D. Sudheendra, M. Dagli, J.I. Mondschein, S. Stavropoulos, R.D. Shlansky-Goldberg, S.O. Trerotola, U. Teitelbaum, R. Mick, M.C. Soulen

Objectives: A previous study reported that only 30% of patients undergoing percutaneous biliary drainage (PBD) normalized their serum bilirubin within 100 days in order to receive chemotherapy, with pre-drainage serum bilirubin level and INR predictive of success. However, for digestive tract cancers, the bilirubin threshold for chemotherapy is either 5 mg/dl or 2 mg/dl depending upon the regimen. We examined the ability of PBD to achieve these clinically relevant endpoints.

Methods: Under IRB approval, retrospective analysis was performed of 117 patients with malignant biliary obstruction who underwent PBD. Time to achieve a bilirubin of 5 mg/dl, 2mg/dl, and survival were estimated by Kaplan-Meier analysis. Potential prognostic factors included pre-drainage bilirubin, creatinine, INR, platelets, type of cancer, presence of liver metastases, drain size, drain location, level of obstruction, % liver drained, and indication for drainage. Categorical variables were analyzed by the log rank test. For continuous variables, hazard ratios were calculated by Cox regression. These were also categorized by quartiles and analyzed by log rank test.

Results: 11 patients were excluded for pre-drainage bilirubin \leq 2 (9) or missing data (2). Among the 88 patients with a pre-drainage bilirubin > 5mg/dl, 62% were \leq 5mg/dl within 30 days and 84% within 60 days, median 21 days. Among 106 patients with a pre-drainage bilirubin >2 mg/dl, 37% were \leq 2mg/dl by 30 days and 70% within 60 days, median 43 days. Pre-drainage bilirubin was not a significant predictor of time to achieve a bilirubin \leq 2mg/dl (p=0.51 for quartiles, HR=0.96, p=0.083). Pre-drainage bilirubin was a significant predictor of time to achieve a bilirubin \leq 5mg/dl (p<0.0001 for quartiles, HR 0.91 p<0.001); patients with an initial bilirubin of 5-15 came down to 5 within 1-2 weeks, while those with an initial bilirubin of 15-40 took 4-6 weeks. Pre-drainage INR was a significant predictors of time to achieve a bilirubin <5mg/dl (HR 0.23, p=0.036). Among the categorical variables only diagnosis was statistically significant, with biliary primaries taking a median of 69 days to reach a bili of 2 mg/dl vs. pancreatic 37 days and other mets 40 days. Median survival was 100 days with 75% alive at 30 days and 60% at 60 days (Table).

Conclusions: PBD of malignant obstruction achieves clinically relevant reduction in serum bilirubin in the majority of patients within 1-2 months, irrespective of the pre-drainage serum bilirubin. PBD is clinically indicated for reduction of bilirubin to allow administration of systemic chemotherapy.

Serum Bilirubin vs Survival following PBD

	30 d	60 d	90 d
Survival	75%	60%	52.5%
TB <5 mg/dl	62%	84%	92%
TB <2 mg/dl	37%	70%	88%

Poster 49: Infection Rates in Single-Incision versus Conventional Two-Incision Technique for Implantable Chest Port Placement

G. Abbey-Mensah, J. Walsh

Objectives: Traditionally, chest ports are placed using a two-incision technique with direct internal jugular vein puncture via a small incision under ultrasound guidance with a second incision made to implant the chest port. The relatively newer, single-incision technique involves accessing the internal jugular vein under ultrasound guidance from an infraclavicular approach using a micropuncture needle bent into a c-shape, and using this same incision to implant the chest port. The latter technique offers better cosmetic results and is a better option for patients with tracheostomy tubes, however, few studies have been done to compare the complications of the two methods. The purpose of our study is to compare the infection rates of the single-incision technique versus the two-incision technique for implanted chest ports.

Methods: A retrospective review of all chest ports placed at a single institution by interventional radiology under fluoroscopic and ultrasound guidance over a 3 year period was performed. All patients gave consent for the procedure. The hospital records of all patients were reviewed to determine the outcome of the ports. All of the ports were placed for chemotherapy.

Results: Placement was technically successful in 137 procedures. Ninety-nine were placed using the conventional two-incision technique and 38 were placed using the single-incision technique. Post-procedure infection (pocket infection or systemic catheter-related septicemia) occurred in 6 patients that underwent the two-incision technique (6%) and 1 patient that underwent the single-incision technique (2.6%). All infected ports were removed. The average time to infection for ports placed by the two-incision technique was 2.8 months and for single incision was 0.5 months.

Conclusions: The conventional two-incision technique for implantable chest port placement has an increased rate of infection than the single-incision technique, likely due to the fact that with two incisions, there are two potential niduses for infection. This should be further studied in a prospective randomized study, which is currently in progress at our institution.

Poster 50: Longitudinal Quality of Life Assessment in Patients with Hepatic Tumors Treated with CT-Guided Radiofrequency Ablation

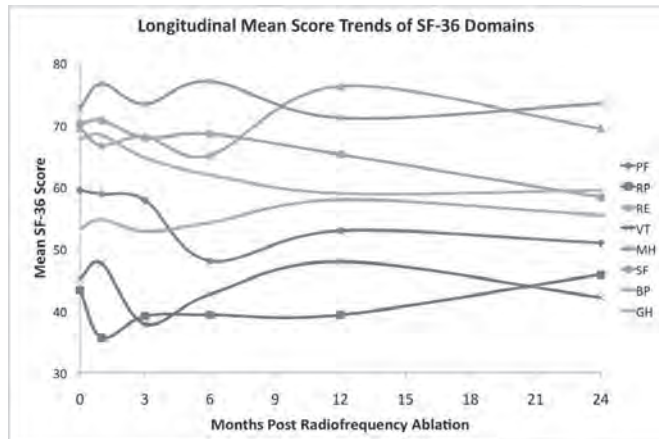
B. Cramer, M. Xing, G. Webber, H.S. Kim

Objectives: To determine the longitudinal effects of CT-guided radiofrequency ablation therapy (RFA) on health-related quality of life (HRQOL) in patients with hepatic tumors.

Methods: Single-center IRB-approved prospective health-related quality of life study using the Short-Form 36 (SF-36) assessment tool before and after CT-guided radiofrequency ablation. Baseline HRQOL scores were evaluated for significant ($p < 0.05$) change within the total patient population at 1 month, 3 months, 6 months, 12 months, and 24 months following radiofrequency ablation using the paired t-test. Baseline HRQOL scores were also correlated with overall survival. Patient HRQOL norm-based summary scores before and after treatment with radiofrequency ablation were also compared to the U.S. healthy population.

Results: 41 patients (20 males, 21 females) with hepatic tumors were enrolled. Tumor types included hepatocellular carcinoma ($n=17$), colon adenocarcinoma ($n=12$), cholangiocarcinoma ($n=6$), neuroendocrine tumor ($n=2$), non-small cell lung cancer ($n=1$), undifferentiated sinonasal carcinoma ($n=1$), endometrial carcinoma ($n=1$), and adrenal cortical carcinoma ($n=1$). Patient age ranged from 41 to 90 years with a mean of 64.1 years. The median length of time from initial RFA treatment to the first follow-up survey was 48 days. There were no significant differences in any of the 8 domains (General Health, Physical Functioning, Mental Health, Bodily Pain, Social Functioning, Vitality, Role-Physical, or Role-Emotional) when comparing baseline scores to 1, 3, 6, 12, and 24-month follow-up scores. For example, Physical Functioning baseline mean score (59.42) showed no significant change at 1 month (58.85, $p=0.246$), 3 months (57.83, $p=0.601$), 6 months (47.99, $p=0.533$), 12 months (52.86, $p=0.667$), or 24 months (50.88, $p=0.616$) post-treatment. Mental Health baseline mean score (72.68) showed no significant change at 1 month (76.58, $p=0.094$), 3 months (73.35, $p=0.260$), 6 month (77.05, $p=0.263$), 12 months (71.14, $p=0.882$), or 24 months (73.42, $p=0.570$). At the conclusion of data collection, 32 of 41 enrolled patients were living. Of the deceased ($n=9$), mean survival was 11.7 months after RFA. Baseline HRQOL mean scores of living patients were compared to deceased patients. Baseline Social Functioning (SF) and Bodily Pain (BP) domain mean scores were significantly increased in living compared to deceased patients (75.39 vs. 51.39, $p=0.034$; 72.66 vs. 50.00, $p=0.041$). There were no significant differences in any other domain. Enrolled patients had decreased mean baseline HRQOL Mental Component Summary (MCS) and Physical Component Summary (PCS) norm-based scores compared to the U.S. healthy population (MCS 48.2 vs. 50.0; PCS 41.1 vs. 50.0). After treatment, mean MCS and PCS norm-based scores remained decreased compared to the U.S. healthy population at 1, 3, 6, 12, and 24 months (MCS 47.6-49.9 vs. 50.0; PCS 37.7-40.2 vs. 50.0).

Conclusions: Patients with hepatic tumors are not likely to perceive changes in any of the HRQOL domains at 1, 3, 6, 12, or 24 months following radiofrequency ablation treatment. Increased baseline SF and BP domain scores correlate with overall survival.



Poster 51: De Novo Radiologic Button Gastrostomy for Children During Chemotherapy

B. Richioud, A. Kalendarian, P. Marec-Berard, M. Saunier, L. Yolande, M. Cuinet

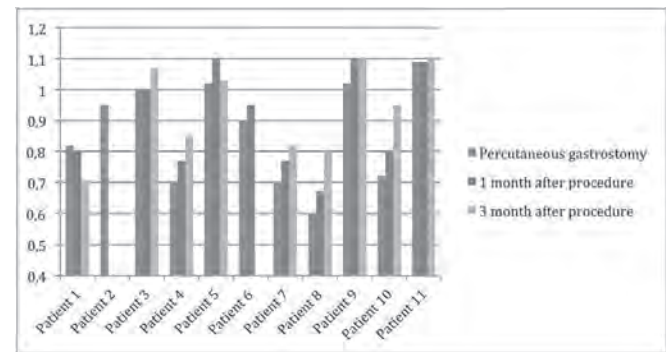
Objectives: To describe the percutaneous radiological button gastrostomy (PRBG) procedure for children in oncology, without the need of a previous tract, and without

any change in the type or the timing of the chemotherapy: safety and effectiveness, weight/height ratio follow-up of three months. Three elements make our work original: - De novo button gastrostomy, without the need of a previous tract, is little described for children - The chemotherapy program was modified to any child, neither in the type nor in the timing of the cycles - Only a few studies have analysed the nutritional outcomes following radiologic gastrostomy placement in children

Methods: PRBG were performed by interventional radiologists for 11 patients (median age 13 yo)(Table 1), according to the classical technic using gastropexy anchors, under general or local anesthesia depending on the ability to cooperate. The button gastrostomy device (MIC-Key G, Ballard Medical Products, Draper, UT) corresponding to the tract length was selected and primary inserted through the peel away dilator. We report acute and late complications. We review heights and weights at different key points of the care with a follow-up of 3 months.

Results: No peroperative complication has been reported. After the placing, one patient necessitated a type 3 analgesic treatment for 48 hours. No major complication occurred, neither early nor late. Minor delayed side-effects were described for 2 patients, all related to local leaks and tissue formation quickly resorbed with a silver nitrate treatment. Patients 2 and 6 respectively died after 2 and 6 weeks following the procedure, due to the evolution of the cancer. During the follow-up, Patient 1 developed vomiting and nausea due to the tumor and the chemotherapy. Hypercaloric feeding was decided, and parenteral feeding had to be added at 3 months. For patient 5, enteral feeding was decreased at 2 month at the request of the family. At 1 month after PRBG, 70% of patients had gained, 20% maintained, and 10% lost weight. At 3 months, 89% had gained weight comparing to initial data, 11 % lost weight (Figure 2).

Conclusions: De novo PRBG in pediatric oncology is safe, including during chemotherapy programs. The hospitalisation period is short; the start of the enteral feeding is quick with an early return home. Procedure and devices are well tolerated by the children and their parents. The effectiveness of PRBG on weight gain appears similar to the other percutaneous techniques of enteral nutrition. This technique can be used in pediatric oncology, respecting at the same time the therapeutic plan.



Weight/Height ratio evolution

Patients Characteristics

Patient	Age (years)	Sex	Pathology
1	3	M	Brain stem astrocytoma
2	8	F	Neuroblastoma
3	9	M	Nasopharyngeal cancer
4	10	F	Osteosarcoma
5	12	M	Nasopharyngeal cancer
6	13	M	Osteosarcoma
7	15	F	Osteosarcoma
8	16	M	Nasopharyngeal cancer
9	17	M	Osteosarcoma
10	18	M	Osteosarcoma
11	20	F	Osteosarcoma

Poster 52: Microwave Ablation of Hepatic Adenomas: Initial Experience with 10 Adenomas

T.A. Potretzke, T. Ziemlewicz, J.L. Hinshaw, M.G. Lubner, D. Kitchin, C.L. Brace, M. Alexander, F.T. Lee

Objectives: The primary indications for the treatment of hepatic adenomas (HA) are to reduce the risk of bleeding and malignant transformation. However, HA are a benign entity that most frequently occur in young, otherwise healthy women, and surgical interventions have significant associated morbidity and even rare mortality. This is the optimal setting for a minimally invasive treatment and image-guided tumor ablation has the potential to fill this role in many of these patients (cautery for the prevention of hemorrhage and cellular necrosis to obviate the risk of malignant transformation). Microwave (MW) ablation is a promising technology that offers several advantages over radiofrequency (RF) ablation, but the application of MW for treatment of hepatic adenomas has not been previously described. The purpose of this study was to retrospectively review the results of the MW ablation of 10 hepatic adenomas utilizing a high-power, gas-cooled MW device at a single center.

Methods: This retrospective study was IRB approved and HIPAA compliant. Between May 2011 and October 2013, 10 hepatic adenomas in 5 patients were treated utilizing US and/or CT guidance. There were 4 female patients and 1 male patient with a mean age of 39.6 years (range 33-45). All procedures were performed with a high-powered, gas-cooled microwave system (Certus 140, Neuwave Medical, Madison, WI) using either a percutaneous (n=8) or open (n=2) approach. Complications were recorded according to the Clavien-Dindo classification.

Results: Tumors ranged in size from 0.8 to 8.3 cm (mean 2.8 cm) and median imaging follow-up was 15 months (range 0-18). Mean power was 78 Watts (range 45 –95 Watts) and mean ablation time was 6.2 minutes (range 2-15 minutes). Technical success was achieved in a single session for 8 of the 10 treated adenomas with complete ablation at immediate post-ablation imaging. The largest adenoma (8.3 cm) was partially ablated in one intra-operative session and then completed in a second session (percutaneous) approximately 10 weeks later with technical success. One 3.8 cm adenoma was partially ablated with a small area of residual tumor on immediate follow up imaging, but the enhancement subsequently resolved. Primary treatment effectiveness by imaging is 100% for the 9 of 10 lesions with follow up imaging. One treated adenoma has not yet been imaged in follow up. There were no complications and there have been no episodes of spontaneous hemorrhage to date.

Conclusions: MW ablation of hepatic adenomas is a logical application of this technology. These initial results suggest that it is safe and effective, although longer term follow up will be needed to confirm efficacy in the prevention of hemorrhagic complications and malignant transformation.

Poster 53: Image-guided Percutaneous Argon-Helium Cryoablation For Painful Bone Tumors

L. Haibo

Objectives: To investigate the analgesic effect of cryosurgery on bone tumor-induced pain.

Methods: 34 patients with bone malignancy were given percutaneous cryosurgery for a total of 43 times. Bone biopsies and PET-CT were performed to observe the metabolic activity after cryosurgery. NRS score were recorded and analyzed to evaluate the pain-killing effect of cryosurgery.

Results: After cryosurgery most of the metastatic foci (10/13) showed necrosis. 7 out of 9 showed significant inhibition of metabolism and 2 partial inhibitions. Three days after cryosurgery, NRS score showed a complete response (CR) to pain in 18 patients (52.9%), partial response (PR) in 10 patients (29.4%), stable disease (SD) in 4 patients (11.8%), and progressive disease (PD) in 2 patients (5.9%). At 10 days after cryosurgery, complete response (CR) of pain was seen in 25 patients (73.5%), partial response (PR) in 6 patients (17.6%), stable disease (SD) in 2 patients (5.9%), and progressive disease (PD) in 1 patient (2.9%). 20 (58.8%) major complications were observed which included 12 cases of local subcutaneous dropsy, 1 case of skin necrosis on local small area, 7 cases of fever; no fracture occurred during the hospitalizations. 6 patients died at 34 days, 58 days, 69days, 88days, 105 days and 16 months respectively after cryosurgery. Among them two patients died of dyscrasia failure, 1 died of airway obstruction and lung infection, 1 died of encephalic metastasis, 2 died of liver and renal failure. No cause of death was directly related to cryosurgery. The remission time of pain of other patients was 46 – 232 days, median time was 128 days. Nine patients' tumors (26.5%) were recurrent or had a progressive destruction of bone.

Conclusions: Cryosurgery can be accepted as a relatively safe and effective procedure for the palliative treatment of bone tumors, especially for stopping the pain.

Poster 54: Combination Treatment With Comprehensive Cryoablation and Immunotherapy in Metastatic Pancreatic Cancer

C. Jibing

Objectives: The aim of this study was to retrospectively assess the effect of comprehensive cryosurgery (ablation of intrapancreatic and extrapancreatic tumors) plus immunotherapy in metastatic pancreatic cancer.

Methods: We divided 106 patients (57 men, 49 women; median age, 65 years) into the cryoimmunotherapy (31 patients), cryotherapy (36 patients), immunotherapy (17 patients), and chemotherapy groups (22 patients). Pretreatment immune function was tested in patients who underwent immunotherapy. Overall survival (OS) after diagnosis of metastatic pancreatic cancer was assessed after a 4-year follow-up.

Results: Median OS was higher in the cryoimmunotherapy (13 months) and cryotherapy groups (7 months) than in the chemotherapy group (3.5 months; both P < 0.001) and was higher in the cryoimmunotherapy group than in the cryotherapy (P < 0.05) and immunotherapy groups (5 months; P < 0.001). In both the cryoimmunotherapy and cryotherapy groups, median OS was higher after multiple cryoablations than after a single cryoablation (P = 0.0048 and 0.041, respectively). In both groups, the median OS was higher in patients with normal immunologic function than in those with immune dysfunction (P < 0.0001 and P = 0.0004, respectively).

Conclusions: Cryoimmunotherapy significantly increased OS in metastatic pancreatic cancer. Multiple cryoablations and normal pretreatment immunologic function were associated with better prognosis.

Poster 55: Outcome of Covered Stents for Treatment of Hepatic and Mesenteric Arterial Injuries in Cancer Patients

M. Danial, R.H. Siegelbaum, E.N. Petre, J.P. Erinjeri, K.T. Brown, S.B. Solomon, M. Maybody, A.M. Covey, G.I. Getrajdman, R. Thornton, J.C. Durack, H. Yarmohammadi, A. Aguado, L. Brody, W. Alago, C.T. Sofocleous

Objectives: To evaluate the technical outcome, patency duration, and factors predicting angiographic success of covered stent placement in the treatment of hepatic and mesenteric arterial injuries.

Methods: A retrospective, HIPAA-compliant review of consecutive patients treated with covered stents (VIABAHN) for hepatic and mesenteric arterial injuries between 4/2009 and 9/2013 was performed. Angiographic success was defined as the ability of the stent to exclude the arterial injury with preservation of patency. Patient demographics and procedural details were analyzed in relation to angiographic success. Follow-up imaging was reviewed in order to evaluate patency duration.

Results: Fifteen patients (10 men, 5 women) with a mean age of 60 ± 13 years formed the patient cohort. Primary tumor type was colorectal (n = 10), pancreas (n = 4) and bile duct (n = 1). In 10 patients, indication for stent placement was bleeding at the site of a hepatic artery infusion catheter. In the other 5 patients, pseudoaneurysms of celiac artery (n = 1), superior mesenteric artery (n = 1), gastroduodenal artery (n = 2), and common hepatic artery (n = 1) were treated. Twenty covered stents were placed (1 stent in 11 patients, 2 stents in 3 patients, and 3 stents in 1 patient). Balloon angioplasty was performed in 7/15 (47%) at the discretion of the operator. Intraprocedural unfractionated heparin was administered along with post-procedural aspirin/clopidogrel in 2/15 (13%) cases. No intraprocedural or post-procedure anticoagulation was used in the remaining 13/15 (87%) cases. Overall angiographic success rate was 87% (13/15). The two failures were immediate stent thrombosis after angioplasty and an endoleak that persisted after balloon angioplasty. Age, sex, primary tumor type, and stent placement indication were not significant factors in predicting angiographic success (p > 0.05). There was a trend toward a higher rate of angiographic success in patients who did not undergo angioplasty compared with those who did (100% vs 71%, p = 0.10). Follow-up imaging was available in 10 of the 13 successful cases. Two of the stents became occluded during followup after 65 and 852 days, respectively. The remaining 8 stents stayed patent during followup that ranged from 39 to 608 days (median 223 days). **Conclusions:** Covered stents are effective in treating injuries of the hepatic or mesenteric arteries with a high angiographic success rate and low occlusion rate. Balloon angioplasty should be carefully considered after covered stent placement.

Poster 56: Resource Utilization During Chemoembolization

J. Redmond, S. Stavropoulos, J.I. Mondschein, M. Dagli, D. Sudheendra, M.C. Soulen

Objectives: To compare equipment, contrast, and fluoroscopy usage during lipiodol chemoembolization among interventional radiology staff, and to identify practices contributing to increased cost per case.

Methods: A retrospective review was performed of chemoembolizations performed between 10/1/2012 and 6/10/2013. Six attending physicians were performing chemoembolization; one was excluded due to low number of cases (7). The remaining 5 performed 25-46 chemoembolizations each for a total of 185 procedures. Fluoroscopy time, contrast volume, and equipment usage were analyzed on a per attending, per case basis. Comparison was also made by grouping attendings into those with greater than 5 years experience (3) and those with 5 or fewer (2). Average numbers of specific inventory items per case as well as average cost per category of item per case were calculated. T-tests were used to determine if differences were statistically significant.

Results: The range of attending experience was 2 – 22 years. Individual usage data is shown in the Table. Mean contrast volume was 62 ml for senior staff vs. 74 ml for junior staff (P < 0.001). Mean fluoroscopy time was 17.4 minutes for senior staff vs. 21.7 minutes for junior staff (P = 0.002). The senior staff's average inventory cost per case was \$886 vs. \$1111 for the junior staff (P < 0.001). Specific practices that statistically significantly increased cost were increased use of micropuncture sets, number and type of microwires, more vials of embolics, and use of vascular closure devices.

Conclusions: Junior staff consume an average of 25% more material and time-based resources when performing chemoembolization, which negatively impacts throughput and divisional efficiency. Detailed inventory analysis provides opportunities for targeted interventions to decrease cost through altering practice.

Resource Utilization by Attending

Years Experience	Mean Fluoroscopy Time/Case (min)	Mean Contrast/Case (mL)	Mean # of Vials of Embolics/Case	% Cases Microcatheter Used	Items Significantly Increasing Cost	Cost/Case (USD)
22	19.6	58	1.07	80%	-	\$833
14	14.5	56	0.92	100%	-	\$935
12	16.8	72	1.05	100%	-	\$914
5	22.3	71	1.65	97%	Transcend Microwire, Embolics, Closure Devices	\$1115
2	21.2	77	1.43	93%	Closure Devices, Embolics	\$1108

Poster 57: Longitudinal Quality of Life Assessment in Patients with Renal Cell Carcinoma Treated with Cryoablation

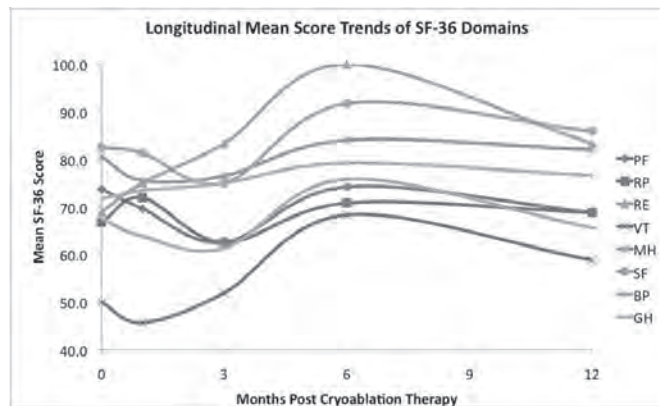
B. Cramer, M. Xing, G. Webber, H.S. Kim

Objectives: To determine the longitudinal effects of cryoablation therapy on health-related quality of life (HRQOL) in patients with renal cell carcinoma (RCC).

Methods: Single-center IRB-approved prospective health-related quality of life study using the Short-Form 36 (SF-36) assessment tool before and after cryoablation. Pre-treatment baseline HRQOL scores were evaluated for significant (p<0.05) change within the total patient population at 1 month, 3 months, 6 months, and 12 months following treatment using the paired t-test. Patient HRQOL norm-based summary scores before and after cryoablation were also compared to the U.S. healthy population.

Results: 15 patients (12 males, 3 females) with RCC were enrolled. Patient age ranged from 53 to 77 years with a mean of 66.1 years. The median length of time from cryoablation to the first follow-up survey was 48 days. There were no significant differences in any of the 8 domains (General Health, Physical Functioning, Mental Health, Bodily Pain, Social Functioning, Vitality, Role-Physical, or Role-Emotional) when comparing pre-treatment scores to 1, 3, 6, and 12-month post-treatment scores. For example, mean scores in Physical Functioning showed no significant change from baseline to post-treatment at 1 month (73.67 vs. 69.55, p=0.070), 3 months (73.67 vs. 62.5, p=0.573), 6 months (73.67 vs. 74.17, p=0.296), or 12 months (73.67 vs. 68.75, p=0.115). Mean scores in Mental Health showed no significant change from baseline to post-treatment at 1 month (80.53 vs. 75.50, p=0.098), 3 months (80.53 vs. 76.5, p=0.351), 6 months (80.53 vs. 84.00, p=0.749), or 12 months (80.53 vs. 82.00, p=0.567). Enrolled patients with RCC had decreased mean baseline HRQOL Mental Component Summary (MCS) and Physical Component Summary (PCS) norm-based scores compared to the U.S. healthy population (MCS 49.8 vs. 50.0; PCS 47.2 vs. 50.0). After treatment, the MCS was higher compared to the U.S. healthy population at 3 months (51.2 vs. 50.0), 6 months (57.6 vs. 50.0), and 12 months (53.8 vs. 50.0). After treatment, PCS remained lower compared to the U.S. healthy population at 1, 3, 6, and 12 months (44.2-47.6 vs. 50.0).

Conclusions: Patients with RCC are not likely to perceive changes in any of the HRQOL domains at 1, 3, 6, or 12 months after cryoablation.



Poster 58: Improved Quality of Life Following Percutaneous Management of Extra-Abdominal Desmoids

P.M. Guzzetta, R.S. Williams, D.B. Yim, D. Monson

Objectives: Extra-abdominal desmoids may be treated by many methods, including radiation and surgical resection; however, local recurrence limits treatment effectiveness. This article investigates our results with percutaneous cryoablation of extra-abdominal desmoid tumors in eight patients with an emphasis on quality of life improvement.

Methods: A retrospective review of the patients who underwent cryoablation from April 2012 to December 2013 for extra-abdominal desmoid tumors was performed. Patients were referred for local regional therapy that failed surgical, chemotherapy or conservative management. The patient population included an age range of 25-70 years

old with 3 males and 5 females. The soft tissue lesions ranged from 5-22 cm in maximal dimension with locations in thighs, paraspinal tissues and flank. One to eight probes were used depending on the size of the lesion, with an average of 3.35 probes. All lesions followed were stable or decreased in size between treatments. A quality of life score was created for the patients with EAD. Symptoms of pain, swelling and neurologic involvement all were given a point value of one with a total range of 0 (asymptomatic) to 3 (all three of the aforementioned symptoms consistent with poor quality of life). Complications were seen in two patients that developed sciatic nerve injury after treatment of their thigh injury. Short-term follow-up has not been completed on two of the patients. Long-term follow-up has not been completed on these patients (12+ months post-treatment). Statistical analysis of the data with a paired t-test was performed.

Results: Five patients presented with thigh lesions with interval symptomatic improvement with 3 of the 5 patients (3 quality of life (QOL) score on initial consult to 0 QOL score post-treatment), one patient without short-term follow-up and one patient with worsening neurologic and pain symptoms (1 to 2 QOL score). The sixth patient had a thoracolumbar paraspinal mass, after three cryoablations; there was decreased pain (1 to 0 QOL score). The last two patients had abdominal wall masses, one demonstrated post treatment improvement of pain and swelling (2 to 0 QOL score) and one has yet to follow up. The improvement of the quality of life score was statistically significant (p value = 0.042) with a mean score improvement of 1.7.

Conclusions: Cryoablation was successful in treating a majority of the patients with extra-abdominal desmoids. There were neurologic complications associated in only two patients, both with desmoid tumors in close proximity or involved with the sciatic nerve. The quality of life score demonstrated statistically significant improvement after percutaneous treatment. Cryoablation of extra-abdominal desmoids remains a good alternative to surgical or radiation therapy with significant improvement of quality of life for a majority of treated patients.

Poster 59: DEB-TACE With Small Particles (70-150µm): Initial Clinical Experience and Safety Profile

A. Ashton, A.L. Tam, S. Gupta, M.J. Wallace, B.C. Odisio

Objectives: To assess the safety of transarterial chemoembolization using 70-150µm drug-eluting beads (DEB-TACE^{MI}) in patients with hepatic malignancies.

Methods: This is a retrospective analysis of 24 patients (hepatocellular carcinoma (n=15), metastatic disease (n=9)) with 34 hepatic lesions treated with 28 sessions of DEB-TACE^{MI}. Segmental/subsegmental DEB-TACE^{MI} was performed with doxorubicin loaded at 25mg/mL of LC BeadTM (22 sessions), 37.5 mg/mL of LC beadTM (2 sessions) or irinotecan loaded at 50mg/mL of LC BeadTM (3 sessions). Clinical-laboratorial and cross-sectional imaging findings post DEB-TACE^{MI} were utilized to identify and classify adverse events (AE) utilizing the National Cancer Institute Common Terminology Criteria for Adverse Events (Version 4).

Results: The mean lesion size was 3.4 cm. Hepatic tumor burden was: <25% (n=20), 25-50% (n=2), and 50-75% (n=2). The mean number of DEB-TACE^{MI} sessions per patient was 1.16. Mean imaging follow-up period was 164 days. Four patients had percutaneous ablation performed within 24 hours before the DEB-TACE^{MI} and none demonstrated AE. The median hospital length of stay after DEB-TACE^{MI} was 1 day (range 0-4 days). There were no Grade 4 or 5 complications. Grade 3 abdominal pain was noted in one session (1/28), requiring an overnight admission for pain control. Postembolization Syndrome (PES) grade 1 or 2 was observed in 75% of the sessions (21/28). PES was absent in 21.4% of the sessions (6/28). Clinically asymptomatic grade 1 liver/biliary injuries were observed on imaging follow-up in 20.8% of the patients (5/24) and consisted of: segmental biliary dilatation (n=2), biloma (n=1), hepatic infarct (n=1) and portal vein thrombosis (n=1).

Conclusions: Segmental/subsegmental DEB-TACE^{MI} is safe and does not result in increased complications when compared with series using larger diameter beads. Combination therapy using percutaneous ablation followed immediately by DEB-TACE^{MI} was also well tolerated and did not result in any AE.

Poster 60: Sustained Release Cisplatin from a Microsphere Formulation Demonstrates Improved Safety and Efficacy in a Xenograft Bladder Cancer Rodent Model

K. Mani, V. Sanna, P. Blaskovich, X. Guan, R. Verma, A. Mathur, H. Sard, A. Singh, M. Jaggi, R. Ohri

Objectives: Cisplatin is one of the most potent anticancer agents against many kinds of cancer, including liver and bladder tumours. However, the serious side effects and resistance phenomena associated with cisplatin administration limits its overall efficacy potential 1, 2. We have developed a microsphere based sustained-release formulation of cisplatin, with the goal of mitigating the side effects of cisplatin while enhancing its efficacy of on the basis of its slower sustained-release and bioavailability compared to un-encapsulated drug.

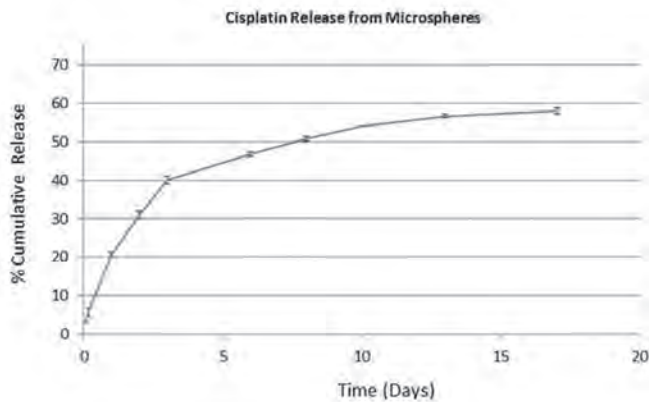
Methods: Our cisplatin microsphere formulation, called "Cis-MS-30", contains cisplatin at 27% (w/w) and was prepared with PLGA as the encapsulating polymer [PLGA i.e. poly (D,L-lactide-co-glycolic acid with a 75:25 ratio between lactide and

glycolide], and with a size range of 105 μm – 150 μm in diameter. Figure 1 is representative of the in-vitro release profile achieved with this formulation over about a 2 week period in ideal sink conditions. The anti-tumor potential and safety-profile of Cis-MS-30 microspheres was evaluated in a xenograft tumor model in athymic nude mice which underwent subcutaneous inoculation with the human 5637 urinary bladder cancer cell-line. Following the growth of subcutaneous solid tumors to a mean volume of $\sim 150 \text{ mm}^3$, Cis-MS-30 microspheres and un-encapsulated Cisplatin were administered through intra-tumoral injections at a dosage of 4.05 mg Cisplatin normalized per kg of animal weight, the frequency of the intra-tumoral administration being once every 12 days. Using vernier caliper measurements of length and width, tumor volume was monitored as a function of time, with tumor volume measurements made twice a week.

Results: Following 4 cycles of intra-tumoral administration (i.e. every 12 days), a reduction in tumor-volume by 88.7% was observed for the Cis-MS-30 microsphere formulation (16.8 mm^3) in comparison to free cisplatin (148 mm^3), which was statistically significant ($p < 0.001$). In addition, 3 animals out of 8 in the group of animal administered with Cis-MS-30 microspheres achieved full tumor regression (defined as no measurable tumor for 3 consecutive time-points). In comparison, none of the group of animals administered with un-encapsulated cisplatin achieved full tumor regression. Additionally, there was 2x greater mortality of animals undergoing administration of un-encapsulated Cisplatin compared to Cis-MS-30 microspheres (4 Vs 2), and also a greater loss of weight (10% compared to none).

Conclusions: The data suggests that the Cis-MS-30 formulation of cisplatin microspheres is capable, over-time, of demonstrating better anti-tumor efficacy compared to the intra-tumoral administration of free cisplatin at the same dose. At the same time, the cisplatin microspheres offer the potential of reduced side-effects by virtue of the slow-release at a lower concentration of the cisplatin for the same dose spread over a longer period of time, rather than a high concentration from the dose that would result with free cisplatin administration. Significant advantages could therefore be offered for interventional oncology applications.

Figure 1: Cisplatin release profile from microsphere formulation



Poster 61: A Comparison of Tissue Contraction During Radiofrequency and Microwave Ablation in Ex Vivo Liver

D. Liu, C.L. Brace

Objectives: Tissue contraction is an important factor affecting device characterization and clinical treatment assessment post ablation. The objective of this study was to compare the amount and evolution of tissue contraction during radiofrequency (RF) and microwave (MW) ablations.

Methods: A total of 46 aluminum fiducial markers were positioned in a 60 mm x 45 mm grid, in a single plane, around a RF or MW ablation probe in ex vivo liver. Each sample was placed on a bed of a 64-slice CT scanner with the probe parallel to be bed. A total of 4 RF ablations with peak power of 140 W and six MW ablations at 100 W were performed for 10 minutes. During each ablation, CT data was acquired over the entire liver sample volume every 30 seconds. Coronal maximum intensity projection (MIP) images were generated and fiducials were segmented using a threshold of 500 HU. A custom block matching algorithm was used to acquire fiducial displacement vectors in both radial (transverse to the probe) and longitudinal (along the probe) directions. The mean displacement vector maps were then created by interpolating discrete fiducial displacements onto a full 2D grid with 0.1 mm isotropic resolution. The final displacement maps of RF and MW ablation provide a distinct way to compare amount of the total tissue contraction during ablation. Through tracking the temporal curves of displacements in radial and longitudinal direction respectively, the growth rates of tissue contraction of the two were also compared and analyzed.

Results: Mean total radial displacements 5 mm, 10 mm, 15 mm radially from the microwave antenna were 1.7 mm, 3.3 mm, 3.8 mm. By contrast, the radial displacements

of RF ablation were much smaller with values of 0.8 mm, 0.6 mm and 0.3 mm at 5 mm, 10 mm and 15 mm radially from the RF probe, respectively. The total longitudinal displacements of microwave ablations were negligible near the distal tip of the antenna, but peaked to 6.0 mm at 45 mm proximal to the antenna tip. By contrast, the longitudinal displacements of RF ablations were greatest near the active electrode, with a peak value of 0.8 mm at the electrode tip. Overall, RF ablations measured at gross pathology were 20 mm in diameter after 1.2 mm contraction while MW ablations were 38 mm after 7.8 mm contraction. 80% of tissue contraction occurred within the first 2 minutes during RF ablations, but contraction during microwave ablations took longer to evolve, reaching the 80% level after 6 minutes (Fig.1).

Conclusions: Tissue contraction reduced the ablation zone diameter for both RF and MW ablation. Greater contractions were observed during MW ablation (approximately 25% diameter reduction) than RF ablation (approximately 10% diameter reduction). Most of the contraction occurred in the first 2 min for RF ablations, while contraction persisted up to 6 min during microwave ablations.

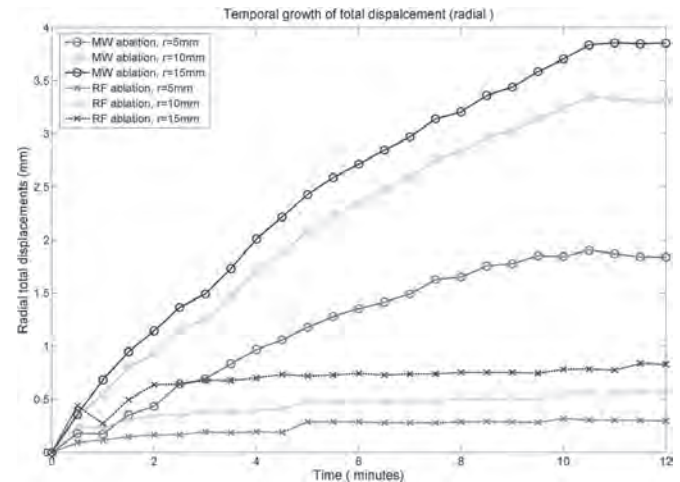


Fig.1 Temporal growth of tissue contraction during RF and MW ablation

Poster 62: Title: Simultaneous Activation of Multiple Microwave Antennas Improves Circularity and Ablation Zone Volume Compared to Sequential Overlapping Ablations

C. Harari, M. Magagna, M. Bedoya, F.T. Lee, C.L. Brace

Objectives: Multiple applicator ablation has been shown to increase ablation zone size and confluence compared to sequential overlapping ablations when using RF energy. While multiple antennas have also been shown to create large, confluent ablations with microwave energy, simultaneous and sequential overlapping ablations have not been compared with microwaves. The purpose of this study was to evaluate the size and shape of ablation zones created with simultaneous and sequential activation of microwave (MW) antennas in ex vivo and in vivo livers.

Methods: MW ablations were performed using two or three antennas at 1.6 or 2.0cm apart, respectively, and either simultaneous activation of all antennas or sequential ablation from each antenna in the array. A total of 32 ablations were performed in ex vivo bovine livers (eight per group) and 24 in in vivo porcine livers (six per group). Temperatures were recorded at four locations throughout ex vivo ablation zones. After each ablation, the ablation zone was excised and sliced transverse to the antenna insertion track. Each slice was digitally scanned, and assessed for circularity, maximum and minimum diameter, area, and maximum inscribed diameter (the largest circle that would fit inside the ablation zone of each slice). Each metric was compared between sequential and simultaneous activation groups in each tissue model using Student's t-tests with $P < 0.05$ indicative of statistical significance.

Results: In ex vivo liver, ablations performed using simultaneous activation were more circular and yielded both higher maximum temperatures and faster heating rates than ablations utilizing sequential activation (mean circularity: 0.89 vs. 0.74 and 0.93 vs. 0.84 for two- and three-antenna ablations, respectively [$P < 0.001$]; mean maximum temperature: 104 vs. 95.2 degrees Celsius and 102.76 vs. 93.17 degrees Celsius; mean heating rate in first two minutes: 15.96 vs 10.19 degrees Celsius per second and 13.98 vs 8.74 degrees Celsius per second for two- and three-antenna ablations, respectively [$P < 0.001$]). Total ablation zone volume did not vary significantly across the ex vivo techniques ($P > 0.05$). In vivo, more circular and larger ablations were observed when using simultaneous activation of multiple antennas. Differences between simultaneous and sequential ablations were statistically significant with three antennas (mean circularity: 0.94 vs. 0.82 for two- and three-antenna ablations, respectively [$P < 0.01$]; mean ablation volume 52.82 vs. 30.50 cm^3 for two- and three-antenna ablations, respectively [$P < 0.01$]). Similar trends were observed with two antennas but the differences failed to meet statistical significance for circularity and total ablation volume (mean circularity: 0.83 vs. 0.75 [$P=0.35$]; total ablation volume: 23.79 vs 17.46 cm^3 [$P=0.30$]).

Conclusions: Activating multiple antennas simultaneously yields an ablation that is more spherical, larger and hotter than sequentially creating multiple overlapping ablations with a single antenna. Simultaneous activation may therefore have beneficial implications for minimally invasive treatment of tumors.

Poster 63: A New Constant-Permittivity Radiating Tip Antenna Increases Predictability of Microwave Ablations (MWA) In Liver Tissue InVivo and In Vivo

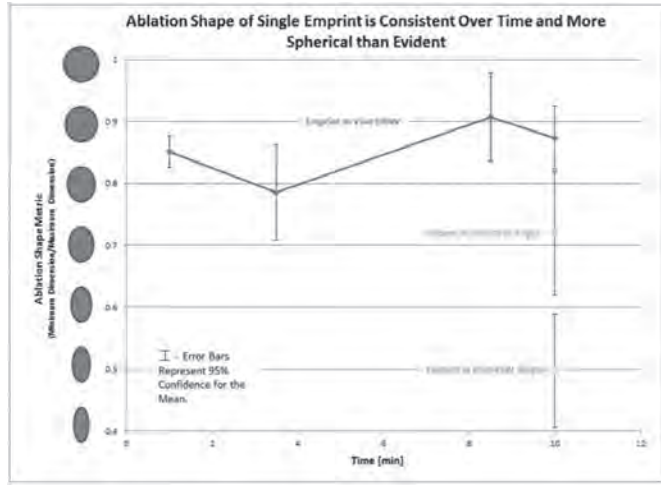
R. Seshadri, D. Niemeyer, K.J. Thompson, J.D. Brannan, J. Swet, I.H. McKillop, D.A. Iannitti

Objectives: The use of MWA technology to destroy hepatic lesions in situ is gaining in prominence. The aim of this study was to evaluate the efficacy and reproducibility of ablations created using a new 2450MHz MWA system (Emprint™, Covidien), employing a novel antenna tip that incorporates a patented Thermosphere™ technology, compared to an existing 915MHz MWA system (Evident™, Covidien) in vitro and in vivo.

Methods: Initial ablations were performed in ex vivo bovine liver to determine equivalency for power-time settings for the Evident and Emprint systems. Hepatic ablations were then performed in swine under general anesthesia (n=7 per time-power combination (45, 75, 100W; 1-10mins). Animals were euthanized, ablations measured, and ablation shape/volume defined and calculated.

Results: Using the Evident (45W;10min), ablations were predominantly ellipsoid in shape and ablation volumes were significantly different when calculated as spheres vs. ellipsoids (1.1±0.31 vs 5.1±1.6cm³, p<0.05). In contrast the Emprint (100W; 3.5min) generated a spherical ablation with no significant difference in calculated volumes as spheres vs. ellipsoids (5.8±1.3 vs 8.8±1.7, p=0.096). Analysis of power-time curves demonstrated equivalent ablation diameter/volume for the Emprint at 100W/3.5mins (2.26±0.18cm/10.06±1.41cm³) and 75W/5mins (2.23±0.21cm/7.16±1.59cm³), with no significant increase in ablation size at additional time settings for the same power. However, at 100W/8:30mins it was noted that charring occurred at the tissue-antenna interface, an event that did not occur at a 100W/3:30min setting, despite equivalent ablation volumes being achieved.

Conclusions: The 2.45GHz generates equivalent ablation volumes in a shorter time period than existing 915MHz technology, an optimal ablation size being achieved within 3.5mins at 100W. Moreover, the new water jacketed radiating antenna tip generates a predictable, spherical ablation in liver in vivo that emanates from the antenna tip. These data indicate the Emprint system will provide more predictable/reliable ablations than existing 915MHz technology (Evident). This may have implications for the development of algorithms for output control in the future



Poster 64: Single Incision Technique For PleurX Catheters: A Novel Approach

M. Meka, J. Salsamendi, S. Bhatia, G. Narayanan

Objectives: To study a single incision technique for PleurX catheter placement and to understand the pros and cons of this approach as opposed to the conventional double incision technique.

Methods: PleurX catheters are placed for management of refractory ascites and pleural effusions. The idea of single incision technique is to decrease the morbidity from the procedure. 15 patients underwent the procedure with this technique in the past 6 months at our institution. All 15 patients were free of catheter related infection, skin incision leak, catheter malfunction, and bleeding.

Results: A PleurX catheter from Care Fusion(Sandiego, California) is used at our institution. The steps of the procedure are discussed in detail including single incision for skin entry, orientation and direction of the tunnel (obliquely oriented caudo-cranial direction for pleural catheter and cranio-caudal direction for peritoneal catheter), customized 45° angle bent tips of the micro puncture needle, 4F micro sheath, 8F and 12F dilators, and 16F peel away sheath. A 0.035" Terumo stiff guidewire is used in this technique to avoid wire kinking during peel away sheath advancement. The risk of bleeding remains low as the pleural entry site remains just superior to the rib and the tunnel is always parallel to the intercostal space avoiding catheter kinking. The risk of infection and leak is low possibly due to single incision as opposed to conventional double incision.

Conclusions: Single incision technique is a simple, safe and effective method for PleurX catheter placement. However, this hypothesis needs to be validated in large cohort of patients in a randomized fashion.

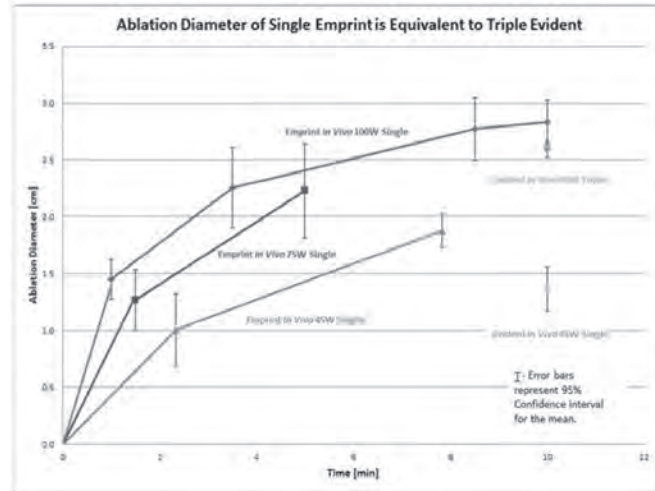
Poster 65: CT-Guided Pulmonary Fiducial Marker Placement: A Tailored Approach for Successful Outcome

D. Irwin, D. Sada, D. Smith, K. Kobayashi, M.A. Sultenfuss

Objectives: 1. Understand appropriate fiducial marker placement for successful stereotactic radiosurgery. 2. Review technical challenges encountered during CT-guided pulmonary fiducial marker placement. 3. Establish a tailored approach for overcoming commonly encountered technical challenges. 4. Review complications related to CT-guided pulmonary fiducial marker placement.

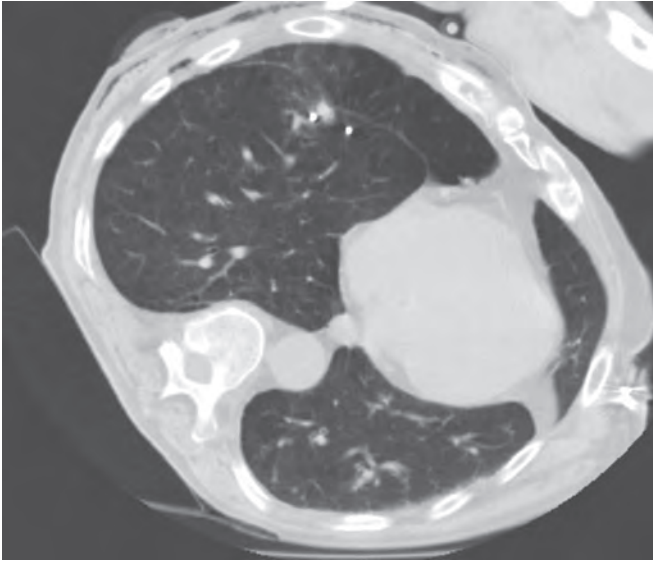
Methods: CT-guided fiducial marker placement for malignant pulmonary lesions assists the delivery of stereotactic radiotherapy. In our institution, these patients are often non-surgical candidates due to poor pulmonary functional status or extensive comorbidities. Earlier detection and diagnosis of lung cancer at our institution leads to increasing patient referrals for fiducial marker placement for small pulmonary malignancies. A total of 75 patients underwent 76 pulmonary fiducial marker placement procedures between February 2011 and December 2013. We reviewed pre- and intra-procedural imaging, establishing a tailored approach for successful fiducial marker placement, including pre-procedural planning strategies to optimize patient position, prioritizing marker placement in more technically challenging locations, and real-time adjustment procedure plan, based on initial fiducial marker placement.

Results: Technical challenges encountered include lesions <2cm in size, lesion location near the pleura or fissure, peri-vascular location, developing intra-procedural pneumothorax, and suboptimal initial fiducial marker placement. Technical considerations for overcoming these obstacles are discussed. Procedures were complicated by pneumothorax in 54 patients (71%), 35 of which required chest tube placement (46%). Pulmonary parenchymal hemorrhage complicated the procedure in 10 patients (13%), with hemoptysis occurring in 1 patient (1.3%) and hemorrhage obscuring the lesion,



precluding additional marker placement in another patient (1.3%). Inadvertent marker placement in the pleural space occurred in 6 procedures (7.9%).

Conclusions: Percutaneous pulmonary fiducial marker placement can be technically challenging, with a high incidence of complications. A tailored approach can overcome common obstacles, leading to a successful outcome.



Post-deployment image demonstrating fiducial markers placed anterior to a lesion located adjacent to the pleural surface.

Author Index

A

Abbey-Mensah, Geraldine - Poster 49
Abel, E. J - Poster 6, Poster 10
Abu Hilal, Mohammad - Poster 21
Agarwal, Harsh - Poster 11
Agarwal, Parul - Paper 11
Aguado, Allison - Paper 21, Poster 12, Poster 55
Ahuja, Chaitanya - Poster 35
Ajwichai, Khobkoon - Poster 26
Al-Tariq, Quazi - Poster 8
Alago, William - Paper 13, Paper 22, Poster 12, Poster 55
Alexander, Marci - Paper 11, Paper 16, Poster 52
Alexopoulou, Efthymia - Poster 44
Alle, Nisha - Poster 7
Allen, Peter J - Paper 7
Amalou, Hayet - Poster 11
Amir, Yasmin - Paper 3
Anaokar, Jordan - Poster 8
Ashton, Aaron - Poster 59
Aulmann, Sebastian - Paper 31

B

Banerjee, Arjun - Poster 34
Bao, Shanshan - Poster 47
Bates, Benjamin J - Poster 30
Bedoya, Mariajose - Poster 62
Bellemann, Nadine - Paper 31, Paper 32
Bennett, Bonita - Paper 37
Bermejo, Justo - Poster 18
Best, Sara L - Poster 6
Bhagat, Nikhil - Paper 4
Bhatia, Shivank - Poster 64
Bitterman, Therese - Paper 1
Blaskovich, Phillip - Poster 60
Bluemmel, Jacques - Paper 28, Poster 20
Boulin, Mathieu - Poster 20
Brace, Christopher L - Paper 11, Paper 16, Paper 18, Paper 26, Paper 30, Paper 35, Poster 6, Poster 10, Poster 13, Poster 52, Poster 61, Poster 62
Brandt, Ryan J - Poster 28
Brannan, Joseph D - Poster 63
Breen, David - Poster 21
Brinckerhoff, Susan - Paper 19
Brittain, Rick - Poster 30
Brocone, Matthew - Paper 41
Brody, Lynn - Paper 13, Paper 21, Paper 22, Poster 12, Poster 55
Broutzos, Elias - Poster 44
Brown, Karen T - Paper 6, Paper 7, Paper 13, Paper 21, Poster 12, Poster 55
Bryant, Timothy - Poster 21
Buckner, Gregory - Poster 1
Butters, Kim A - Poster 2

C

Callstrom, Matthew R - Poster 2
Camacho, Juan C - Paper 8, Paper 9, Paper 25, Paper 36, Paper 38, Poster 22, Poster 23, Poster 32, Poster 38

Carrafiello, Gianpaolo - Poster 15, Poster 16
Carrasquillo, Jorge - Paper 22
Chadha, Meghna - Poster 35
Chao, Cherng - Poster 36, Poster 37
Chapiro, Julius - Paper 4, Paper 20
Chen, Jeane - Paper 27, Paper 33
Chen, Rongxin - Paper 4, Paper 20
Chen, Yi-Jen - Poster 33
Chen, Yizhe - Poster 24
Chervonenko, Daniil - Paper 39
Chiang, Jason - Paper 30
Choyke, Peter - Poster 11
Cornelis, Francois - Paper 21, Poster 14
Covey, Anne M - Paper 6, Paper 7, Paper 21, Paper 22, Poster 12, Poster 55
Coyne, John - Poster 21, Poster 31
Cramer, Brandon - Poster 43, Poster 50, Poster 57
Cristescu, Mircea - Poster 10
Critchfield, Jeffrey J - Poster 35
Cuinet, Marie - Poster 51

D

D'Angelica, Michael - Paper 7, Paper 13
Dagli, Mandeep - Poster 36, Poster 37, Poster 48, Poster 56
Danial, Mir - Poster 55
Dauer, Lawrence - Poster 12
de Baere, Thierry - Paper 12
Deitrick, Ginna - Paper 5
DeMatteo, Ronald P - Paper 7
Denys, Alban - Poster 20
Deschamps, Frederic - Paper 12
Devic, Zlatko - Poster 34
Dhanasekaran, Renumathy - Paper 9
Do, Richard - Paper 6, Paper 22
Durack, Jeremy C - Paper 13, Poster 12, Poster 14, Poster 55
Duran, Rafael - Paper 4, Paper 20

E

Edalat, Faramarz - Poster 22, Poster 23, Poster 32, Poster 38
Erinjeri, Joseph P - Paper 6, Paper 7, Paper 13, Paper 21, Paper 22, Poster 12, Poster 14, Poster 55

F

Fan, Daiming - Paper 14
Farsad, Khashayar - Poster 35
Felker, Ely - Poster 7, Poster 26
Filippidis, Dimitrios - Poster 44
Fischman, Aaron - Paper 3, Poster 6
Fisher, George A - Poster 34
Floridi, Chiara - Poster 15, Poster 16
Flowers, David - Poster 21, Poster 31
Fong, Yuman - Paper 7
Fontana, Federico - Poster 15, Poster 16
Frangakis, Constantine - Paper 4
Fritz, Stefan - Paper 31
Furgeson, Darin Y - Poster 24

G

Gade, Terence - Poster 25

Galt, James - Paper 36, Paper 38
Garcia, Alessandra - Paper 22
George, Steve - Poster 21
Georgiades, Christos - Paper 29, Poster 4, Poster 5, Poster 9
Germann, Günter - Paper 32
Geschwind, Jean-François - Paper 4, Paper 20
Getrajdman, George I - Paper 6, Paper 7, Poster 12, Poster 14, Poster 55
Giantonio, Bruce - Paper 5
Gilbert, Carl W - Paper 28
Giri, Shivrman - Paper 19
Gockner, Theresa - Paper 31
Gockner, Theresa Luise - Paper 32
Goldin, Dmitry - Poster 40
Gonda, Elizabeth - Paper 19
Gonen, Mithat - Paper 7, Paper 13, Paper 22
Gordon, Andrew Christian - Paper 19
Guan, Xiao-Pei - Poster 60
Guillame, Nicolas - Paper 37
Guiu, Boris - Poster 20
Guo, Yang - Paper 27
Gupta, Sanjay - Poster 59
Guzzetta, Paul Michael - Poster 58

H

Haaga, John - Paper 41
Hacking, Christopher - Poster 21
Haibo, Li - Paper 15, Poster 53
Hamza, Samia - Poster 20
Handel, Jeremy - Poster 40
Harari, Colin - Poster 62
Harris, Kathleen R - Paper 33
Harrison, Neil - Poster 25
Hartung, Michael P - Paper 40
Hellan, Minia - Poster 30
Hinshaw, J. L - Paper 11, Paper 18, Poster 6, Poster 10, Poster 52
Hinshaw, Louis - Paper 16, Paper 35, Poster 13
Hoffmann, Katrin - Poster 18
Hollywood, Coral - Poster 21
Hoteit, Maarouf - Paper 1
Huang, Jiaoti - Poster 7
Hukuoka, Yasushi - Paper 28
Hunt, Stephen - Paper 1, Poster 25

I

Iannitti, David A - Poster 63
Ierardi, Anna Maria - Poster 15, Poster 16
Inaba, Yoshitaka - Paper 24
Irwin, David - Poster 65

J

Jack, Daniel - Poster 40
Jagait, Harvinder S - Poster 28
Jaggi, Manu - Poster 60
Jarnagin, William R - Paper 7, Paper 13
Jernigan, Shaphan R - Poster 1
Jibing, Chen - Poster 41, Poster 54

K

Kalenderian, Anne-Charlotte - Poster 51
Kanaev, Sergey - Paper 39

Kannengiesser, Stephan - Paper 19
Karagulle-Kendi, Ayse K - Paper 38
Kato, Mina - Paper 24
Kauczor, Hans U - Paper 31
Kauczor, Hans-Ulrich - Paper 32, Poster 18
Kauffman, Shannon - Poster 30
Kauffman, John A - Poster 35
Kelekis, Alexios - Poster 44
Kelekis, Nikolaos - Poster 44
Kemeny, Nancy - Paper 6, Paper 13, Paper 22
Kessler, Jonathan - Poster 33
Kharoti, Yama - Poster 35
Khazaie, Khashayarsha - Paper 34
Kichikawa, Kimihiko - Paper 28
Kim, Dong-Hyun - Paper 27, Paper 34
Kim, Edward - Paper 3
Kim, Hyun S - Paper 8, Paper 9, Paper 25, Paper 36, Paper 38, Poster 22, Poster 23, Poster 32, Poster 38, Poster 43, Poster 50, Poster 57
Kim, Joseph - Poster 33
Kim, Young Jun - Poster 19
King, David - Paper 40
Kingham, Peter - Paper 7
Kitchin, Douglas R - Paper 11
Kitchin, Douglas - Paper 18, Poster 10, Poster 52
Knaus, Marion - Poster 25
Kobayashi, Katsuhiko - Poster 65
Kokabi, Nima - Paper 9, Paper 25, Paper 36, Paper 38, Poster 22, Poster 23, Poster 32, Poster 38
Kolbeck, Kenneth J - Poster 35
Köllensperger, Eva - Paper 32
Kumar, Pradesh - Poster 21
Kunz, Pamela L - Poster 34

L

Lakshmanan, Manojkumar - Poster 14
Larson, Andrew C - Paper 19, Paper 27, Paper 33, Paper 34
Leal, Julie N - Paper 7
Lee, Fred T - Paper 11, Paper 16, Paper 18, Paper 35, Poster 6, Poster 10, Poster 13, Poster 52, Poster 62
Lee, Min Woo - Paper 2, Paper 23
Lee-Felker, Stephanie - Poster 7, Poster 26
Lessne, Mark - Paper 29, Poster 4, Poster 5, Poster 9
Levy, Jennifer - Poster 48
Lewandowski, Robert J - Paper 19, Paper 34
Li, Duan - Poster 12
Li, Tao - Paper 14
Li, Weiguo - Paper 19
Liang, Ping - Paper 10
Lim, Hyo Keun - Paper 2, Paper 23
Lin, MingDe - Paper 4, Paper 20
Lippert, Marguerite C - Poster 6
Liu, Dong - Poster 61
LlZhi, Niu - Poster 42
Longerich, Thomas - Poster 18
Longing, Anne P - Paper 22
Lookstein, Robert A - Paper 3

Louie, John D - Poster 34
Lu, David - Paper 17, Poster 7, Poster 8,
Poster 26
Lubner, Meghan G - Paper 11, Paper 16,
Paper 18, Paper 35, Poster 6,
Poster 10, Poster 13, Poster 52
Lutat, Carolin - Poster 3

M

Magagna, Michelle - Poster 62
Malagari, Aikaterini - Poster 44
Mammariappallil, Joseph George -
Poster 47
Mani, Kamraj - Poster 60
Marec-Berard, Perrine - Poster 51
Masada, Tetsuya - Paper 28
Master, Viraj - Paper 25
Mathur, Archana - Poster 60
Matsushima, Shigeru - Paper 24
Maybody, Majid - Paper 13, Paper 22,
Poster 12, Poster 14, Poster 55
McKillop, Iain H - Poster 63
Mckinney, J. Mark - Poster 29
McWilliams, Justin P - Paper 17
Meka, Murali - Poster 64
Metz, David C - Paper 37
Mick, Rosemary - Poster 48
Miller, Frank - Paper 19
Min, Ji Hye - Paper 23
Mishchenko, Andrey - Paper 39
Mittal, Pardeep K - Paper 25, Poster 22,
Poster 23
Moeslein, Fred - Poster 39
Mogler, Carolin - Paper 32
Moin, Adnaan - Poster 39
Mokry, Theresa - Paper 31, Paper 32
Mondschein, Jeffrey I - Paper 5,
Poster 36, Poster 37, Poster 48,
Poster 56
Monson, David - Poster 46, Poster 58
Moreland, Anna J - Poster 6
Mortell, Kelly - Paper 41

N

Nadolski, Gregory - Paper 1, Poster 25
Nakamoto, Dean - Paper 41
Narayanan, Govindarajan - Poster 64
Nash, Kathryn - Poster 21
Nayak, Nita - Poster 26
Negussie, Ayele - Poster 11
Neilson, John - Paper 40
Nelson, Rebecca - Poster 33
Nicolai, Jodi - Paper 27, Paper 34
Niemeyer, David - Poster 63
Nishiofuku, Hideyuki - Paper 28
Nowakowski, F Scott - Paper 3

O

Obayashi, Chiho - Paper 28
Odisio, Bruno C - Poster 59
Ohri, Rachit - Poster 60
Ouellette, James - Poster 30

P

Pandit-Taskar, Neeta - Paper 22
Parekh, Samir - Paper 9
Park, John J - Poster 33
Park, Jonathan - Poster 8
Patel, Amish - Paper 3
Patel, Rahul - Paper 3
Pattaras, John - Paper 25

Pearce, Neil - Poster 21
Pereira, Philippe L - Paper 31, Paper 32
Petre, Elena N - Paper 13, Paper 22,
Poster 55
Petrillo, Mario - Poster 16
Pierami Neto, Rubens J - Poster 27,
Poster 29
Pinto, Peter - Poster 11
Plotnik, Adam Nehemiah - Paper 17
Pohl, Theresa - Poster 20
Potretzke, Theodora A - Poster 52
Prajapati, Hasmukh J - Paper 8
Primrose, John - Poster 21
Pryma, Daniel A - Paper 37

R

Raatschen, Hans Juergen - Poster 3
Radeleff, Boris A - Paper 31, Paper 32,
Poster 18
Raman, Steven - Paper 17, Poster 7,
Poster 26
Redmond, Jonas - Poster 56
Reinhardt, Sven - Paper 28, Poster 20
Ren, Jane - Paper 28
Ren, Weihua - Paper 14
Requarth, Jay - Poster 47
Rhim, Hyunchul - Paper 2, Paper 23
Richioud, Bertrand - Poster 51
Richter, Götz - Poster 18
Riff, Brian P - Paper 37
Ringe, Kristina I - Poster 3
Rodriguez, Ron - Paper 29, Poster 4,
Poster 5, Poster 9

S

Sada, David - Poster 65
Sag, Alan - Poster 12
Sakaria, Sonali - Paper 9
Sako, Eric Y - Paper 17
Salem, Riad - Paper 19
Salsamendi, Jason - Poster 64
Sampson, Lisa - Paper 35, Poster 13
Sanna, Vinod - Poster 60
Sano, Tsuyoshi - Paper 24
Sard, Howard - Poster 60
Sato, Takeshi - Paper 28
Sato, Yozo - Paper 24
Saunier, Marie - Poster 51
Savelyeva, Valentina - Paper 39
Savin, Michael - Poster 40
Schafer, Markus - Paper 28
Schemmer, Peter - Poster 18
Schernthaler, Ruediger - Paper 20
Schirmacher, Peter - Poster 18
Schmitt, Antonin - Poster 20
Schmitz, Anne - Paper 31
Schuster, David M - Paper 36, Paper 38
Seale, Thomas - Poster 46
Sella, David - Poster 27
Seshadri, Ramanathan - Poster 63
Shady, Waleed - Paper 13, Paper 22
Sharma, Navesh - Poster 39
Shea, Lonnie D - Paper 33
Shenkman, Noah S - Poster 6
Sheu, Alexander Yowei - Paper 34
Shlansky-Goldberg, Richard D -
Poster 48
Siegelbaum, Robert H - Paper 13,
Paper 21, Paper 22, Poster 12,
Poster 55
Silk, Mikhail - Paper 6
Simon, Celeste - Poster 25
Sinclair, Philip - Poster 17

Singh, Anu - Poster 60
Singh, Gagandeep - Poster 33
Siripongsakun, Surachate - Paper 17
Smith, Darryl - Poster 65
Smolock, Amanda - Paper 18
Sofocleous, Constantinos T - Paper 7,
Paper 13, Paper 21, Paper 22,
Poster 12, Poster 14, Poster 55
Solomon, Stephen B - Paper 13,
Paper 21, Paper 22, Poster 12,
Poster 14, Poster 55
Sommer, Christof M - Paper 31, Paper 32
Sommer, Christof-Matthias - Poster 18
Song, Kyungdo - Paper 2
Soulen, Michael C - Paper 5, Paper 37,
Poster 25, Poster 36, Poster 37,
Poster 48, Poster 56
Spivey, James - Paper 9
Srimathveeravalli, Govindarajan -
Poster 14
Stampfl, Ulrike - Paper 31, Paper 32,
Poster 18
Stavropoulos, S William - Paper 5,
Poster 36, Poster 37, Poster 48,
Poster 56
Stedman, Brian - Poster 21, Poster 31
Suchy, Hannah B - Paper 6
Sudheendra, Deepak - Poster 36,
Poster 48, Poster 56
Sultenfuss, Mark A - Poster 65
Sun, Lee - Paper 28
Swet, Jacob - Poster 63
Sze, Daniel Y - Poster 34

T

Tacher, Vania - Paper 4
Takaki, Haruyuki - Poster 14
Takano, Masato - Paper 28
Tam, Alda L - Poster 59
Tan, Nelly - Paper 17, Poster 7, Poster 26
Tanaka, Toshihiro - Paper 28
Techasith, Tust - Poster 34
Teitelbaum, Ursina - Paper 5, Paper 37,
Poster 48
Tewari, Sanjit - Poster 12
Thompson, Kyle J - Poster 63
Thompson, Scott M - Poster 2
Thornton, Raymond - Paper 7, Paper 13,
Paper 22, Poster 12, Poster 55
Trerotola, Scott o - Poster 48
Tsapakos, Michael - Poster 28
Turkbey, Baris - Poster 11
Turkevich, Vladimir - Paper 39
Tutton, Sean M - Paper 40

V

van Houten, Diana - Paper 5
Velonakis, George - Poster 44
Verma, Ritu - Poster 60
Violari, Elena - Paper 21, Paper 22
Vollherbst, Dominik - Paper 31

W

Wachter, Frederic M - Paper 31
Wacker, Frank - Poster 3
Wallace, Michael J - Poster 59
Walsh, Edward - Poster 40
Walsh, James - Poster 49
Wang, Jianhong - Paper 14
Wang, Qinglin - Paper 14
Wang, Zhijun - Paper 4, Paper 20

Webber, Grant - Poster 43, Poster 46,
Poster 50, Poster 57
Weber, Charles N - Poster 25
Weiss, Karl Heinz - Poster 18
Wells, Shane A - Poster 6
Wendremaire, Maeva - Poster 20
Werner, Jens - Paper 31
White, Sarah Beth - Paper 27, Paper 33,
Paper 40
Wild, Damian - Paper 37
Willey, Bridgett J - Paper 30, Poster 13
Williams, Roger - Paper 36, Poster 46
Williams, Roger S - Poster 58
Wilson, Iain D - Poster 31
Wood, Bradford - Poster 11
Woodrum, David A - Poster 2
Wortley, Phillip Guy - Poster 46
Wright, Mark - Poster 21
Wu, Po-hung - Paper 26

X

Xiao, Yueyong - Poster 45
Xing, Minzhi - Paper 9, Paper 25,
Paper 36, Paper 38, Poster 22,
Poster 23, Poster 43, Poster 50,
Poster 57
Xu, Ruidan - Paper 14
Xu, Sheng - Poster 11

Y

Yamaura, Hidekazu - Paper 24
Yang, Yu-Xiao - Paper 37
Yangué, Yannick - Poster 15
Yap, Jonathan W - Paper 33
Yarmohammadi, Hooman - Paper 4,
Paper 41, Poster 12, Poster 55
Yenokyan, Gayane - Paper 20
Yim, Douglas B - Poster 58
Yolande, Lallemand - Poster 51
Youn, Pilju - Poster 24
Yu, Jie - Paper 10

Z

Zelzer, Sascha - Paper 31, Paper 32
Zhang, Hua - Paper 14
Zhang, Zhuoli - Paper 34
Zhong, Xiaodong - Paper 19
Ziemlewicz, Timothy - Paper 11,
Paper 16, Paper 18, Paper 35
Ziemlewicz, Timothy J - Poster 6,
Poster 10
Ziemlewicz, Timothy - Poster 13,
Poster 52



WCIO 2015

HILTON NEW YORK
NEW YORK, NEW YORK USA
6-9 MAY 2015

WCIO is *the* interventional oncology conference to attend, featuring leading, innovative IO experts, state-of-the-art lectures, panel discussions on current IO topics, unique live case presentations, and the latest scientific advances.

— Brought to you by —

WCIO

Advancing Interventional Oncology

www.wcioevents.org

Your Imaging Partner in Diagnostic and Interventional Radiology

Please visit us at Booth 113

Guerbet proudly supports WCIO.

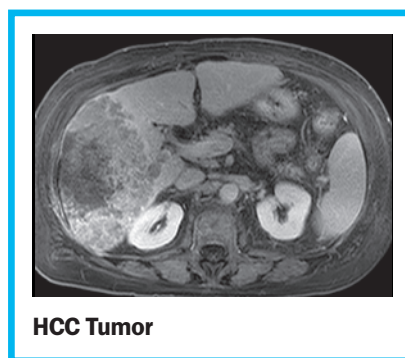
Guerbet | 
Contrast for Life

TheraSphere®

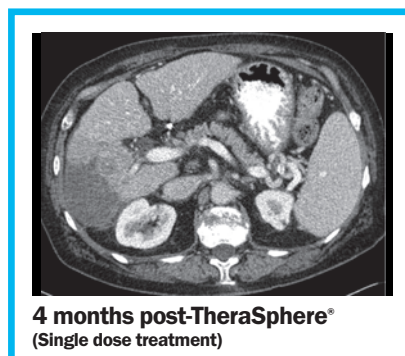
For HCC Patients With or Without
Partial or Branch PVT

TheraSphere® glass Y-90 microspheres give patients a clear advantage

TheraSphere® has a clear advantage because it is a powerful,¹ well-tolerated yttrium-90 glass microsphere therapy for transarterial radioembolization (TARE) in hepatocellular carcinoma (HCC).²



Sato KT, et al. Treatment of Unresectable Primary and Metastatic Liver Cancer with Yttrium-90 Microspheres (TheraSphere®): Assessment of Hepatic Arterial Embolization. Cardiovascular and Interventional Radiology. 2006; 29:522-529.



Tumor response varies, the tumor response shown is for illustrative purposes and may not be representative.



TheraSphere®: In the EU, TheraSphere® is used in the treatment of hepatic neoplasia. In Canada, TheraSphere® may be used in the treatment of hepatic neoplasia in patients who have appropriately positioned arterial catheters. In the USA TheraSphere® is authorised by Federal Law (USA) for use as a humanitarian device in radiation treatment or as a neoadjuvant to surgery or transplantation in patients with unresectable HCC who can have placement of appropriately positioned hepatic arterial catheters. The device is also indicated for HCC patients with partial or branch portal vein thrombosis/occlusion, when clinical evaluation warrants the treatment. The effectiveness of this device for this use has not been demonstrated.³

For full instructions for use and important safety information, please refer to the TheraSphere® package insert or IFU at www.TheraSphere.com. TheraSphere® is manufactured by Nordion (Canada) Inc. TheraSphere is a trademark of Theragnostics Corporation used under license by BTG International Canada Inc. TheraSphere is a registered trademark in US, EU and certain other territories. "See More. Reach Further. Treat Smarter", "Imagine where we can go", BTG and the BTG roundel logo are trademarks of BTG International Ltd. BTG and the BTG roundel logo are registered trademarks of BTG International Ltd in the US, EU and certain other territories. All rights reserved. © 2014 BTG International Ltd. US-USTHSP-2014-0279.

References:

1. Refers to high specific activity
2. Hilgard P, Hamami M, Fouly AE, et al. Radioembolization with Yttrium-90 Glass Microspheres in Hepatocellular Carcinoma: European Experience on Safety and Long-term Survival. Hepatology, 2010; 52: 1741-1749
3. TheraSphere® [US Package Insert] Ottawa, ON; Nordion (Canada) Inc. 2011.

SEE MORE.
REACH FURTHER.
TREAT SMARTER.

There are no limits to where our ideas will take us.

Imagine where we can go.

